STRUCTURAL BASIS OF LIGAND BINDING TO 3',5"-AMINOGLYCOSIDE *O*-PHOSPHOTRANSFERASE TYPE IIIa

Desiree Ho-Chi Fong

Doctor of Philosophy

Department of Biochemistry

McGill University

Montreal,Quebec

2006-03-28

A thesis submitted to McGill University
in partial fulfilment of the requirements of the degree of
Doctor of Philosophy

Your file Votre référence
ISBN: 978-0-494-25146-1
Our file Notre référence
ISBN: 978-0-494-25146-1

ACKNOWLEDGEMENTS

I would like to extend a million thank-yous to my supervisor, Dr. Albert Berghuis, for his guidance, patience, and unfailing optimism. This dissertation could not have been written without his supervision and encouragement throughout my academic program. I am grateful for the opportunity to do research in a relaxed and open environment. I would also like to thank all past and present Berghuis lab members, especially, Oliver Bättig, Dr. David Burk, Noboru Ishiyama, Magdalena Korczynska, Ahmad Mirza, Nicolas Skouris, Dr. Bing Xiong, and Veronica Yim, for listening to my complaints and frustrations. I am thankful for their assistance in the lab and the camaraderie we share. I will never forget the many trying, adventurous, and sometimes fruitful synchrotron trips. I would like to acknowledge Nicolas Skouris for his help in translating the abstract of this thesis. A special thank you to David Burk, for being a wonderful friend and for his advice and assistance throughout my graduate study. I am also indebted to him for proofreading this thesis. I would like to thank the International Centre for Diffraction Data, McGill University, Ontario Ministry of Education and Training, and McMaster University for the awards given. Last but not least, a heartfelt thank you to my family for their unconditional love, patience, and endless support.

CONTRIBUTIONS OF AUTHORS

Text and images from the following three published articles were incorporated into this thesis.

1. Fong, D.H., Burk, D.L., and Berghuis, A.M. (2005) Aminoglycoside kinases and antibiotic resistance. In Pinna, LA and Cohen, PTW (eds.), *Inhibitors of Protein Kinases and Protein Phosphatases.* Springer, Berlin, Vol. 167, pp. 157–188.

   This review article was structured and drafted based on a review written by D.L.B. and A.M.B. (Burk, DL and Berghuis, AM (2002) Protein kinase inhibitors and antibiotic resistance. Pharmacol Ther. ***93****: 283–292) My contributions to this article included writing and editing the majority of the text and figures according to the criteria specified by the publisher and the addition of new information acquired and published since the aforementioned review article. In whole, I was responsible for approximately 60% of the article.*

2. Fong, D.H. and Berghuis, A.M. (2004) Crystallization and preliminary crystallographic analysis of 3'-aminoglycoside kinase type IIIa complexed with a eukaryotic protein kinase inhibitor, CKI-7. *Acta crystallogr. D.* **60**: 1897–1899.

3. Fong, D.H. and Berghuis, A.M. (2002) Substrate promiscuity of an antibiotic resistance enzyme due to target mimicry. *EMBO J.* **21**: 2323–2331.

   I performed all experiments, analyzed the data and wrote the manuscripts of articles 2 and 3. A.M.B. provided comments and suggestions throughout the course of the work.

ABSTRACT

3',5"-aminoglycoside *O*-phosphotransferase type IIIa (APH(3')-IIIa) is an enzyme produced by pathogenic Gram-positive bacteria such as *Enterococci* and *Staphylococci*. It is capable of conferring resistance to a broad range of clinically important aminoglycoside antibiotics *via* the ATP-dependent addition of a phosphate to specific hydroxyl groups on the drug. The phosphorylated aminoglycoside loses its toxic effects due to reduced affinity for its target, the A-site of 30S ribosome. Crystal structures of several ternary complexes have been elucidated in an effort to understand the promiscuity of substrate recognition by APH(3')-IIIa. They are APH(3')-IIIa bound with ADP and kanamycin or neomycin to resolutions of 2.4 Å and 2.7 Å, respectively, as well as the structures of APH(3')-IIIa bound with AMPPNP and butirosin or 5"-monophosphorylated butirosin to resolutions of 2.4 Å and 2.7 Å, respectively. These structures reveal that the basis for this enzyme's broad substrate spectrum is the presence of a flexible antibiotic-binding loop and a versatile antibiotic-binding pocket composed of three sub-sites. A comparison of the A-site of the bacterial ribosome and APH(3')-IIIa shows a high degree of similarity in the pattern of hydrogen bonds to the aminoglycoside. However, they differ in their van der Waals interactions with the substrate, suggesting a potential strategy for the design of novel antibiotics and adjuvants. Another strategy for overcoming antibiotic resistance resulting from the effects of APH(3')-IIIa is the development of inhibitors that target the nucleotide-binding pocket of the enzyme. It has been shown that

APH(3')-IIIa possess striking structural and functional similarity to eukaryotic protein kinases (ePKs). In particular, APH(3')-IIIa is sensitive to several ATP-competitive protein kinase inhibitors. To aid the design of ligands with high specificity to the nucleotide-binding pocket of APH(3')-IIIa, the crystal structure of APH(3')-IIIa bound with CKI-7, a casein kinase 1 inhibitor, has also been determined to 2.5 Å resolution. Distinct features can be identified upon detailed comparisons between CKI-7-bound and nucleotide-bound APH(3')-IIIa and isoquinolinesulfonamide-bound ePKs. It is hoped that these results will contribute to the design of compounds that will allow aminoglycoside antibiotics to remain useful components of the antibacterial armamentarium.

ABRÉGÉ

3',5"-aminoglycoside *O*-phosphotransferase de type IIIa (APH(3')-IIIa) est une enzyme produite par des bactéries pathogéniques Gram-positives telles que les entérocoques et les streptocoques. Elle a la capacité de conférer une résistance à un grand spectre d'antibiotiques cliniquement important du type aminoglycoside en catalysant le transfert d'un phosphate à des groupes hydroxyles spécifiques par un mécanisme dépendant de l'ATP. L'aminoglycoside phosphorylé perd ainsi ces effets toxiques en ayant une affinité réduite pour sa cible, le site A du ribosome 30S. Nous avons élucidé plusieurs structures cristallines de cet enzyme afin de comprendre le mécanisme par lequel APH(3')-IIIa reconnaît son substrat. Nous avons complexé APH(3')-IIIa avec de l'ADP et avec kanamycin ou neomycin a des résolutions de 2.4 Å et de 2.7 Å, respectivement, et avec AMPPNP et butirosin ou butirosin-5"-monophosphorylé, encore a des résolutions de 2.4 Å et 2.7 Å, respectivement. Ces structures ont démontré que la raison derrière la grande variété de substrat que cet enzyme peut phosphoryler est dû à la présence d'un segment flexible responsable de la liaison de l'enzyme au substrat et à cause d'une cavité de liaison qui est très versatile et qui est composée de trois sous-sites. Une comparaison du site A du ribosome bacterien avec APH(3')-IIIa démontre un haut degré de similarité dans l'agencement des liens hydrogènes avec l'aminoglycoside. Il existe, par contre, une différence entre les interactions van der Waals avec le substrat, suggérant une stratégie possible pour la conception

de nouveaux antibiotiques et adjuvants. Une autre stratégie possible pour surmonter la résistance bactérienne est le développement d'inhibiteurs ciblant le site d'attachement nucléotidique de l'enzyme. Il à déjà été demontré que APH(3')-IIIa possède une ressemblance structurelle et fonctionnelle aux kinases protéiques des eucaryotes (ePKs). En particulier, APH(3')-IIIa est sensible à plusieurs inhibiteurs de kinases protéiques qui sont compétitifs avec l'ATP. Pour aider dans la conception d'inhibiteurs ciblant le site d'attachement nucléotidique, la structure de APH(3')-IIIa a aussi été déterminée en présence du composé CKI-7, un inhibiteur de la kinase de caséine de type 1, et ce à une résolution de 2.5 Å. En comparant la structure de APH(3')-IIIa complexé avec CKI-7 et un nucléotide avec les structures des ePKs complexé avec isoquinolinesulfonamide, certaines caractéristiques sont facilement identifiables. Il est espéré que ces résultats vont contribuer à la conception de composés qui permettront aux antibiotiques du type aminoglycoside de demeurer des outils efficaces dans notre armement antibacterien.

TABLE OF CONTENTS

ACKNOWLEDGEMENTS ii

CONTRIBUTIONS OF AUTHORS iii

ABSTRACT iv

ABRÉGÉ vi

LIST OF TABLES xii

LIST OF FIGURES xiii

LIST OF ABBREVIATIONS xvii

1 Introduction 1

1.1 Infectious Diseases, Antibiotics, and Antibiotic Resistance . . . 1

1.2 Aminoglycosides and Aminoglycoside Resistance 4

1.2.1 Aminoglycoside Antibiotics 4

1.2.2 Resistance to Aminoglycosides 7

1.2.3 Aminoglycoside Phosphotransferases 8

1.3 3'-Aminoglycoside *O*-Phosphotransferase-IIIa Structure and Similarity to Eukaryotic Protein Kinases 17

1.3.1 Tertiary Structure 17

1.3.2 Apo and Nucleotide-bound Structures of APH(3')-IIIa . 19

1.3.3 ATP-binding Site 22

1.3.4 Aminoglycoside-binding Site 25

1.4 Circumvention of Aminoglycoside Inhibition by 3'-Aminoglycoside *O*-Phosphotransferase 29
1.4.1 Targeting the Aminoglycosides and Their Binding Pocket 29
1.4.2 Targeting the Nucleotide-Binding Pocket 38
1.4.3 Exploiting the Bridged Binding Site 41
1.4.4 Alternative Strategies for Circumventing Antibiotic Resistances 43
1.5 Thesis Objectives 46

2 Overview of Experimental Procedures 47

2.1 APH(3')-IIIa Production and Purification 47
2.1.1 Materials 47
2.1.2 Procedures 49
2.2 Phosphotransferase Activity Assay 52
2.2.1 Materials 53
2.2.2 Methods 54
2.3 Crystallization 54
2.3.1 Materials 55
2.3.2 General Crystallization Techniques Employed 56
2.4 Data Collection and Processing 57
2.5 Molecular Replacement 59
2.5.1 Rotational Search 60
2.5.2 Translational Search 61
2.6 Model Refinement 62

3 Structural Basis of Plasticity in Substrate Specificity 66

3.1 Introduction 66
3.2 Experimental Procedures 68
3.2.1 Crystallization and Data Collection 68
3.2.2 Structure Determination and Refinement 70

3.3 Results 75
3.3.1 Overall Structure of Aminoglycoside-bound APH(3')-IIIa 75
3.3.2 Aminoglycoside-binding Site 81
3.4 Discussion 86
3.4.1 Substrate-binding Mechanism of other Multiple-substrate Recognizing Enzymes 86
3.4.2 Comparison of Aminoglycoside-binding Mode in 16S Ribosomal RNA versus APH(3')-IIIa 88
3.4.3 Comparison to the Crystal Structure of APH(3')-IIa . . 94
3.4.4 Binding of Aminoglycosides with a 4-amino-2-hydroxybutyrate (AHB) 99
3.4.5 Sequential and Regiospecific Diphosphorylation of 4,5 -disubstituted Aminoglycosides 100

4 3'-Aminoglycoside Phosphotransferase Type IIIa complexed with a Eukaryotic Protein Kinase Inhibitor, CKI-7 105

4.1 Introduction 105
4.2 Experimental Procedures 107
4.2.1 Crystallization 107
4.2.2 Data Collection and Processing 109
4.2.3 Structure Determination and Refinement 110
4.2.4 Inhibitor Design 112
4.3 Results and Discussion 113
4.3.1 Overall Structure of CKI-7-bound APH(3')-IIIa 113
4.3.2 Inhibitor Binding Site 117
4.3.3 Comparison of inhibitor-bound APH(3')-IIIa and eukaryotic protein kinases 120
4.3.4 Inhibitor Design 135

5 Summary and Conclusions 149

5.1 Summary of Experimental Results 149

5.2 Future Directions 151
5.3 Concluding Remarks 153

Appendix 155

LIST OF TABLES

Table		page
1–1	Some aminoglycoside-modifying enzymes	9
1–2	Substrate profiles of selected aminoglycoside-modifying enzymes	15
2–1	Salt step gradient program for 50 mL Q-Sepharose	50
2–2	Salt step gradient program for 6 mL Resource Q	51
3–1	Diffraction data collection statistics for APH(3')-IIIa complexed with ADP and kanamycin A or neomycin B, and AMPPNP and butirosin A.	71
3–2	Refinement statistics for APH(3')-IIIa complexed with ADP and kanamycin A or neomycin B, and AMPPNP and butirosin A.	74
4–1	Data collection statistics for APH(3')-IIIa in complex with eukaryotic protein kinase inhibitor, CKI-7	110
4–2	Refinement statistics for APH(3')-IIIa in complex with eukaryotic protein kinase inhibitor, CKI-7	112
5–1	Summary of APH(3')-IIIa complexes determined	152

LIST OF FIGURES

Figure page

1–1 Structures of representative aminoglycosides from different classes. 6

1–2 Amino acid sequence alignment of twenty-eight APH enzymes. . . 11

1–3 Structures of substrates of APH(3')-IIIa. 14

1–4 Comparison of the crystal structures of APH(3')-IIIa and cAPK. . 20

1–5 Superposition of the α-carbon trace of the APH(3')-IIIa–ADP, APH(3')-IIIa–AMPPNP, and APH(3')-IIIa apoenzyme structures. 22

1–6 The nucleotide-binding site of APH(3')-IIIa. 23

1–7 Structures of aminoglycosides lacking a 3'-hydroxyl group – tobramycin and dibekacin. 30

1–8 Aminoglycosides with substitutions at the 1-amino group of the central 2-deoxystreptamine ring – butirosin, amikacin, and isepamicin. 31

1–9 Four synthetic aminoglycosides based on the structure of neamine. 35

1–10 Two types of mechanism-based inhibition. 37

1–11 Examples of eukaryotic protein kinase inhibitors that target the nucleotide-binding site. 40

1–12 A tethered derivative of adenosine and neamine that targets both the nucleotide- and substrate-binding sites of aminoglycoside-modifying enzymes. 42

1–13 Superposition of APH(3')-IIIa–ADP and APH(3')-IIIa–ADP–ankyrin repeat crystal structures. 45

2–1 Coupled enzyme ATPase assay for the detection of phosphotransferase activity by APH(3')-IIIa. 53

2–2 Ramachandran plot for APH(3')-IIIa–ADP–kanamycin A complex. 65

3–1 Crystal structures of APH(3')-IIIa in complex with ADP and kanamycin A or neomycin B and electrostatic potential surface of the nucleotide-bound enzyme. 76

3–2 Simulated annealing F_o-F_c omit maps for kanamycin A, neomycin B, butirosin A and 5"-monophosphorylated butirosin A. 77

3–3 Structural changes observed in APH(3)-IIIa upon aminoglycoside binding. 78

3–4 Superposition of AMPPNP- and butirosin A-bound structures of APH(3')-IIIa. 80

3–5 Schematic representation of hydrogen bond interactions between APH(3')-IIIa and 4,5-disubstituted aminoglycosides. 85

3–6 Comparison of aminoglycoside binding to APH(3')-IIIa versus the bacterial ribosome. 93

3–7 Superposition of APH(3')-IIIa and APH(3')-IIa bound with kanamycin A. 95

3–8 Schematic representation of hydrogen bonds made by kanamycin A with APH(3')-IIIa and APH(3')-IIa. 97

4–1 Crystals of the APH(3')-IIIa–CKI-7 complex at various stages of optimization. 109

4–2 Calcium binding site in CKI-7-bound APH(3')-IIIa. 116

4–3 Superposition of the α-carbon trace of CKI-7-bound and ADP-bound APH(3')-IIIa. 117

4–4 The inhibitor-binding pocket of APH(3')-IIIa. 119

4–5 Structures of CKI-7-bound APH(3')-IIIa and CK1. 121

4–6 Comparison of the CKI-7-/nucleotide-binding pockets of APH(3')-IIIa and CK1. 123

4–7 Chemical structures of ATP and several eukaryotic protein kinase inhibitors of the isoquinolinesulfonamide family. 127

4–8 Superposition of the α-carbon trace of H89-bound and AMPPNP-bound cyclic-AMP-dependent protein kinase (cAPK). 129

4–9 Comparison of the binding modes of H-isoquinolinesulfonamide inhibitors. 131

4–10 Comparison of the inhibitor-binding pocket of APH(3')-IIIa, CK1, and cAPK. 132

4–11 Hydrogen bonding interactions between various isoquinolinesulfonamides and APH(3')-IIIa or cAPK. 134

4–12 Comparison of the binding mode between the modelled H7, CKI-7, and ADP in APH(3')-IIIa. 136

4–13 Pharmacophore model of the APH(3')-IIIa ADP-binding site. . . . 141

4–14 Examples of ligands derived from 8-isoquinolinesulfonamide. . . . 144

4–15 Examples of ligands derived from isoquinoline modelled in the binding pocket by analogy to CKI-7. 145

4–16 Examples of ligands derived from 5-isoquinolinesulfonamide positioned according to the modelled binding mode of H7 in APH(3')-IIIa. 146

4–17 Examples of ligands derived from isoquinoline positioned according to the modelled binding mode of H7 in APH(3')-IIIa. 147

LIST OF ABBREVIATIONS

Å	Ångstrom (1 Å = 0.1 nm)
AAC	aminoglycoside *N*-acetyltransferase
ADP	adenosine 5'-diphosphate
AHB	4-amino-2-hydroxybutyrate
AME	aminoglycoside-modifying enzyme
AMoRe	Automated Package for Molecular Replacement
AMPPNP	β,γ-imidoadenosine 5'-triphosphate
AR	ankyrin repeat
ANT	aminoglycoside *O*-nucleotidyltransferase
APH	aminoglycoside *O*-phosphotransferase
APH(3')-IIIa	3',5"-aminoglycoside *O*-phosphotransferase type IIIa
ATP	adenosine 5'-triphosphate
BNL	Brookhaven National Laboratories
cAPK	cyclic-AMP-dependent protein kinase
CCD	charge-coupled device
CCP4	Collaborative Computational Project, Number 4
CKI-7	*N*-(2-aminoethyl)-5-chloro-isoquinoline-8-sulfonamide
CKI-8	1-(5-chloro-8-isoquinolinesulfonyl)-piperazine
CNS	Crystallography and NMR System
CK1	casein kinase 1
Da	Dalton (1 Da = 1 g/mol)

DTT	dithiothreitol
EDTA	ethylenediamine tetraacetic acid
ePK	eukaryotic protein kinase
H1152P	(S)-(+)-2-Methyl-1-[(4-methyl-5-isoquinolynyl)sulfonyl]homopiperazine
H7	1-(5-isoquinolinesulfonyl)-2-methylpiperazine
H8	*N*-[2-(methylamino)-ethyl]-5-isoquinolinesulfonamide
H9	*N*-(2-aminoethyl)-5-isoquinolinesulfonamide
H89	*N*-[2-(*p*-bromocinnamylamino)ethyl]-5-isoquinolinesulfonamide
HA1004	*N*-(2-guanidinoethyl)-5-isoquinolinesulfonamide
HA1077	1-(5-isoquinolinesulfonyl)-homopiperazine hydrochloride
IPTG	isopropyl β-D-thiogalactopyranoside
K	degree Kelvin
LB	Luria broth
MRSA	methicillin-resistant *Staphylococcus aureus*
NADH	β-nicotinamide adenine dinucleotide, reduced form
NMR	nuclear magnetic resonance
NSLS	National Synchrotron Light Source
PEG	polyethylene glycol
PhK	phosphorylase kinase
PMSF	phenylmethylsulfonyl fluoride
rmsd	root mean square deviation
SDS-PAGE	sodium dodecyl sulfate polyacrylamide gel electrophoresis
Tris	2-amino-2-(hydroxymethyl)1,3-propanediol

CHAPTER 1
Introduction

Text and figures in sections 1.2, 1.3, and 1.4 were adapted from the following book chapter: Fong, D.H., Burk, D.L. and Berghuis, A.M. (2005) Aminoglycoside Kinases and Antibiotic Resistance. In Pinna, L.A. and Cohen, P.T.W. (eds.), Inhibitors of Protein Kinases and Protein Phosphatases. Springer, Berlin, Vol. 167, pp. 157–188. With kind permission of Springer Science and Business Media.

Figure 1–3 was taken from from the journal article: Fong, D.H. and Berghuis, A.M. (2002) Substrate promiscuity of an aminoglycoside antibiotic resistance enzyme *via* target mimicry. *EMBO J.* **21**: 2323–2331. With permission from Nature Publishing Group.

1.1 Infectious Diseases, Antibiotics, and Antibiotic Resistance

Infectious diseases, particularly those caused by bacterial pathogens, have remained a major cause of mortality and morbidity throughout history. These diseases include the Bubonic plague in 14th century Eurasia, and more recently, a highly contagious and lethal strain of *Clostridium difficile* in Montreal, and ongoing cholera epidemics in Africa. In 1900, infections were the leading cause of death in the United States (Yoshikawa, 2002). Although infection-related deaths

and complications have declined precipitously since the introduction of antibiotics some 60 years ago, infections remain one of the major causes of death worldwide, particularly in the poorest nations (World Health Organization, 1999). In fact, one third of the global population is currently infected with tuberculosis (World Health Organization, 2000) and infectious diseases account for approximately 50,000 deaths each day around the world (Yoshikawa, 2002). Compounding this problem is the emergence of antimicrobial-resistant pathogens.

Antimicrobials are used in all facets of our lives, most obviously in human and veterinary medicine (Conly, 2002; Teale, 2002). The use of an antibiotic for any purpose, in any amount and over any time period, causes a selective pressure for bacteria that have evolved mechanisms to escape the effects of these drugs. While the emergence of resistance to antibacterial agents is a natural biological phenomenon and is unavoidable, the injudicious and widespread use of antibiotics exacerbates the situation and undermines the therapeutic efficacy of existing agents. For example, in the United States, approximately 126 million courses of antibiotics were prescribed in the ambulatory setting in 2000 (McCaig *et al.*, 2003) and many of these were for upper respiratory tract infections such as the common cold and bronchitis (Rutschmann and Domino, 2004). Nonetheless, human usage only accounts for approximately half of the over 22 million kilograms of antibiotics produced each year; the remaining 50% are used in the agriculture, aquaculture, and horticulture industries (Conly, 2002). The predominant use of antibiotics in animal husbandry is as growth promoters or as preventive measures (Conly, 2002; Teale, 2002). These practices may contribute

to a rise in the number of resistant microbes, which could be transmitted between animals and humans.

Nearly all of the antibiotics in current clinical use were discovered before the 1980s (Chopra *et al.*, 2002; World Health Organization, 2000). Only one new class of antimicrobial agents, the oxazolidinones, has been introduced in the last 20 years (Moellering, 2003). Unfortunately, each antibiotic developed and introduced into routine usage has invariably been enervated by the emergence of bacterial strains showing resistance. Subsequently, the level of resistance rises with use, ultimately leading to resistance-associated treatment failures (Moellering, 2003). All major bacterial pathogens are resistant to at least one drug and oftentimes, they are resistant to many (Chopra *et al.*, 2002; Moellering, 2003). Some resistant strains of opportunistic pathogens, such as vancomycin resistant *enterococci* (VRE), methicillin-resistant *Staphylococcus aureus* (MRSA), and vancomycin resistant *Staphylococcus aureus* (VRSA), are capable of surviving the effects of most, if not all, antibiotics currently in use (Cohen, 2000; Nicolaou and Boddy, 2001; Schentag *et al.*, 1998; Walsh, 2000; Chang *et al.*, 2003). For example, *enterococci* are a common cause of bloodstream infections in North America (Pfaller *et al.*, 1998; Georgopapadakou, 2002). Among *Enterococci* spp., 80% of *Enterococcus faecium* strains are resistant to ampicillin, 49-61% are resistant to quinolones, 31-38% to aminoglycosides, 12-13% to vancomycin, and 74-80% to streptogramins (Georgopapadakou, 2002).

Antibiotic resistance has become a serious global health problem. It threatens to reverse 60 years of progress made in human health and welfare, and raises

the spectre of a post-antibiotic era. Controlling antibiotic resistance requires global efforts and a multifaceted approach. A comprehensive strategy as suggested by the World Health Organization in the WHO Global Strategy for Containment of Antimicrobial Resistance (`http://www.who.int/emc-documents/antimicrobial_resistance/docs/EGlobal_Strat.pdf`) emphasizes the need to curtail the inappropriate use of antimicrobial agents, to improve infection control in order to reduce the transmission of resistant organisms, to better educate and inform the public, and to continually develop new antimicrobial agents. Moreover, surveillance of the trends in resistance will enable policies and guidelines to be kept current. Attempts to conserve our antibacterial armamentarium should focus on the management rather than elimination of antibiotic resistance, with the objective of retarding or delaying the development of new resistance while continuing to develop new agents (Conly, 2002; Livermore, 2003).

1.2 Aminoglycosides and Aminoglycoside Resistance

1.2.1 Aminoglycoside Antibiotics

The first aminoglycoside, streptomycin, was isolated from the soil bacterium *Streptomyces griseus* in 1944 (Schatz *et al.*, 1944). Streptomycin proved to be the first successful drug against *Mycobacterium tuberculosis* and became widely popular in the 1940s and 1950s. The impact of streptomycin was of such significance that Selman A. Waksman was awarded the Nobel Prize in Medicine in 1952 for its discovery. While streptomycin remains an integral part of modern chemotherapy for tuberculosis over 50 years after its clinical introduction, a variety of natural and semisynthetic aminoglycosides with broad antimicrobial

spectra have also been discovered and developed. These antibiotics are often used to treat serious nosocomial infections. Despite some toxic effects on the kidney and the inner ear (Forge and Schacht, 2000), aminoglycosides are among the most commonly used antibiotics due to their low cost and high efficacy against both Gram-positive and Gram-negative bacteria, and in some cases, protozoan infections (Berman and Fleckenstein, 1991).

From a chemical perspective, aminoglycosides are a group of structurally diverse, water soluble, polycationic molecules. They contain an aminocyclitol nucleus and two or three aminosugar rings linked to the nucleus *via* glycosidic bonds. They can be grouped into two main categories based on the structure of the central aminocyclitol ring. The first group, which includes streptomycin, contains a streptidine derivative; the second, larger group, which includes neomycin and kanamycin, contains a 2-deoxystreptamine ring derivatized at either the 4- and 5-positions or the 4- and 6-positions (Figure 1–1). Conventionally, the numbering of the 6-aminohexose ring linked to the 4-position of the 2-deoxystreptamine is designated the prime (') ring, and the pentose or hexose ring linked to the 5- or 6-position is designated double prime (").

Unlike many antibiotics which are bacteriostatic, most aminoglycosides are bactericidal compounds, specifically those containing the 2-deoxystreptamine core structure. The primary target of these drugs in the bacterial cell is the 30S ribosomal subunit, as shown by chemical footprinting experiments (Moazed and Noller, 1987), nuclear magnetic resonance (NMR) experiments (Fourmy *et al.*, 1996), and more recently, evidence from crystallographic studies (Carter *et al.*,

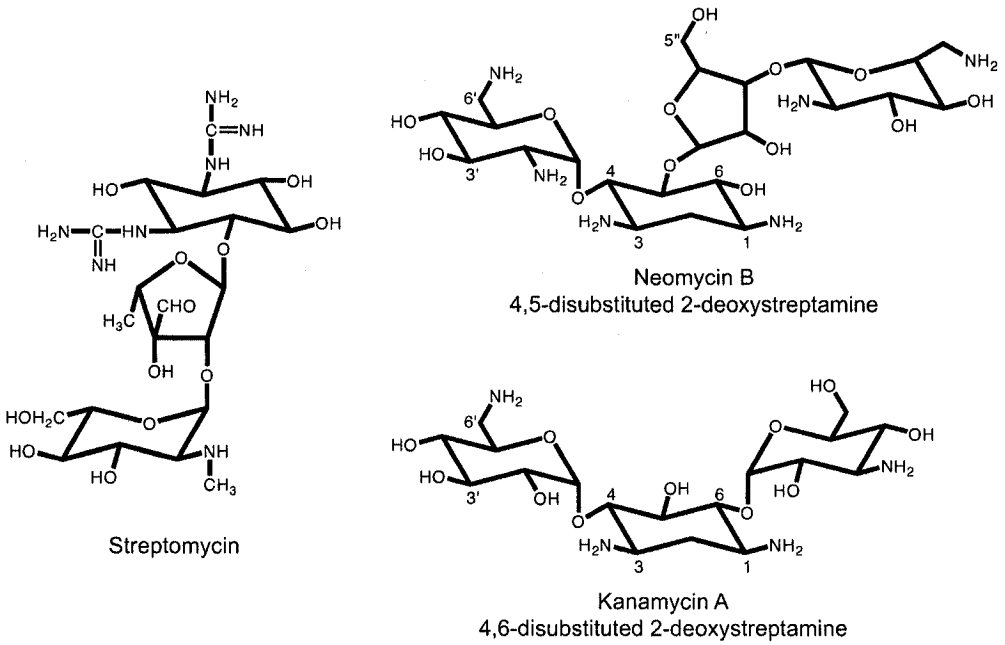

Figure 1–1. Structures of representative aminoglycosides from different classes. Streptomycin is a streptidine-containing aminoglycoside. Neomycin B and kanamycin A are both examples of aminoglycosides containing a 2-deoxystreptamine core. Neomycin B has a 4,5-disubstituted 2-deoxystreptamine, whereas kanamycin A has a 4,6-disubstituted 2-deoxystreptamine.

2000). Nonetheless, some details concerning the uptake and action of aminoglycosides remain elusive. Existing evidence indicates that the first step of aminoglycoside uptake involves an energy-requiring transport across the cell membrane (Wright *et al.*, 1998). Once inside the cell, the aminoglycosides bind to the A-site (the decoding site) of the 16S rRNA (Moazed and Noller, 1987) and trigger certain conformational changes in the A-site that normally occur only when there is a correct interaction between cognate tRNA and mRNA (Pape *et al.*, 2000; Ogle *et al.*, 2001, 2002; Rodnina *et al.*, 2002). As a result, the stability of the binding of near-cognate aminoacyl-tRNA to this site is increased and the ribosome is unable to discriminate between cognate and near- or non-cognate tRNA-mRNA

complexes and the production of defective proteins ensues. The faulty proteins are presumably inserted into the cytoplasmic membrane, leading to the loss of membrane integrity. Additional aminoglycosides are then rapidly transported across the damaged membrane, leading to the accumulation of the drug in the cytoplasm, saturation of all ribosomes and ultimately cell death (Wright *et al.*, 1998).

1.2.2 Resistance to Aminoglycosides

Unfortunately, the extensive use of aminoglycosides has undermined their potency due to the emergence of resistance in bacteria. There are three principal mechanisms of bacterial resistance to antibiotics. First, the bacteria can prevent accumulation of antibiotics inside the cell either *via* changes in membrane permeability or *via* efflux pumps that export the drug from the cell. Second, the bacteria can also alter, by mutation or chemical modification (Cundliffe, 1989; Thompson *et al.*, 1985) the target of the antibiotic (such as the ribosome) to preclude the effects of the antibiotic. Lastly, antibiotics that manage to enter the cell can be enzymatically degraded or modified such that the affinity for their target is lost or reduced and, therefore, the altered antibiotics can no longer exert their antimicrobial effects (Llano-Sotelo *et al.*, 2002). Enzymatic modification is the most prevalent means of resistance to aminoglycosides in clinical isolates (Davies, 1991). Three families of aminoglycoside-modifying enzymes (AMEs) have been identified. They are aminoglycoside *N*-acetyltransferases (AACs), aminoglycoside *O*-phosphotransferases (APHs) and

aminoglycoside *O*-nucleotidyltransferases (ANTs). They render aminoglycoside antibiotics inactive by catalysing the transfer of an acetyl group (from acetyl CoA), a phosphate group or an adenyl group (both from adenosine 5'-triphosphate (ATP)) to the aminoglycoside. Over 50 AMEs have been identified (Table 1–1) and they are named using nomenclature proposed by Shaw *et al.* (1993). First, each enzyme is identified by the reaction they carry out — AAC for acetylation, APH for phosphorylation, and ANT for adenylation. This is followed by the regiospecificity of the group transferred, designated in parentheses. Next follows a Roman numeral which specifies the unique aminoglycoside substrate profile. A final lower case letter identifies the distinct genes which confer identical resistance phenotypes.

1.2.3 Aminoglycoside Phosphotransferases

Although many AMEs are capable of conferring a resistant phenotype, generally only APHs yield high levels of resistance (Vakulenko and Mobashery, 2003). APHs constitute the second largest group of AMEs, carrying out the phosphorylation of specific hydroxyl groups of aminoglycosides using ATP as a cofactor. Over 20 distinct aminoglycoside phosphotransferases (or kinases) have been identified and they show significant sequence similarity (Figure 1–2). APHs are classified into seven types (Table 1–1) (Shaw *et al.*, 1993) and among them, APH(3') enzymes make up the largest group, comprising eight sub-classes (APH(3')-I to APH(3')-VIII). APHs have been isolated from both Gram-positive and Gram-negative bacteria, including aminoglycoside-producing organisms (Shaw *et al.*, 1993).

Table 1–1. Some aminoglycoside-modifying enzymes

AAC		APH		ANT	
AAC(2')	Ia, Ib, Ic, Id, Ie	APH(3')	Ia, Ib, Ic	ANT(4')	Ia
	IIa, IIb		IIa, IIb		IIa
AAC(6')	Ia-In, Ip-Ix, Iz		IIIa	ANT(6)	Ia
	IIa, IIb		IVa	ANT(9)	Ia
AAC(1)	Ia		Va, Vb, Vc		Ib
AAC(3)	Ia, Ib		VIa	ANT(2")	Ia
	IIa, IIb, IIc		VIIa	ANT(3")	Ia
	IIIa, IIIb, IIIc		VIIIa		
	IVa	APH(4)	Ia, Ib		
	VIa	APH(6)	Ia, Ib, Ic, Id		
	VIIa	APH(9)	Ia, Ib		
	VIIIa	APH(2")	Ia, Ib, Ic, Id		
	IXa	APH(3")	Ia, Ib		
	Xa	APH(7")	Ia		

APH(3')-IIIa. APH(3')-IIIa is the most studied aminoglycoside phosphotransferase. It was originally isolated from *Streptococcus faecalis* (Trieu-Cuot and Courvalin, 1983) and *S. aureus* (Gray and Fitch, 1983). Subsequently, the gene was detected in *Campylobacter coli*, which became a precedent for the transfer of an antibiotic resistance gene between Gram-positive and Gram-negative bacteria (Papadopoulou and Courvalin, 1988; Taylor *et al.*, 1988). The *aph(3')-IIIa* gene from *Enterococcus faecalis* has been cloned and the protein expressed and purified from *Escherichia coli* (McKay *et al.*, 1994a). The purified APH(3')-IIIa enzyme can exist as either a monomer or a covalent dimer linked *via* a disulfide bridge. The two active sites in the dimer are independent of each other and thus, the catalytic activity in the two states are indistinguishable

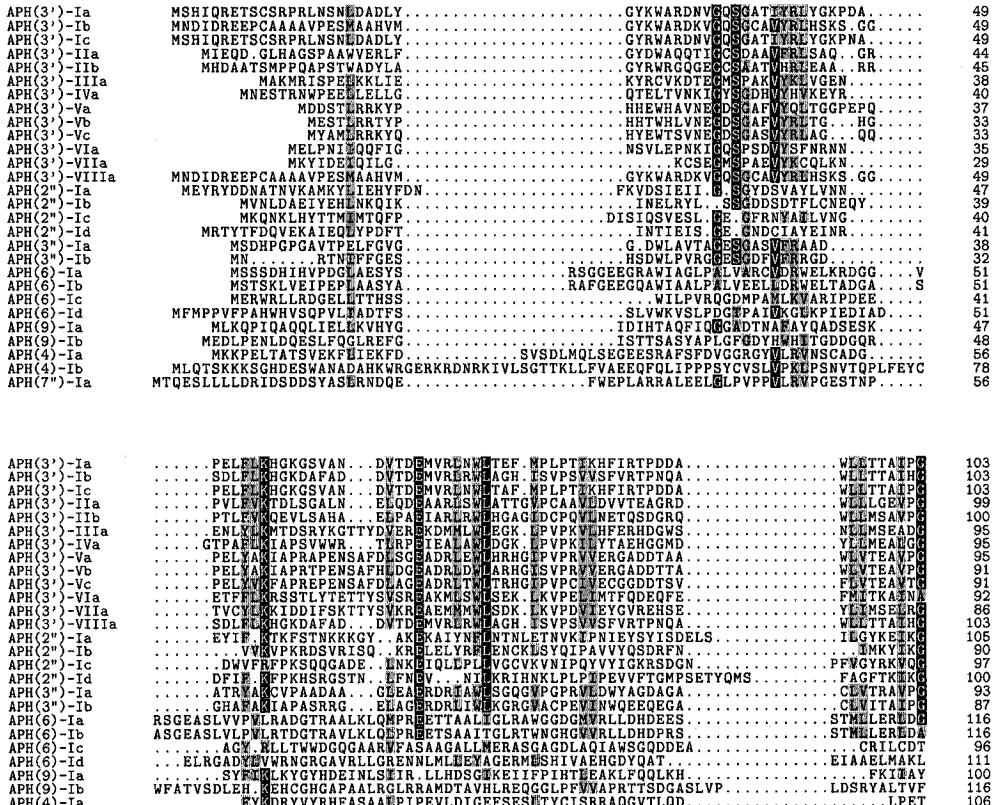

X non conserved
X similar
X conserved

Figure 1–2. Amino acid sequence alignment of twenty-eight APH enzymes, including thirteen APH(3') isozymes, four APH(2") isozymes, three APH(6) isozymes, two each of APH(3"), APH(9), and APH(4) isozymes, as well as one APH(7"). Multiple sequence alignment was performed using Clustal X version 1.83 (Chenna *et al.*, 2003). Conserved residues are shaded black and similar residues are in grey background. Residues with similar properties are defined as follows: FYW, ILVM, RK, DE, GA, ST, NQ. GenBank Protein IDs are CAA23656 (APH(3')-Ia), AAA26412 (APH(3')-Ib), CAA44024 (APH(3')-Ic), AAA73390 (APH(3')-IIa), AAG07506 (APH(3')-IIb), CAA24789 (APH(3')-IIIa), CAA27061 (APH(3')-IVa), AAA26699 (APH(3')-Va), AAC32025 (APH(3')-Vb), AAB21326 (APH(3')-Vc), CAA30578 (APH(3')-VIa), AAA76822 (APH(3')-VIIa), AAA26412 (APH(3')-VIIIa), AAA26865 (AAC(6')-Ia–APH(2")-Ia), AAK63040 (APH(2")-Ib), AAB49832 (APH(2")-Ic), AAC14693 (APH(2")-Id), AAA26700 (APH(3")-Ia), AAA26442 (APH(3")-Ib), CAA68516 (APH(6)-Ia), CAA29136 (APH(6)-Ib), AAA73392 (APH(6)-Ic), AAA26443 (APH(6)-Id), AAB58447 (APH(9)-Ia), AAB66655 (APH(9)-Ib), CAA24743 (APH(4)-Ia), CAA52372 (APH(4)-Ib), and CAA27276 (APH(7")-Ia).

(McKay *et al.*, 1994a). APH(3')-IIIa has one of the broadest substrate profiles among all single-function AMEs (Figure 1–3 and Table 1–2). As its name implies, APH(3')-IIIa catalyzes the transfer of a phosphate group to the 3'-hydroxyl of the antibiotic substrate. Interestingly, it is also able to transfer a phosphategroup from ATP to the 5"-hydroxyl of neomycin type aminoglycosides (Thompson *et al.*, 1996b). Hence, aminoglycosides which lack the 3'-hydroxyl, such as lividomycin, are also substrates for APH(3')-IIIa, since they can be modified at the 5"-position. In this sense, the enzyme would be more appropriately named APH(3')(5")-IIIa. The enzyme is 264 amino acid residues in size, with a molecular mass of 31,000 Da. Product and dead-end inhibition (McKay and Wright, 1995), along with solvent viscosity, thio, and solvent isotope effects (McKay and Wright, 1996), indicate that the phosphorylation reaction catalyzed by APH(3')-IIIa follows a Theorell-Chance mechanism (Theorell and

Chance, 1951) where ATP binds to the enzyme first, followed by the aminoglycoside; phosphorylated-aminoglycoside is then quickly released, followed by the rate-limiting step — the release of adenosine 5'-diphosphate (ADP). Evidence from site-directed mutagenesis and positional isotope exchange methods suggests that the phosphoryl transfer occurs through direct attack of the 3'-hydroxyl group of the aminoglycoside on the γ-phosphate of ATP *via* a dissociative manner (Thompson *et al.*, 1996a; Boehr *et al.*, 2001b). APH(3')-IIIa is the first aminoglycoside phosphotransferase to be structurally characterized. The three-dimensional atomic structure of the enzyme complexed with ADP was determined to 2.2 Å by X-ray crystallography (Hon *et al.*, 1997, Section 1.3). Subsequently, structures of APH(3')-IIIa in the apoenzyme form (i.e. no substrate or cofactor) and in complex with the non-hydrolyzable ATP analogue β,γ-imidoadenosine 5'-triphosphate (AMPPNP) have been determined (Burk *et al.*, 2001).

APH(3')-Ia and APH(3')-IIa. Two other APH(3') enzymes, APH(3')-Ia and APH(3')-IIa, have also been extensively characterized. The amino acid sequences of APH(3')-Ia, APH(3')-IIa and APH(3')-IIIa enzymes share approximately 30% identity but APH(3')-Ia and APH(3')-IIa show a generally higher specificity for aminoglycoside substrates, as demonstrated by the higher k_{cat}/K_m values (Siregar *et al.*, 1994, 1995). APH(3')-Ia is the most commonly disseminated APH in Gram-negative bacteria. The *aph(3')-Ia* gene was discovered on transposon Tn*903* in *E. coli* (Oka *et al.*, 1981), encoding an enzyme that is able to phosphorylate a range of clinically useful aminoglycoside antibiotics (Table

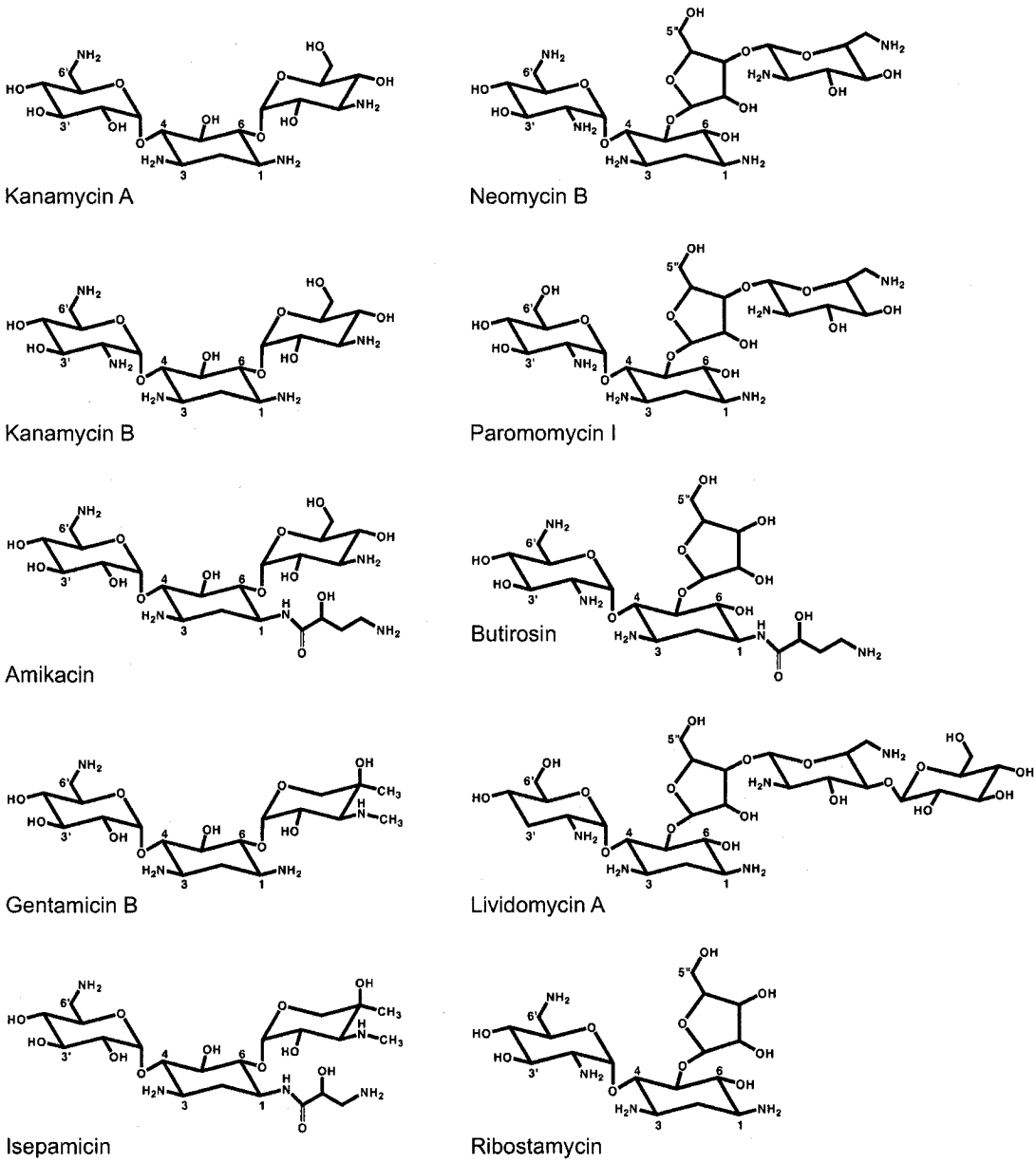

Figure 1–3. Structures of known substrates of APH(3')-IIIa. The enzyme modifies all 4,6-disubstituted aminoglycosides at the 3'-hydroxyl group. All 4,5-disubstituted aminoglycosides, except lividomycin A, are modified at the 3'- and 5"-hydroxyl groups. Lividomycin A has no hydroxyl group at the 3' site, hence it can only be phosphorylated at the 5" position. *Reproduced with permission from Nature Publishing Group.*

1–2) (Shaw *et al.*, 1993). Steady state kinetic studies of APH(3')-Ia indicate that the phosphorylation reaction occurs *via* a rapid equilibrium random mechanism and, like APH(3')-IIIa, the phosphoryl group is believed to be transferred in a direct displacement manner (Siregar *et al.*, 1995).

Table 1–2. Substrate profiles of selected aminoglycoside-modifying enzymes

Enzyme	Profile	Reference(s)
APH(3')-Ia	kanamycin, neomycin, lividomycin, paromomycin, ribostamycin	(Oka *et al.*, 1981)
APH(3')-IIa	kanamycin, neomycin, butirosin, paromomycin, ribostamycin	(Beck *et al.*, 1982)
APH(3')-IIIa	kanamycin, amikacin, isepamicin, gentamicin B, butirosin, lividomycin, paromomycin, ribostamycin	(Gray and Fitch, 1983; Trieu-Cuot and Courvalin, 1983)
APH(2")-Ia (bifunctional enzyme)	kanamycin, amikacin, tobramycin, dibekacin, gentamicin, isepamicin, sisomicin, netilmicin, neomycin, butirosin, lividomycin, paromomycin, ribostamycin, neamine	(Daigle *et al.*, 1999a; Ferretti *et al.*, 1986)

Although APH(3')-IIa is rarely found in clinical isolates, it is still a well-known APH. The *aph(3')-IIa* gene, encoded on transposon Tn*5* (Beck *et al.*, 1982) is widely used in molecular biology as a selectable marker in both eukaryotic and prokaryotic studies. APH(3')-Ia and APH(3')-IIa have almost identical substrate spectra (Table 1–2). Recently, the crystal structure of APH(3')-IIa

complexed with kanamycin was solved (Nurizzo *et al.*, 2003). It is essentially identical to the structure of APH(3')-IIIa. See section 3.4.3 for a detailed comparison of the structures of APH(3')-IIa and APH(3')-IIIa.

APH(2")-Ia. Another important resistance factor in Gram-positive pathogens is APH(2")-Ia. The gene *aph(2")-Ia* is located downstream of *aac(6')-Ie*, and they are conjointly expressed as one enzyme with two reaction centres. This bifunctional enzyme is capable of inactivating essentially all clinically available aminoglycosides containing a 2-deoxystreptamine ring (Ferretti *et al.*, 1986; Leclercq *et al.*, 1992) (Table 1–2) and is most prevalent in MRSA isolates in many parts of the world (Schmitz *et al.*, 1999; Udo and Dashti, 2000; Ida *et al.*, 2001). The substrate specificity of AAC(6')-Ie–APH(2")-Ia is not very stringent. In addition to acetylating the amino group at the 6'-position, the AAC domain can also acetylate the 6'-hydroxyl of lividomycin and paromomycin. Whereas APH(2") denotes the transfer of a phosphate group to the 2"-hydroxyl of the drug, phosphorylation at the 3'- and 3"-positions of most 4,5-disubstituted aminoglycosides, and the 5"-position of lividomycin, has also been observed (Daigle *et al.*, 1999a). The phosphorylation reaction of APH(2")-Ia proceeds through a random rapid equilibrium mechanism (Martel *et al.*, 1983). The amino acid sequence of APH(2")-Ia is about 15% identical to that of APH(3')-IIIa.

1.3 3'-Aminoglycoside *O*-Phosphotransferase-IIIa Structure and Similarity to Eukaryotic Protein Kinases

APH(3')-IIIa from *Enterococci* and *Staphylococci* is perhaps the best understood of the AMEs. As a result, APH(3')-IIIa has become a useful model for the study of aminoglycoside phosphotransferases. Experiments on APH(3')-IIIa have revealed much about the kinetic properties, mechanism, and structure of this enzyme. These studies contribute to our knowledge in the underlying principles of enzyme mechanism. In particular, structural studies elucidating the non-covalent interactions between the target protein and its substrates are essential to our understanding in the molecular basis of enzymatic catalysis.

1.3.1 Tertiary Structure

Two molecules of APH(3')-IIIa–nucleotide complex were found in the asymmetric unit, covalently linked by two cysteine bridges between Cys19 and Cys156 in a head-to-tail-tail-to-head fashion (Hon *et al.*, 1997). Although the active sites face each other, they are about 20 Å apart and are unlikely to have any cooperative or antagonistic influences on each other. This observation is consistent with steady-state kinetic results which showed that the monomer is the biologically relevant unit (McKay *et al.*, 1994a). The disulfide-linked APH(3')-IIIa dimer is therefore an artifact of the purification procedure (Kadokura *et al.*, 2003). The APH(3')-IIIa enzyme is composed of two lobes, a 94-residue N-terminal lobe and a larger 157-residue C-terminal lobe. The two lobes are joined by a 12-residue linker region containing a short β-strand and α-helix. The N-terminal lobe consists of a five-stranded antiparallel β-sheet, with an α-helix located between two

β-strands and a short 3_{10} helix preceding the first β-strand. The architecture of the N-terminal lobe of APH(3')-IIIa is similar to that observed in eukaryotic protein kinases (ePKs) such as the catalytic subunits of cAPK, casein kinase 1 (CK1) and phosphorylase kinase (PhK) (Knighton *et al.*, 1991; Owen *et al.*, 1995; Xu *et al.*, 1995). For structurally conserved main-chain atoms in the N-terminal lobe, the root mean square deviation (rmsd) in atomic position is only 1.8 Å between APH(3')-IIIa and cAPK. This is remarkable, given the fact that the sequence identity between the two enzymes is less than 6% for these residues (Burk *et al.*, 2001).

The 12-residue linker that connects the N- and C-terminal lobes of APH(3')-IIIa is also structurally similar to the equivalent region in the structures of protein kinases such as cAPK. The linker consists of a short α-helix flanked by sections of random coil. The C-terminal lobe of APH(3')-IIIa can be divided into three sections: (i) a central core composed of two α-helices and a long hairpin-shaped loop incorporating two short sections of antiparallel β-sheet, (ii) an insert region composed of two α-helices connected by long loop and (iii) a C-terminal region composed of two α-helices.

There are four areas in which APH(3')-IIIa differs significantly from ePKs such as cAPK (Figure 1–4). First, in APH(3')-IIIa, the loop between β-strands 1 and 2 contains a one-residue insertion and adopts a different conformation than that observed in ePKs (red). While this loop is the location of the conserved GXGXXG motif in protein kinases, the motif is not observed in APH(3')-IIIa.

Second, as a consequence of differences in the C-terminal lobes of APH(3')-IIIa and the protein kinases, the location of the α-helix in the linker region is shifted in APH(3')-IIIa with respect to where it is usually located in the protein kinases (yellow). Third, APH(3')-IIIa has a 60-residue insert in its C-terminal lobe (blue). Consisting of two α-helices and a 19-residue loop, this insertion occupies the space of a smaller section of polypeptide found in ePKs (orange). The latter has a distinctly different conformation from that seen in APH(3')-IIIa and has been identified as important in substrate selectivity and specificity (Madhusudan *et al.*, 1994; Taylor *et al.*, 1992). This section of the ePK sequence also corresponds to the activation segment in some protein kinases, containing sites of phosphorylation that switch the enzyme from an inactive to an active conformation (Yamaguchi and Hendrickson, 1996; Johnson *et al.*, 1996). Lastly, the positions of the two α-helices at the end of the C-terminal lobes are significantly different in the APH(3')-IIIa and ePK structures (magenta).

1.3.2 Apo and Nucleotide-bound Structures of APH(3')-IIIa

Three crystal structures of APH(3')-IIIa have been solved: the apoenzyme, the ADP-bound and the AMPPNP-bound complexes (Hon *et al.*, 1997; Burk *et al.*, 2001). These three structures are remarkably similar (Figure 1–5). The rmsd value between all main chain atoms of the two nucleotide-bound structures is 0.3 Å and that between the apoenzyme structure and the nucleotide-bound complexes is 1.5 Å. The majority of the positional variability is localized to four regions: residues 22–29, residues 100–112, residues 147–170, and residues 226–238. Residues 100–112 and 226–238 are located in surface loop regions where

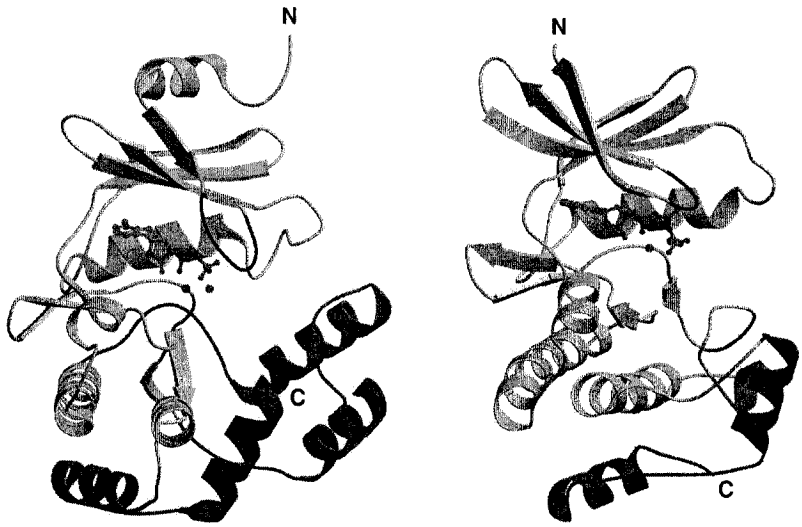

Figure 1–4. A comparison of the structures of APH(3')-IIIa (left) and cAPK (right) highlighting, in colour, the areas with significant differences. These areas include: 1. the loop between strands β1 and β2 (red), 2. the linker region between the N- and C-terminal domains (yellow), 3. a 60-residue insert in APH(3')-IIIa (blue), 4. a smaller insertion found in ePKs (orange) and 5. the last two α-helices of the C-terminal domain (magenta). The ATP cofactor and its associated magnesium ions are depicted as green balls-and-sticks. *Reproduced with permission from Springer Science and Business Media.*

flexibility is not unexpected. The segment comprised of residues 147–170 has a different conformation in all three structures, but more significantly between the apoenzyme and nucleotide-bound complexes. However, this difference in conformation is unlikely associated with the absence or presence of nucleotide but is ascribed to the different crystal contacts between the apoenzyme and nucleotide-bound enzyme in this region. The nucleotide-bound complexes were crystallized with two molecules per asymmetric unit, linked by a disulfide bridge; whereas the apoenzyme is crystallized with one molecule in the asymmetric unit and the disulfide bond is made between adjacent asymmetric units. Lastly, the only positional deviation that appears to be a direct result of the binding

of nucleotide resides in the region encompassing residues 22–29. This flexible segment forms a cover for the phosphate groups of the nucleotide and is analogous to the phosphate-positioning motif with the signature sequence GXGXXG in the catalytic cores of ePKs. However, in the apoenzyme structure, the polypeptide backbone of this region shifts down to occupy the phosphates-binding space (Burk *et al.*, 2001). The flexibility of this region of the active site in APH(3')-IIIa may facilitate the binding and release of the nucleotide that occur over the course of the reaction cycle. Kinetic evidence from site-directed mutants suggested that this loop, in particular Met26 and Ser27, may also play a role in stabilizing the transition state during phosphoryl transfer (Thompson *et al.*, 2002).

In contrast to many protein kinases that undergo a substantial conformation change from the open to closed state upon binding of the nucleotide (Taylor *et al.*, 2004), the structural differences between apo and nucleotide-bound APH(3')-IIIa are minor and localized. The rigidity of APH(3')-IIIa can be attributed to the more extensive network of interactions in the domain hinge region located on the opposite side of the nucleotide-binding pocket (Burk *et al.*, 2001). The domain hinge has been proposed to act as the pivot about which the two lobes in ePK move and the higher number of interactions between the two lobes in APH(3')-IIIa would make interdomain movement energetically unfavorable. The lack of interdomain movement required for phosphoryl transfer, and thus aminoglycoside inactivation, in APH(3')-IIIa is probably advantageous

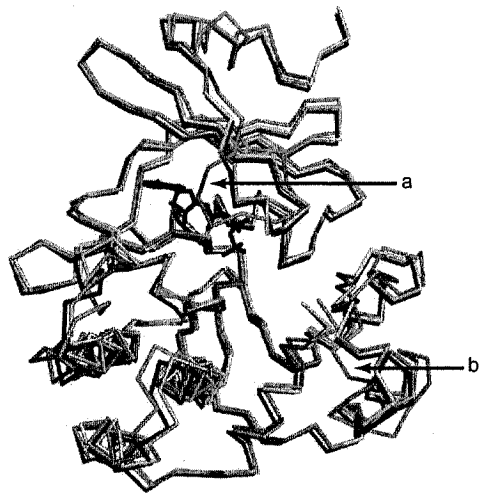

Figure 1–5. Superposition of the α-carbon trace of the APH(3')-IIIa–ADP (yellow), APH(3')-IIIa–AMPPNP (blue), and APH(3')-IIIa apoenzyme (grey) structures. The AMPPNP molecule is drawn in dark blue to highlight the nucleotide-binding pocket. Two areas of significant positional deviation are indicated: (a) the loop over the nucleotide-binding pocket (residues 22–29) and (b) the proposed antibiotic-binding loop (residues 147–170).

to cell survival. ePKs are involved in important cell functions and signal transduction. The conformation change observed in protein kinases plausibly confer supplementary substrate specificity, thereby tightly controlling various cellular processes. Contrarily, pathogenic bacteria would benefit from having an enzyme that is less restrained in substrate specificity and is always primed to inactivate aminoglycoside molecules (Burk *et al.*, 2001).

1.3.3 ATP-binding Site

The binding site for ATP and its associated magnesium ions in APH(3')-IIIa is located in a deep cleft between the N- and C-terminal lobes. The only notable difference between the ADP- and AMPPNP-bound complexes is a change in the

coordination of the metal ions to accommodate the γ-phosphate of AMPPNP (Figure 1–6). Only three residues are absolutely conserved in both eukaryotic protein kinases and aminoglycoside phosphotransferases — Asp190, Asn195 and Asp208. These residues plus two additional highly conserved residues — Lys44 and Glu60, are all located in the ATP-binding pocket. The positions of these residues, as well as those of the two magnesium ions, are essentially the same in the two structures. These conserved residues, along with the magnesium ions, form a network of interactions that stabilizes the phosphate groups of the nucleotide.

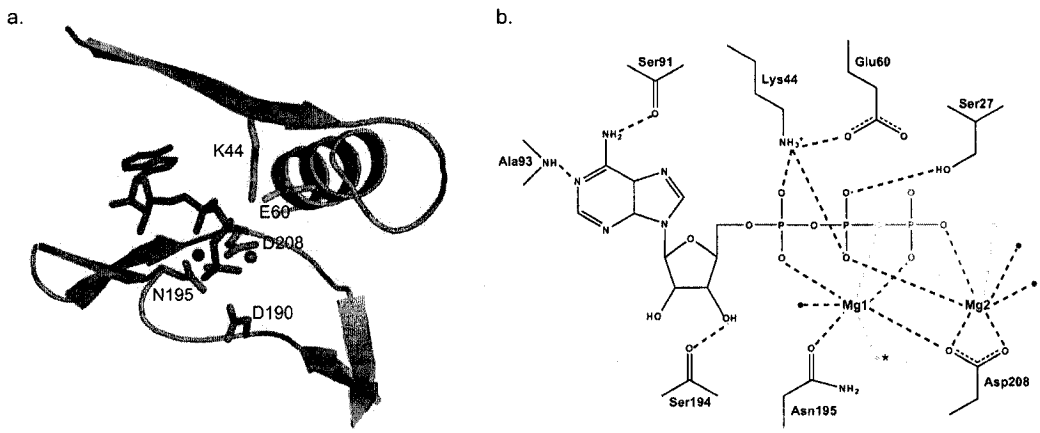

Figure 1–6. *a.* The nucleotide-binding pocket of APH(3')-IIIa. The backbone is shown in grey and the AMPPNP and the magnesium ions are in light blue. Residues that are absolutely conserved and conserved between APH(3')-IIIa and ePK are depicted as sticks and coloured in orange and light orange, respectively. *b.* Schematic representation of the hydrogen bonding network between the ADP or ATP and APH(3')-IIIa. Interactions observed in both APH(3')-IIIa–ADP and APH(3')-IIIa–AMPPNP complexes are represented in black, while those unique to ADP are shown in yellow and those unique to ATP are shown in light blue. The asterisk denotes a water molecule that is not observed in the AMPPNP complex. Note that the ATP depicted in the figure has an oxygen atom bridging the β- and γ-phosphate atoms, whereas the nucleotide in the APH(3')-IIIa–AMPPNP complex has an NH group.

In protein kinases, the residue corresponding to Asp190 has been proposed as a general base assisting in substrate deprotonation (Madhusudan *et al.*, 1994). Although mutagenesis of Asp190 in APH(3')-IIIa results in drastically lower activity — supporting a role for this residue in catalysis, its specific role in catalysis has not been definitively identified (Hon *et al.*, 1997; Zhou and Adams, 1997). Asp190 is positioned at the tip of the phosphate-binding area of APH(3')-IIIa and does not make any direct interactions with the nucleotide or the metal ions. The function of Asp190 may be limited to positioning the reactive hydroxyl group of the substrate during phosphoryl transfer (Boehr *et al.*, 2001b).

Mutagenesis studies of Asn195 indicated that this residue was important for ATP binding (Boehr *et al.*, 2001b). Since Asn195 interacts with ATP *via* a magnesium ion, it has been suggested that the decrease in ATP affinity is the result of a non-optimally coordinated metal ion. Asp208 is a ligand of both active site metal ions, and an Asp208Ala mutation results in a protein without detectable aminoglycoside phosphotransferase activity (Boehr *et al.*, 2001b). Thus, Asp208 appears to be critical for catalysis in APH(3')-IIIa, facilitating the generation or stabilization of the transition state.

Lys44 is positioned over the binding site, interacting with the α- and β-phosphates of the cofactor. Evidence from mutagenesis studies suggests that Lys44 influences the K_m for ATP and thus makes an important contribution to ATP binding (Hon *et al.*, 1997). The analogous lysine residue in the protein kinase family is also positioned to interact with the α- and β-phosphates of ATP. Glu60 is positioned in such a way that it hydrogen bonds to the side chain of

Lys44, orienting it so that it interacts with the α- and β-phosphates of ATP. However, mutagenesis studies show that Glu60 does not have any direct effects on substrate affinity or catalysis (Boehr *et al.*, 2001b).

1.3.4 Aminoglycoside-binding Site

In order to fully understand the catalytic mechanism of APH(3')-IIIa, information regarding the recognition and the conformation of enzyme-bound aminoglycoside substrates must be obtained. It is particularly intriguing in this case due to the number of substrates that can be modified and the non-distinct regiospecificity of APH(3')-IIIa.

Many studies have been carried out in an effort to resolve the gap in our knowledge regarding the binding properties of aminoglycosides to APH(3')-IIIa. First, McKay *et al.* (1996) showed that electrostatic interactions play a key role in aminoglycoside recognition by APH(3')-IIIa. Aminoglycosides are inherently positively charged at physiological pH due to the presence of multiple amino groups (Shaw *et al.*, 1993). Using aminoglycoside derivatives lacking specific amino functional groups in steady-state kinetic analyses, it was shown that the protonated amine at position 1 of the 2-deoxystreptamine ring and a heteroatom (either amino or hydroxyl group) at positions 2' and 6' were important for aminoglycoside binding. These results corroborated the hypothesis, based on the crystal strucutre of ADP-bound APH(3')-IIIa, that the anionic groove adjacent to the phosphate groups is the location of the aminoglycoside-binding site (Burk *et al.*, 2001; Hon *et al.*, 1997).

Subsequently, mutagenesis studies were carried out in order to delineate the key residues involved in aminoglycoside binding (Thompson *et al.*, 1999). These experiments showed that the C-terminal amino acid sequence, which is highly conserved among APH(3') enzymes, imparts the bulk of substrate specificity. Specifically, analysis of the deletion mutant ΔPhe264 indicated that the carboxylate of the terminal residue Phe264 is crucial for the proper binding and efficient phosphorylation of the aminoglycosides, especially those substrates that are 4,6-disubstituted. This mutant is impaired in its ability to phosphorylate the 3'-hydroxyl group of the substrates, and is thus unable to diphosphorylate, 4,5-disubstituted aminoglycosides. Asp261 is absolutely conserved among APH(3') enzymes. Mutation of this residue to alanine interferes with the binding of aminoglycosides that are substituted at the N1 position, such as amikacin and butirosin. In addition, the Asp261Ala mutant has diminished capability to phosphorylate aminoglycosides. The effects of this mutation on catalysis are more pronounced for 4,5-disubstituted aminoglycosides. Glu262 is also completely conserved among APH(3')s. The Glu262Ala mutant shows that Glu262 exerts only minor effects on aminoglycoside phosphorylation but appears to be involved in the binding of aminoglycosides such as kanamycin, ribostamycin, and neamine. This residue has also been suggested to direct the 5"-phosphorylation of 4,5-disubstituted aminoglycosides.

Prior to the availability of structural information, speculations were made regarding the conformation of APH(3')-IIIa-bound aminoglycoside substrates

based on the observed enzymatic modification pattern of antibiotics. For example, it is assumed that in the active site of APH(3')-IIIa, the prime and double prime rings of 4,5-disubstituted aminoglycosides are in proximity to each other since a hydoxyl group on each of the two rings can be phosphorylated by the enzyme (Serpersu *et al.*, 2000).

The conformations of several APH(3')-IIIa-bound aminoglycosides have been determined by NMR spectroscopy (Cox *et al.*, 1996; Cox and Serpersu, 1997; Mohler *et al.*, 1997; Cox *et al.*, 2000; Serpersu *et al.*, 2000). These studies suggest that different aminoglycosides may assume markedly different conformations. It was observed that amikacin, a 4,6-disubstituted aminoglycoside, seem to adopt an extended conformation in the active site of APH(3')-IIIa. Such an arrangement would place the reactive 3'-hydroxyl approximately 4 Å from the γ-phosphate of ATP (Cox *et al.*, 1996; Cox and Serpersu, 1997). Although, isepamicin, another 4,6-disubstituted aminoglycoside, is also in an extended conformation, at least two major orientations of the double prime ring can be observed (Cox *et al.*, 2000).

In contrast to amikacin and isepamicin, butirosin A, a 4,5-disubstituted substrate, does not appear to adopt an extended conformation. The prime and double prime rings of butirosin A are in a stacking arrangement such that both 3'- and 5"-hydroxyl groups would be proximal to the γ-phosphate of ATP (Cox *et al.*, 1996; Cox and Serpersu, 1997). While only one conformation was observed in enzyme-bound butirosin A, other 4,5-disubstituted aminoglycosides examined (ribostamycin and lividomycin A) were found to adopt two conformations in the

active site. The stacking arrangement seen in butirosin was also observed in ribostamycin (Cox *et al.*, 2000). Alternatively, the prime and double prime rings of ribostamycin, as well as a small fraction of APH(3')-IIIa-bound lividomycin A, can be orthogonal to each other (Mohler *et al.*, 1997; Cox *et al.*, 2000). In the major observed conformer of lividomycin A, the prime and double prime rings appear to adopt a conformation that is intermediary between stacking and being orthogonal to each other.

These results suggest that APH(3')-IIIa can plausibly place the 3'- and 5"-hydroxyl groups of 4,5-disubstituted aminoglycosides in the proper position for catalysis *via* minor shifts in the positions of the 2-deoxystreptamine and prime rings. Hence, it can be inferred that these rings provide the principal interactions with the enzyme required for the functional alignment of the hydroxyl groups (Serpersu *et al.*, 2000). Moreover, the 2-deoxystreptamine and prime rings of isepamicin and ribostamycin superimpose well with those of RNA-bound gentamycin C_{1a} and paromomycin, respectively, suggesting that these two rings make crucial contacts with the RNA (Cox *et al.*, 2000). Docking experiments have been performed with kanamycin, ribostamycin, and butirosin (Thompson *et al.*, 1999). These results confirmed that aminoglycoside substrate could take on dramatically different conformations in the active site of APH(3')-IIIa and the conformations produced are in agreement with those obtained from NMR studies.

1.4 Circumvention of Aminoglycoside Inhibition by 3'-Aminoglycoside *O*-Phosphotransferase

Two main principles are followed in the search for ways to circumvent the inactivation of aminoglycosides by modifying enzymes. The first involves abolishing the resistance mechanism such that antibacterial activity can be restored. The second approach requires the development of new antibiotic compounds that are effective inhibitors of bacterial protein translation and can also evade resistance mechanisms. Most of these studies have been done with the phosphotransferase class of AMEs due to the amount of information available. Many compounds were developed based on the binding properties of the aminoglycosides, as well as on the kinetic mechanism of the AMEs. Structural information has added much insight in the development of aminoglycoside derivatives and inhibitors targeted at the cofactor-binding site or the whole binding cleft of AMEs.

1.4.1 Targeting the Aminoglycosides and Their Binding Pocket

Most studies of possible strategies to circumvent the effects of resistance factors have focussed on aminoglycoside binding. The advantage of such an approach is that since the compound would necessarily mimic features of an aminoglycoside, it could be a universal inhibitor for all three classes of AMEs.

Removing the Target Functional Group. There have been some successes in modifying existing aminoglycoside antibiotics to generate new compounds that bind, but are not inactivated by, resistance enzymes. For example, tobramycin (3'-deoxykanamycin B) (Umezawa *et al.*, 1971b) and dibekacin (3',4'-dideoxykanamycin B) (Umezawa *et al.*, 1971a), both lacking the 3'-hydroxyl, are

competitive inhibitors for APH(3')s (McKay and Wright, 1995) (Figure 1–7). Both molecules evade modification by the APH(3') enzymes. However, they can be deactivated by other classes of AMEs.

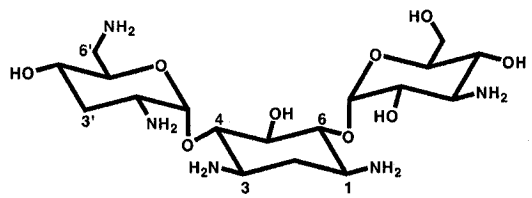

Tobramycin
(3'-deoxykanamycin B)

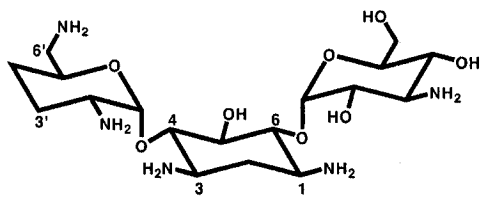

dibekacin
(3',4'-dideoxykanamycin B)

Figure 1–7. Structures of the aminoglycosides tobramycin (top) and dibekacin (bottom). Both molecules lack a 3'-hydroxyl group, making them resistant to modification by APH(3')-IIIa. *Reproduced with permission from Springer Science and Business Media.*

Reducing the Binding Affinity. Another approach involves modifying the antibiotic in such a way that it can no longer bind to the AMEs. This strategy is based on the observation that the naturally occurring butirosins, which possess a 4-amino-2-hydroxybutyrate (AHB) on the amine at the 1-position of the 2-deoxystreptamine ring, are resistant to many inactivating enzymes yet retain their bactericidal properties (Tsukiura *et al.*, 1973) (Figure 1–8). It is thought that the AHB and other side chains at the 1-amino position hinder

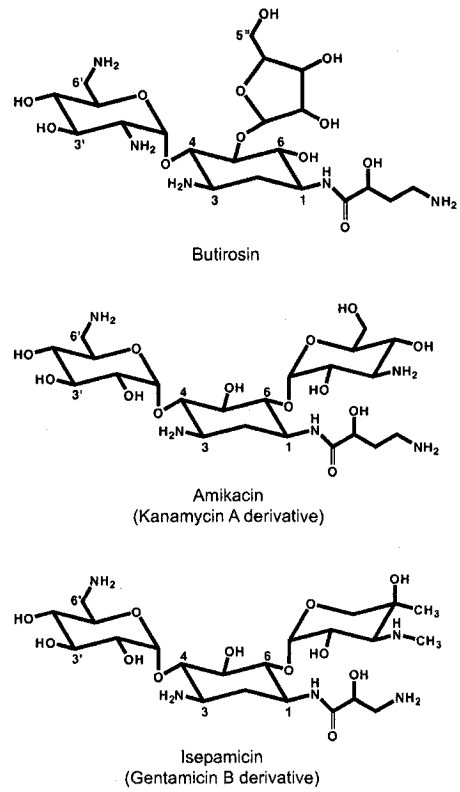

Figure 1–8. Three aminoglycosides with substitutions at the 1-amino group of the central 2-deoxystreptamine ring. Butirosin is naturally-occurring, while amikacin and isepamicin are semisynthetic aminoglycosides. The 1-amino substitutions are believed to hinder binding to aminoglycoside-modifying enzymes, making these compounds resistant to inactivation. *Reproduced with permission from Springer Science and Business Media.*

binding to the AME (Kondo and Hotta, 1999). This observation led to the development of second generation semisynthetic aminoglycoside antibiotics such as amikacin (Figure 1–8) and arbekacin (kanamycin A and dibekacin derivated at the N1 by an AHB group, respectively) (Kondo *et al.*, 1973a,b; Holm *et al.*, 1983; Kawaguchi *et al.*, 1972), isepamicin (gentamicin B substituted with a 4-amino-2-hydroxypropionyl at N1) (Figure 1–8) (Nagabhushan *et al.*, 1978), as well as netilmicin (sisomicin with ethyl group introduced at N1) (Wright,

1976). These compounds have been shown to be clinically useful, especially arbekacin, which is effective against MRSA infections (Kondo and Hotta, 1999) and whose antibiotic activity is unaffected by 2'- and 3"-acetylation (Hotta *et al.*, 1996, 1998). Unfortunately, some level of resistance has been noted, chiefly as a consequence of inactivation by the bifunctional enzyme AAC(6')-Ie–APH(2")-Ia (Kondo *et al.*, 1993b; Fujimura *et al.*, 1998, 2000). Subsequently, two derivatives of arbekacin, 2"-amino-2"-deoxyarbekacin and 2"-amino-5,2"-dideoxy-5-epiaminoarbekacin (Kondo *et al.*, 1993a, 1994), have been developed and shown to be active *in vivo*, yet less toxic to mammals than their parent compound (Inouye *et al.*, 1996).

Another scheme for diminishing the binding affinity of aminoglycosides for APHs is by minimizing the electrostatic interactions between the aminoglycoside and the resistance enzyme. This is achieved through the deletion of amino or hydroxyl groups at important positions on neamine and kanamycin B (Roestamadji *et al.*, 1995a; McKay *et al.*, 1996). These modified drugs retain their antibacterial activity but have a significantly reduced rate of phosphorylation and affinity for APH(3')-Ia and APH(3')-IIa, probably due to the removal of specific ionic and hydrogen bond interactions between the substrate and the enzyme. However, the affinity of these analogues for APH(3')-IIIa is only moderately affected.

Neamine Derivatives. Neamine is a poor antibiotic and is not clinically useful. However, it serves as an invaluable template for the design of new antibiotics. It has been shown that neamine is the minimal structural motif required for binding to the A-site of 16S subunit of rRNA (Fourmy *et al.*, 1996, 1998).

Hence, it is sensible, in designing new aminoglycosides, to preserve the minimum structural motif required for RNA binding and antibiotic activity, but to deviate from typical aminoglycoside structures, in order to elude the various modifying enzymes.

Previous studies showed that the antibiotic activity can be retained when ring IV of neomycin B is substituted with a diaminoalkane group, even though the analogue binds to RNA with diminished specificity (Alper *et al.*, 1998). Subsequently, Greenberg *et al.* (1999) synthesized derivatives of neamine by appending various poly amino, amino alcohol, or aromatic substitutions at the O5-position. The results showed that the compounds substituted with a diaminoalkyl group enhanced the binding to RNA while exhibiting antibiotic activity equivalent to neamine.

More recently, several neamine derivatives were synthesized based on the interactions observed in the NMR solution structure of paromomycin bound to an A-site rRNA template, as well as extensive searches in the Cambridge Structural Database and the National Cancer Institute 3-D Database (Haddad *et al.*, 2002). These compounds are composed of a neamine core, with an AHB group or its analogue at the N1-position of the 2-deoxystreptamine (as in butirosin and amikacin), plus a diaminoalkane group of various lengths at the O6-position (Figure 1–9a). An AHB group was selected as a substituent, since aminoglycosides such as butirosin and amikacin, which possess this structure at N1, have reduced affinity for AMEs (see section 1.4.1). The terminal amine-containing aliphatic component was added in order to improve the interaction between the

O6 and the phosphate backbone of the target rRNA. Many of the designed compounds were shown to be capable of binding to a fragment modelling the A-site of the *E. coli* rRNA, and demonstrated broad spectrum antibiotic activity that is much higher than their parent compound or equal to that of other commonly used aminoglycosides. Some of these designed antibiotics were shown to be poor substrates of APH(3')-Ia and AAC(6')-Ie–APH(2")-Ia, the bifunctional enzyme. The crystal structure of the A-site rRNA template in complex with a designer neamine derivative of high antibiotic activity has recently been reported (Russell *et al.*, 2003). The structure showed that the binding mode of the designer compound is essentially identical to that of paromomycin (Carter *et al.*, 2000). Comparison of neamine derivatives to the kanamycin A bound to APH(3')-IIIa (Fong and Berghuis, 2002, Chapter 3) also explains the basis of the designer molecules' ability to elude inactivation by AMEs. The AHB moiety at the N1-position forms steric clashes with the antibiotic-binding loop of APH(3')-IIIa, impeding the formation of an active ternary complex (Russell *et al.*, 2003).

It has been shown that neamine binds to the A-site model of prokaryotic rRNA in a 2:1 ratio (Sucheck *et al.*, 2000). A series of neamine dimers were constructed in order to identify bivalent aminoglycosides that would interact with the model target site of aminoglycosides in bacteria, and at the same time resist modification by AMEs due to their unusual structure. Two neamine molecules are joined by either amides or 1,2-hydroxyamine with methylene bridges of variable lengths (Figure 1–9b,c). These compounds were found to possess antibiotic activity that is comparable or even superior to that of neamine. They are

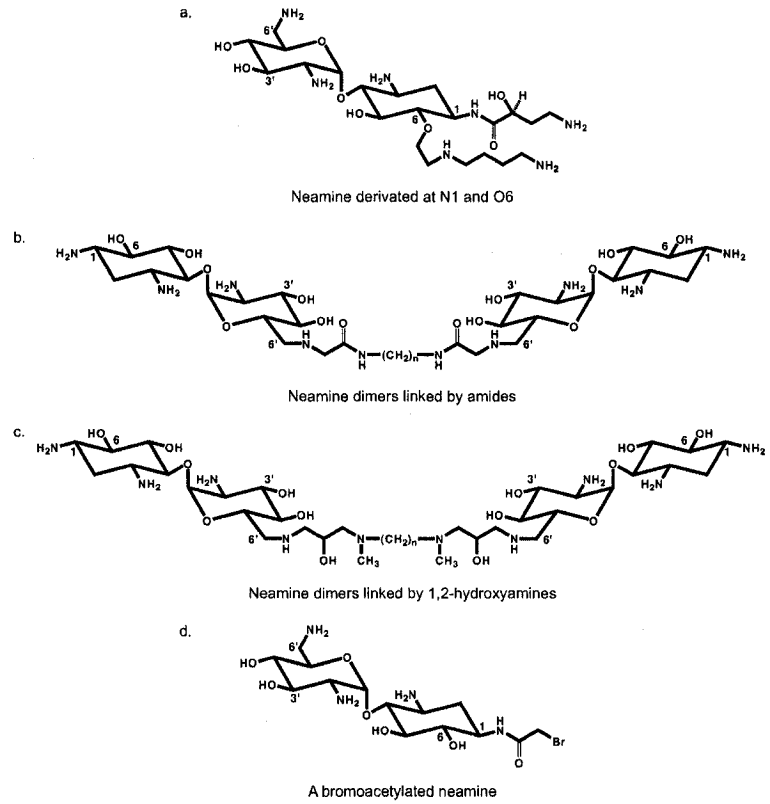

Figure 1–9. Four synthetic aminoglycosides based on the structure of neamine, the minimal structure required for binding to the bacterial ribosome. **a.** A neamine derivative with AHB and diaminoalkane substitutions at the N1 and O6 positions, respectively. **b.** Amine-linked neamine dimers. **c.** 1,2-hydroxyamine-linked neamine dimers. d. A bromoacetylated neamine. *Reproduced with permission from Springer Science and Business Media.*

also potent competitive inhibitors of APH(2") activity of the bifunctional enzyme AAC(6')-Ie–APH(2")-Ia and are poor substrates for APH(3')-IIIa and the AAC(6')-Ie activity of the bifunctional enzyme.

Four derivatives of neamine have also been synthesized by regiospecifically appending a bromoacetyl group to the various amines of the antibiotic (Roestamadji and Mobashery, 1998) (Figure 1–9d). The affinity of the bromoacetylated

compounds for APH(3')-IIa is significantly reduced. In the presence of ATP, the phosphorylation reaction would proceed but at an attenuated rate, whereas in the absence of ATP, the bromoacetylated neamines would inactivate APH(3')-IIa in a time-dependent and saturable manner. Moreover, the activity of the enzyme could not be recovered despite an attempt to remove the modified neamine molecules by extensive dialysis. This observation suggests that the electrophilic bromoacetyl group could form covalent bonds with different nucleophilic residues in the active site. As a result, the modified neamine becomes irreversibly bound to the enzyme and prevents it from binding and inactivating aminoglycosides.

Mechanism-Based Inhibition. The first mechanism-based inhibitors of APH(3')s were described by Roestamadji *et al.* (1995b). The compounds are derivatives of neamine and kanamycin B, in which a nitro (NO_2) group replaces the amine at the 2'-position (Figure 1–10a). These molecules are excellent substrates for APH(3')s but poor antibiotics. Upon phosphorylation by APH(3') enzymes at the 3'-hydroxyl, the phosphoryl group, being an excellent leaving group, is rapidly eliminated, generating an electrophilic nitroalkene. The reactive electrophilic intermediate can in turn capture an active site nucleophilic amino acid side chain and form a covalent bond, irreversibly inactivating the enzymes. They are so-called "suicide" substrates.

A more recent derivative is 3'-oxo-kanamycin A, a self-regenerating aminoglycoside, in which the hydroxyl group at the 3'-position is replaced by a ketone (Haddad *et al.*, 1999) (Figure 1–10b). The hydrated variant of this compound is a good substrate for APH(3') enzymes. However, the phosphorylated product is

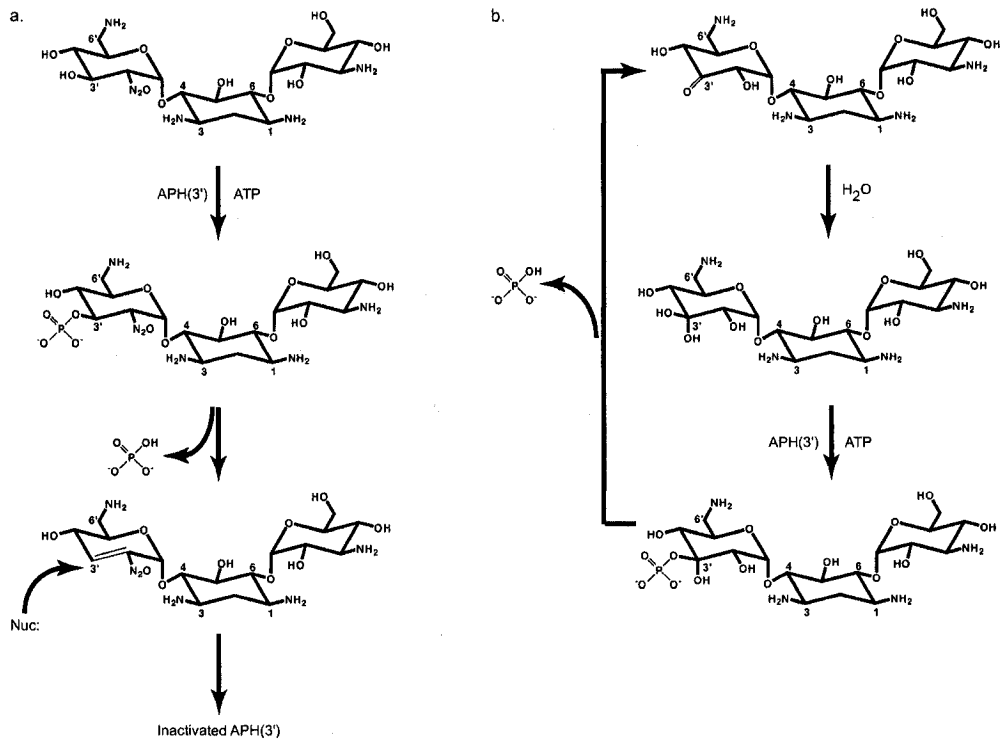

Figure 1–10. Mechanism-based inhibition. **a.** Proposed mechanism of aminoglycoside phosphotransferase inhibition by 2'-nitro aminoglycoside derivatives. Spontaneous loss of phosphate from a phospho-aminoglycoside yields an electrophilic nitroalkene. Trapping of a nucleophilic active site residue (Nuc:) produces an inactivated enzyme. **b.** Reaction cycle of 3'-oxo-kanamycin. Although a good substrate for APH(3') phosphotransferases, the phosphorylated product is unstable and is spontaneously dephosphorylated to regenerate the original compound. *Reproduced with permission from Springer Science and Business Media.*

unstable and releases the inorganic phosphate in a spontaneous non-enzymatic way, regenerating the parent compound. The derivative antibiotic is therefore not inactivated, making the resistance enzymes ineffective. The *in vivo* capabilities of this derivative have also been examined in *E. coli* strains that harbor a plasmid containing the *aph(3')-Ia* gene. It was shown that these strains are sensitive to the 3'-oxo-kanamycin A derivative.

1.4.2 Targeting the Nucleotide-Binding Pocket

Studies on aminoglycoside phosphotransferase inhibitors that target the nucleotide-binding site were prompted by the determination of the three-dimensional structure of APH(3')-IIIa. As discussed above, the overall structure of APH(3')-IIIa is remarkably similar to that of eukaryotic protein kinases, especially in the ATP-binding domain (see section 1.3). This finding led to a survey of the effectiveness of a wide range of ePK inhibitors such as the indole carbazoles, the flavonoids, and the isoquinolinesulfonamides (which are all competitive inhibitors of ATP) against aminoglycoside phosphotransferases (Daigle *et al.*, 1997). The basis of this study was that molecules that target the nucleotide-binding site would prevent the binding of ATP and thus disrupt the enzyme function. One limitation of this approach of inhibitor design is that, at best, only the phosphotransferase class of AMEs would be inhibited. Of the three classes of ePK inhibitors tested, the isoquinolinesulfonamides (Figure 1–11a) have been found to be good competitive inhibitors of ATP for both APH(3')-IIIa and the bifunctional enzyme, AAC(6')-Ie–APH(2")-Ia. Structural studies reveal that these inhibitors bind to the active site of protein kinases by forming a hydrogen bond between the nitrogen of the isoquinoline and the main chain amide hydrogen of the linker peptide that joins the N- and the C-terminal domains (Engh *et al.*, 1996; Xu *et al.*, 1996). An analogous hydrogen bond is also observed between the N1 of the purine ring in ADP or AMPPNP and the linker of APH(3')-IIIa. Therefore, it is inferred that isoquionolinesulfonamides would bind to APH(3')-IIIa in a similar fashion and thus inhibit the function

of APH(3')-IIIa. Unfortunately, these compounds are only able to inhibit the resistance enzymes *in vitro* and cannot reverse antibiotic resistance in enterococcal strains that harbour either the *aph(3')-IIIa* or *aac(6')-Ie-aph(2")-Ia* gene (Daigle *et al.*, 1997).

Protein kinases play key roles in virtually every activity and signalling pathway involved in the development and maintenance of eukaryotic cells. Therefore, care must be taken in the design of inhibitors directed at the nucleotide-binding pocket of aminoglycoside phosphotransferases to avoid cross-reactivity. Structural information about the proteins becomes particularly valuable in this respect. By examining the structures of APHs and ePKs, it is possible to identify distinguishing features that might be utilized in the development of compounds that would selectively inhibit APHs without affecting host protein kinases (Boehr *et al.*, 2002). For example, the crystal structure of APH(3')-IIIa showed that Tyr42 was located near the nucleotide-binding site and that its aromatic ring side chain participates in stacking interactions with the adenine moiety of ATP. This residue is highly conserved as either a tyrosine or phenylalanine among many APH enzymes, but it is predominantly an alanine in protein kinases (Burk *et al.*, 2001). The orientation of the adenine ring in protein kinases and APH(3')-IIIa also differs by a rotation of about 40° due to the difference in electrostatic interactions in the nucleotide-binding site (Burk *et al.*, 2001; Burk and Berghuis, 2002). It is possible that such a difference could be exploited to produce an inhibitor specific to APHs, eluding the problem of protein kinase inhibition by APH inhibitors.

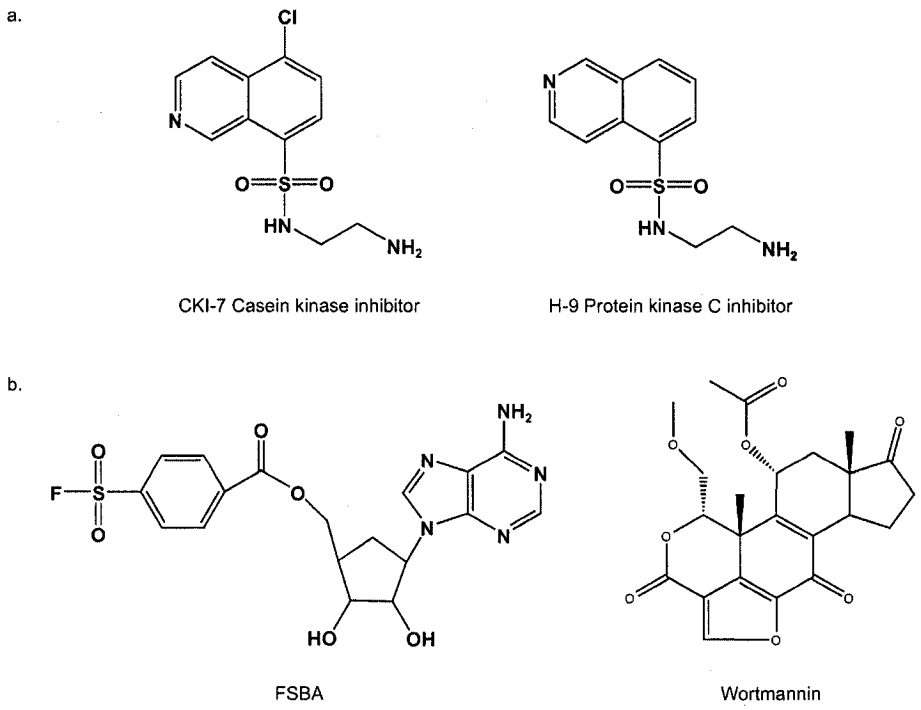

Figure 1–11. Examples of eukaryotic protein kinase inhibitors that target the nucleotide-binding site. **a.** Structures of two isoquinolinesulfonamide compounds. **b.** Structures of FSBA (left) and wortmannin (right). *Reproduced with permission from Springer Science and Business Media.*

Another complication to overcome in the development of broad spectrum antibiotics that target the nucleotide-binding site are the differences in the active sites among the various APHs. As described earlier in this section, APH(3')-IIIa and AAC(6')-Ie–APH(2")-Ia display definite selectivity towards one specific class of protein kinase inhibitor, implying that the nucleotide-binding sites have critical differences (Boehr *et al.*, 2001a). This issue was further illustrated by Boehr *et al.* (2001a) using 5'-[p-(fluorosulfonyl)benzoyl]adenosine (FSBA) and

wortmannin (Figure 1–11b). Previous experiments showed that FSBA, a hydrophilic ATP analogue, inactivates APH(3')-IIIa by covalently linking to invariant Lys44 in the nucleotide-binding site (McKay *et al.*, 1994b). However, FSBA has no effect on the APH(2")-Ia portion of the bifunctional enzyme (Boehr *et al.*, 2001a). Conversely, wortmannin, a potent inhibitor of phosphatidylinositol 3-kinase (Powis *et al.*, 1994), was able to inhibit APH(2")-Ia but not APH(3')-IIIa. Phosphatidylinositol 3-kinase, which shares a similar fold as aminoglycoside and protein kinases (Rao *et al.*, 1998; Walker *et al.*, 2000), can be inhibited by wortmannin by the covalent modification of the lysine residue in the ATP-binding pocket (Wymann *et al.*, 1996; Walker *et al.*, 2000). Wortmannin inactivates APH(2")-Ia in the same manner by covalently binding to Lys52 (homologous to Lys44 in APH(3')-IIIa) (Boehr *et al.*, 2001a).

1.4.3 Exploiting the Bridged Binding Site

The idea of designing inhibitors for resistance enzymes that target the binding sites of both the cofactor and the aminoglycoside is based on the enzyme mechanism of APH(3')s. Whereas APH(3')-Ia functions by a random equilibrium BiBi mechanism (Siregar *et al.*, 1995), APH(3')-IIIa catalyzes its reaction by the Theorell-Chance mechanism — a form of ordered BiBi mechanism (McKay and Wright, 1995). Both mechanisms require that all ligands be present in the active site prior to catalysis. Using this approach, tethered derivatives of adenosine and the aminoglycoside neamine have been synthesized (Liu *et al.*, 2000). These bisubstrate analogues are made by covalently linking the 5'-hydroxyl of adenosine to the 3'-hydroxyl of neamine *via* methylene linkers of various lengths

(Figure 1–12). Appropriate linker lengths that very nearly span the distance between the ATP and the aminoglycoside-binding sites should manifest themselves by showing strong inhibition of the resistance enzyme. When tested against the APH(3')-Ia and APH(3')-IIIa, compounds with linkers of 6–7 carbons in length were found to be the most potent competitive inhibitors of both ATP and kanamycin A.

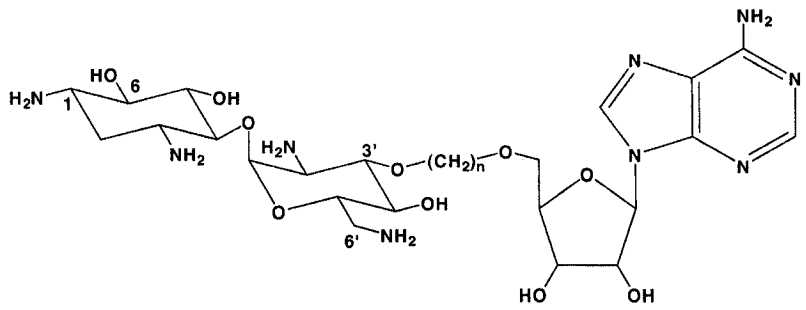

Figure 1–12. A tethered derivative of adenosine and neamine that targets both the nucleotide- and substrate-binding sites of aminoglycoside-modifying enzymes. *Reproduced with permission from Springer Science and Business Media.*

These bisubstrate inhibitors must contain many elements required for binding both regions of the active site of aminoglycoside phosphotransferases. The specificity of the molecule is increased and the problem of cross-reactivity with host protein kinases can be circumvented. Nevertheless, the spectrum of activity of these molecules is reduced, since they are able to bind only those resistance factors that utilize ATP. In addition, the requirement for sufficient specificity in both binding pockets means that compounds that are developed to meet these conditions are likely to be large. Such compounds are unlikely to be effective therapeutic agents, due to issues associated with membrane transport of large molecules (Burk and Berghuis, 2002).

1.4.4 Alternative Strategies for Circumventing Antibiotic Resistances

Peptide Inhibitors. In addition to inspiring the investigation of the inhibition of APHs using ePK inhibitors that target ATP binding, the discovery of the structural similarities between aminoglycoside and protein kinases also led to the examination of the ability of APHs to phosphorylate protein kinase substrates (Daigle *et al.*, 1999b). APH(3')-IIIa and APH(2")-Ia (of the bifunctional enzyme) were shown to be capable of phosphorylating peptide substrates, but at a much slower rate than aminoglycosides. The binding modes of peptide substrates were examined by modelling studies using the structure of APH(3')-IIa. The crystal structure of APH(3')-IIa in complex with kanamycin A is one of the newest addition to the array of structural information on AMEs (Nurizzo *et al.*, 2003). The cAMP kinase inhibitor PKI in the conformation observed in the crystal structure of cAPK (Zheng *et al.*, 1993) was modelled into the active site of APH(3')-IIa (Smith and Baker, 2002). The peptide can be readily accommodated in the binding site of APH(3')-IIa with very few steric hindrances between the inhibitor and the resistance enzyme.

The possibility of using cationic peptides as starting molecules for the development of broad-spectrum inhibitors of resistance enzyme activities was therefore examined (Boehr *et al.*, 2003). Due to the large number of negatively charged residues in the binding pockets of AMEs, positively charged peptides are the preferred ligands. Both APH(3')-IIIa and APH(2")-Ia were inhibited by protegrin, indolicidin and its analogue, CP10A, in a non-competitive manner with both ATP and kanamycin. The inhibition patterns demonstrate that the peptides bind

to both the free enzymes and to enzyme-substrate complexes. Together, these results suggest that the peptide inhibitors have multiple binding modes and may span both the ATP- and aminoglycoside-binding sites. Furthermore, the modelling study of cAMP kinase PKI and APH(3')-IIa corroborated the inhibition kinetics experiments that showed that PKI fully occupied the aminoglycoside-binding site as well as a large portion of the putative ATP-binding site (Smith and Baker, 2002). Although some antimicrobial peptides are able to penetrate into the cytoplasm of bacteria, many are known to act on the cytoplasmic membrane (Wu *et al.*, 1999). Unfortunately, none of the peptides that inhibited resistance enzymes *in vitro* displayed synergistic antimicrobial properties with aminoglycosides in organisms harbouring resistance genes (Boehr *et al.*, 2003).

Ankyrin Repeat Proteins. Recently, designed ankyrin repeat (AR) proteins capable of inhibiting APH(3')-IIIa function both *in vitro* and *in vivo* with high specificity were identified (Amstutz *et al.*, 2005). The AR is one of the most common protein-protein interaction motifs in nature. The core AR module consists of a helix-loop-helix motif and consecutive units are connected by a β-hairpin loop. The AR proteins found in nature are predominantly intracellular enzyme modulators of diverse functions (Forrer *et al.*, 2003; Amstutz *et al.*, 2005).

Several AR protein inhibitors of APH(3')-IIIa were identified from libraries of engineered AR proteins (Forrer *et al.*, 2003). *In vitro* experiments showed that the selected AR protein inhibitors act exclusively on APH(3')-IIIa, not the structurally homologous ePKs and have dissociation constants in the nanomolar

range. Moreover, *in vivo* studies indicated that cells expressing AR proteins manifest a phenotype comparable to an APH gene knockout, completely restoring antibiotic susceptibility in resistant bacteria (Amstutz *et al.*, 2005).

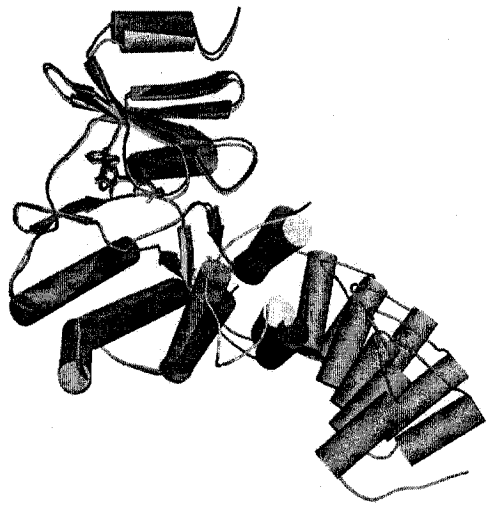

Figure 1–13. Superposition of APH(3')-IIIa–ADP and APH(3')-IIIa–ADP–ankyrin repeat crystal structures (PDB code: 2BKK). The structures are displayed in a cartoon representation in which the α-helices are depicted as cylinders. The ADP-bound APH(3')-IIIa is coloured in light grey and the ADP–AR-bound enzyme is shown in dark grey. The AR protein inhibitor is coloured pink. The parts of the enzyme that underwent significant displacement as a result of AR protein binding, namely α-helices A and B and the C-terminal helix, are highlighted in purple. The equivalent segments in APH(3')-IIIa–ADP are coloured yellow for comparison.

The mode of inhibition of AR protein inhibitors was revealed by X-ray crystallography (Kohl *et al.*, 2005). The structure of APH(3')-IIIa complexed with one of the most potent AR protein inhibitors, AR_3a, showed that the AR inhibitor binds to the C-terminal lobe of APH(3')-IIIa outside the aminoglycoside-binding pocket (Figure 1–13). In contrast to most small molecule kinase inhibitors, the AR protein inhibitors are not confined to binding the enzyme active

site. This attribute enables less conserved regions of the enzyme to be targeted and consequently contributes to increased specificity. While the global architecture of APH(3')-IIIa is maintained, the region in contact with AR_3a, namely α-helices A and B, is significantly distorted, resulting in a considerable displacement in the C-termnal helix. The precise positioning of these helices is crucial to substrate binding and catalysis and the binding of AR_3a traps APH(3')-IIIa in an unproductive active site conformation (Kohl *et al.*, 2005).

1.5 Thesis Objectives

Virtually all antibiotics in use today were discovered by empiric screening based on their ability to inhibit bacterial growth (Chopra *et al.*, 2002). Understanding the mechanisms that confer a resistant phenotype on bacteria at the atomic level will greatly contribute to the development of analogues of existing agents and inhibitors of the resistance enzymes. The objectives of this study is to employ X-ray crystallographic techniques to elucidate the binding mode of different classes of aminoglycosides to APH(3')-IIIa and to identify the binding properties of a prototypal ligand that could be modified to become potent inhibitors for this class of AMEs. The effectiveness and benefits of the co-administration of an antibiotic with an adjuvant can be illustrated by the β-lactam-β-lactamase inhibitor combination. In fact, the amoxicillin-clavulanate combination has been in use for over 20 years and remains to be a highly effective antimicrobial therapy (Paterson, 1999). Therefore the approach of circumventing aminoglycoside resistance by an aminoglycoside-AME inhibitor combination therapy is certainly worth investigating.

CHAPTER 2
Overview of Experimental Procedures

This chapter provides a general overview of the methods used in this study to determine the structures of ligand-bound APH(3')-IIIa. A detailed description of the structure determination procedure pertaining to each complex is presented in subsequent chapters.

2.1 APH(3')-IIIa Production and Purification

2.1.1 Materials

The following solutions were prepared for the production and purification of APH(3')-IIIa.

Luria Broth (LB) :

10 g Tryptone, pancreatic digest of casein (BD, Sparks, MD)

5 g Yeast extract (BD)

10 g NaCl (Sigma-Aldrich, St. Louis, MO)

1 L Deionized distilled water

Sterilized in autoclave at 121 °C for 30 minutes

Lysis Buffer :

50 mM 2-Amino-2(hydroxymethyl)1,3-propanediol (Tris) (Sigma-Aldrich)

5 mM Ethylenediamine tetraacetic acid (EDTA) (Sigma-Aldrich)

200 mM NaCl

0.1 mM Dithiothreitol (DTT) (Sigma-Aldrich)

1 mM Phenylmethylsulfonyl fluoride (PMSF) (Sigma-Aldrich) *or*

1 Protease inhibitor cocktail tablet (Complete Mini; Roche Diagnostics GmbH, Mannheim, Germany) per 1 L of bacterial culture

Adjusted to pH 8.0 with HCl (Fisher Scientific, Nepean, ON) and/or NaOH (BDH Inc., Toronto, ON) as necessary

No Salt Buffer (Buffer A) :

50 mM Tris

1 mM EDTA

Adjusted to pH 8.0 with HCl and/or NaOH as necessary

High Salt Buffer (Buffer B) :

50 mM Tris

1 mM EDTA

1 M NaCl

adjusted to pH 8.0 with HCl and/or NaOH as necessary

Crystallization Buffer :

25 mM Sodium cacodylate (Sigma-Aldrich)

adjusted to pH 7.0 with HCl and/or NaOH as necessary

2.1.2 Procedures

The overexpression and purification schemes of APH(3')-IIIa were based on methods previously established (McKay *et al.*, 1994a). In brief, the gene encoding APH(3')-IIIa was originally cloned and sequenced from a clinical isolate of *Streptococcus faecalis* (Jacob and Hobbs, 1974; Trieu-Cuot and Courvalin, 1983). It was then subcloned into an overexpression vector and the subsequent plasmid, pETSACG1, was used to transform *E. coli* strain BL21 (DE3) (McKay *et al.*, 1994a). A culture of *E. coli* BL21 (DE3) that contains the vector harboring the *aph(3')-IIIa* gene was obtained from Dr. Gerry Wright at McMaster University, Hamilton, ON. The protein produced from this construct lacks the N-terminal methionine residue and hence consists of 263 residues.

25 mL of LB supplemented with 100 μg/mL of ampicillin (BioShop Canada, Burlington, ON) was inoculated with *E. coli* BL21 (DE3) containing the pETSACG1 plasmid and grown overnight in a rotary shaker at 37 °C and 250 rpm. 1 L of LB containing 100 μg/mL of ampicillin was then inoculated with the overnight cell culture and allowed to grow at 37 °C in a rotary shaker at 250 rpm until A_{600} of the culture reached 0.5 (approximately 2–2.5 hours). At this point, the cells were induced with isopropyl β-D-thiogalactopyranoside (IPTG) (Invitrogen, Carlsbad, CA) to a final concentration of 1 mM. The cells were grown for an additional 3 hours and were harvested by centrifugation at 3000 x g for 15 minutes. All centrifugation steps were carried out at 4 °C. The cell pellet was then washed with cold 0.85% (w/v) NaCl solution and centrifuged for 10 minutes at 10000 x g. The cell pellet was resuspended in lysis buffer,

placed on a bed of ice, and lysed by sonication. The removal of cell debris was accomplished by centrifugation at 10000 x g for 20 minutes.

All protein purification was performed at 4 °C using the ÄKTAprime System (Amersham Biosciences Corp., Piscataway, NJ).

Table 2–1. Salt step gradient program for 50 mL Q-Sepharose

Volume (mL)	Buffer B (%)	Fraction Size (mL)
0	0	0
50	0	0
100	15	0
200	15	0
350	30	3.2
550	50	3.2
650	50	3.2
655	100	0
800	100	0
805	0	0
900	0	0

flow rate = 2 mL/min

The supernatant was applied to a column (XK26/20; Amersham Biosciences Corp.) containing 50 mL of Q-Sepharose anion exchange resin (Amersham Biosciences Corp.) equilibrated with buffer A. APH(3')-IIIa was eluted by a 0–100% buffer B step gradient (Table 2–1). Fractions eluted at around 45% buffer B were found to contain APH(3')-IIIa by phosphotransferase activity assay (Section 2.2) or sodium dodecyl sulfate polyacrylamide gel electrophoresis (SDS-PAGE).

Table 2–2. Salt step gradient program for 6 mL Resource Q

Volume (mL)	Buffer B (%)	Fraction Size (mL)
0	0	0
6	0	0
18	20	0
36	20	0
51	25	0.5
96	40	0.5
114	40	0.5
115	100	0
133	100	0
134	0	0
150	0	0

flow rate = 1.5 mL/min

These fractions were pooled and dialysed overnight in buffer A using the Spectra/Por 6 standard regenerated cellulose (RC) dialysis membrane with molecular weight cutoff of 25000 Da (Spectrum Laboratories, Inc., Rancho Dominguez, CA). The protein was quantified by the Bradford assay (Bradford, 1976) using bovine serum albumin (BSA) as the standard (Bio-Rad Laboratories, Inc., Hercules, CA). The sample was subsequently applied to the Resource Q pre-packed anion exchange column (6mL; Amersham Biosciences Corp.) equilibrated with buffer A. The enzyme was recovered by a step gradient to 100% buffer B (Table 2–2). Eluate in approximately 35% buffer B was found to contain APH(3')-IIIa using the activity assay or SDS-PAGE. The enzyme was concentrated using Vivaspin concentrators with polyethersulfone (PES) membranes having a molecular weight cutoff of 10000 Da (Vivascience GmbH, Hannover, Germany). The

concentrated sample was applied to a column (XK16/70; Amersham Biosciences Corp.) filled with 100 mL of Superdex 75 size exclusion media (Amersham Biosciences Corp.) equilibrated with the crystallization buffer. APH(3')-IIIa was confirmed to elute in the largest peak by the presence of phosphotransferase activity and the homogeneity of the preparation was verified using silver-stained SDS-PAGE. The pure enzyme was pooled and concentrated to about 15 mg/mL for storage at 4 °C.

2.2 Phosphotransferase Activity Assay

Phosphorylation of aminoglycoside antibiotics by APH(3')-IIIa was monitored using a coupled enzyme ATPase assay (McKay *et al.*, 1994a). The assay is based on the conversion of phosphoenolpyruvate (PEP) to pyruvate by pyruvate kinase (PK) coupled to the conversion of pyruvate to lactate by lactate dehydrogenase (LDH) (Figure 2–1). Following each cycle of ATP hydrolysis, PK converts one molecule of PEP to pyruvate when ADP is converted back to ATP. Subsequently, pyruvate is converted to lactate by LDH with the concomittant oxidation of β-nicotinamide adenine dinucleotide, reduced form (NADH). NADH absorbs strongly at 340 nm but its oxidized form, NAD^+, does not, thus allowing the rate of NADH oxidation to be monitored by the decrease in absorbace at 340 nm. The decline in OD_{340} can be converted into phosphotransferase activity where 1 molecule of NADH oxidized to NAD^+ corresponds to the production of 1 molecule of ADP by, specifically in this case, APH(3')-IIIa. The change in OD_{340} was monitored using a Cary 50 UV/VIS Spectrophotometer (Varian, Inc., Palo Alto, CA).

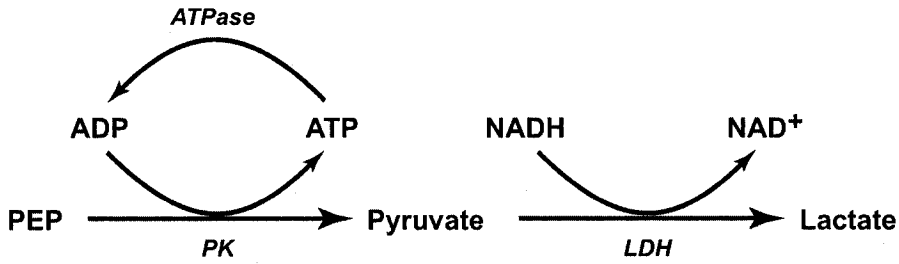

Figure 2–1. Coupled enzyme ATPase assay for the detection of phosphotransferase activity by APH(3')-IIIa. APH(3')-IIIa is the ATPase catalyzing the modification of the aminoglycoside, generating ADP. ATP is then regenerated as pyruvate kinase (PK) converts phosphoenolpyruvate (PEP) to pyruvate. The rate of phosphotransferase activity is mirrored in the decrease in OD_{340} due to the depletion of NADH in the conversion of pyruvate to lactate by lactate dehydrogenase (LDH).

2.2.1 Materials

Assay Buffer :

50 mM Tris pH 7.5

40 mM Potassium chloride (KCl) (BDH Inc.)

10 mM Magnesium chloride ($MgCl_2$) (Sigma-Aldrich)

0.5 mg/mL NADH (Sigma-Aldrich)

2.5 mM Phospho(enol)pyruvate (PEP; 2-[Phosphonooxy]-2-propenoic acid]) (Sigma-Aldrich)

0.1 mM Kanamycin (Sigma-Aldrich)

1 mM ATP (Sigma-Aldrich)

5 μL Pyruvate kinase / Lactate dehydrogenase (PK/LDH) (Sigma-Aldrich) per reaction

20 μL 2–3 mg/mL purified APH(3')-IIIa per reaction

2.2.2 Methods

The assay was performed at 37 °C. 1 mL of assay buffer was required for each reaction. The assay buffer was preincubated at 37 °C for 5 minutes before dispensing 1 mL into each 1.5 mL cuvette. The cuvette was then placed in the spectrophotometer and the machine was zeroed using the assay buffer. OD_{340} was monitored for about 15 seconds before adding the protein sample, or ADP as a positive control or buffer as a negative control. The reaction was monitored for about 2–3 minutes for any changes in the slope.

2.3 Crystallization

The objective of crystallization is to produce a well-ordered protein crystal of sufficient size such that it will produce a diffraction pattern when irradiated by X-rays. This diffraction pattern can then be analyzed to produce a map of the molecule's electron density. The protein sequence can be modelled to fit this density map, thus discerning the protein's three-dimensional structure.

Optimal conditions for crystal nucleation and growth are difficult to predict. Successful crystallization of a protein requires a unique condition influenced by a large number of factors, e.g. protein purity and homogeneity, protein concentration, buffer type, pH, precipitants, salts, and temperature. The variables influencing crystal growth are too large for an exhaustive search to be conducted. Therefore, the sparse matrix sampling method (Jancarik and Kim, 1991) was employed in order to rapidly and efficiently screen wide ranges of pH, salts and precipitants, and their combinations thereof, for their ability to promote crystallization.

2.3.1 Materials

50 mM stock solutions of various ligands of APH(3')-IIIa in crystallization buffer:

- ADP (Sigma-Aldrich)
- AMPPNP (Sigma-Aldrich)
- Kanamycin monosulfate salt (Sigma-Aldrich; catalog # K4000)
- Neomycin trisulfate salt hydrate (Sigma-Aldrich; catalog # N5285)
- Butirosin sulfate salt (Sigma-Aldrich; catalog # B9525)

10 mM stock solution of APH(3')-IIIa inhibitor in dimethyl sulfoxide:

- *N*-(2-aminoethyl)-5-chloro-isoquinoline-8-sulfonamide (CKI-7) (Seikagaku America, MJS BioLynx Inc., Ontario, Canada)

Crystallization materials:

- VDX crystallization plates (Hampton Research, Aliso Viejo, CA)
- Siliconized glass cover slides 12 mm circles (Hampton Research)
- Vacuum grease (Dow Corning, Midland, MI)

Sparse matrix screens:

- Crystal Screens I & II (Hampton Research)
- Wizard I & II (Emerald BioSystems, Bainbridge Island, WA)
- Cryo I & II (Emerald BioSystems)

2.3.2 General Crystallization Techniques Employed

Crystallization Condition Screening. The enzyme concentration was adjusted to 10–15 mg/mL. Prior to crystallization, 3–5 molar excess of various ligands were added to the protein solution which was then filtered using an Ultrafree-MC Centrifugal Filter Device with Durapore (PVDF) membrane of pore size 0.22 μm (Millipore Corporation, Bedford, MA) to remove any particulate matter and/or sample aggregates.

The vapour diffusion method in the hanging drop format was utilized for all crystallization experiments. Briefly, in this technique, a few microliters of the protein sample is mixed with an equal volume of crystallization reagent on a siliconized glass cover slide. The cover slide is then inverted and sealed over a reservoir of the crystallization reagent. The initial reagent concentration in the drop is therefore lower than that in the reservoir. As a result, water vapour diffuses from the droplet to the reservoir until an equilibrium is established. During this process, the concentration of both the protein sample and the crystallization reagent in the drop slowly increases and crystals may start to form.

The initial crystallization conditions for APH(3')-IIIa in the presence of different ligands were determined using several commercially available sparse matrix screening kits from Hampton Research and Emerald Biostructures (288 conditions total). Each VDX plate can sample 24 different conditions. The lip of the reservoirs of the VDX plate was first rimmed with vacuum grease. Next, 700 μL of a crystallization reagent was dispensed into each well. Siliconized cover slides were dusted with canned compressed air. Subsequently, 2 μL each

of the protein sample (ligand added) and the reservoir solution were placed on each cover slide and mixed gently. The cover slide was then inverted over the reservoir solution, gently pressed and turned to ensure a complete seal.

Each crystal trial was performed in duplicate. One was placed at 4 °C and the other at 22 °C in low temperature incubators.

The crystallization experiments were examined after about one week. The experiments would then be re-examined every week for the first month and every 2-4 weeks thereafter for 10-12 months or until the drops and/or the reservoir solution dried up. When crystalline material was observed, the crystallization condition would be refined and optimized.

Crystallization Condition Optimization. Each crystallization reagent in the sparse matrix screens is composed of a buffer, precipitant, and/or salt. During optimization, parameters such as the concentrations of protein, precipitant, and salt, and buffer pH were varied in order to improve crystal quality. Often, this step would suffice to produce crystals suitable for X-ray diffraction analysis. Additional optimization strategies and techniques pertaining to specific APH(3')-IIIa complexes will be described in the relevant chapters.

2.4 Data Collection and Processing

Prior to exposure to X-ray, crystals of APH(3')-IIIa grown in the presence of inhibitor or nucleotides and various substrates were soaked briefly (1–2 minutes) in a suitable cyro-protectant if necessary, and flash frozen in either liquid nitrogen or a stream of cold nitrogen gas. All data collection was performed under cryogenic conditions (110 K). In most cases, data were gathered from a single

crystal at the X8C beamline of the National Synchrotron Light Source (NSLS), Brookhaven National Laboratories (BNL), using an ASDC Quantum charge-coupled device (CCD) detector. The data were collected using the oscillation method, with an oscillation angle of 1.0° and a wavelength of 1.072 Å. In general, 180 frames of data were collected.

The first step of data processing is to determine the crystal parameters and its orientation with respect to the X-ray beam and the detector from a single frame of data. Using the information derived from the single frame, the second step involves integrating diffraction data collected in every image of the data set and reducing them to a file described by reciprocal space coordinates, (h, k, l), and intensity values. These two tasks were carried out by the program Denzo, a part of the HKL suite of programs (Otwinowski and Minor, 1997). The companion program, Scalepack, was utilized for the global refinement of crystal parameters and the ensuing scaling and merging of the integrated data (Otwinowski and Minor, 1997). The intensity measurements are corrected or scaled based on errors associated with the experiment and are subsequently merged. Redundant observations are averaged and the extent of discrepancy among these symmetry-related reflections after scaling is assessed by the R_{sym} value.[1]

[1] $R_{sym}(I) = (\sum_{hkl} \sum_{i} |I_i(hkl) - \overline{I(hkl)}|) \div (\sum_{hkl} \sum_{i} I_i(hkl))$; where $I_i(hkl)$ is the observed intensity and $\overline{I(hkl)}$ is the average intensity of i observations of the equivalent symmetry-related reflection.

2.5 Molecular Replacement

The structures of the APH(3')-IIIa complexes described in this thesis were solved using the molecular replacement method. The molecular replacement technique determines the orientation and position of a molecule in the crystallographic unit cell using knowledge of a previously solved structure of a related protein or the same protein in a different crystal form. The search is made up of two components: the rotational search followed by the translational search. In this case, the ADP-bound enzyme structure was used as the initial search model in solving the APH(3')-IIIa–kanamycin A complex, which in turn was used as the search model for the structure determination of APH(3')-IIIa–butirosin A complex. The search model is first rotated and then translated in the unit cell in order to achieve a maximum overlap between the model and the target molecules. Once a correct orientation and position are found, a preliminary model of the target structure can be obtained and used for model rebuilding and refinement. If the target enzyme complex was crystallized in the same space group and similar cell dimensions as one of the previously determined APH(3')-IIIa structures, such as the neomycin B-, 5"-phosphorylated butirosin A-, or CKI-7-bound APH(3')-IIIa, the rotational and translational searches would be unnecessary since the orientation and position of the protein molecule in the unit cell were already known.

The molecular replacement process was accomplished using algorithms implemented in the Crystallography and NMR System (CNS) (Brünger *et al.*, 1998)

or the Collaborative Computational Project, Number 4 (CCP4)-supported program Automated Package for Molecular Replacement (AMoRe) (Navaza, 1994; Collaborative Computational Project Number 4, 1994).

2.5.1 Rotational Search

The rotation function allows the determination of the orientation of the search molecule such that a maximal overlap with the target molecule can be achieved. This is accomplished by comparing the intramolecular or self vectors of the known and unknown structures at different orientations of the search model. Collectively, the intramolecular vectors are described by the Patterson function[2] and the correlation between the known and unknown structures is monitored by the product of the Patterson functions[3] (Brünger *et al.*, 1998; Grosse-Kunstleve and Adams, 2001; Navaza, 2001). This method is implemented in both AMoRe and CNS (the real-space rotation function). The algorithms differ in the strategy the Patterson functions are calculated (DeLano and Brünger, 1995).

An alternative approach available in the CNS software is the direct rotational function in which the search model itself is rotated prior to the calculation of the Patterson function. Although this method is generally more accurate and may prevail in cases where the real-space Patterson rotation search method fails,

---

[2] $\mathcal{P}(u\,v\,w) = \frac{1}{V} \sum_{hkl} |F(h\,k\,l)|^2\, e^{-2\pi i(hu+kv+lw)}$

[3] $Rot(\Omega) = \int_{\mathcal{U}} \mathcal{P}_{obs}(u)\, \mathcal{P}_{model}(\Omega u)\, du$; where Ω is the 3×3 rotation matrix, $\mathcal{P}_{obs}$ and $\mathcal{P}_{model}$ are the observed and model Patterson functions, respectively, and $\mathcal{U}$ is a location vector in Patterson space $\mathcal{U}$.

it is computationally intensive since a new Patterson function must be computed at each sampled orientation. A more efficient fast direct rotational function, a modified version of the direct algorithm, was used to determine the rotational component. The fast direct rotation function performs an initial coarse grid search followed by finer searches around the top peaks from the initial search. Solutions of the direct rotation function were scored by the linear correlation coefficient (CC) between the observed and calculated normalized structure factors, also known as the Patterson Correlation (PC)[4] (DeLano and Brünger, 1995; Grosse-Kunstleve and Adams, 2001). The top solutions of the CNS rotational search were then subjected to PC refinement, an energy minimization step aiming to improve the accuracy of the overall angular orientation of the search model and thus enhancing the the probability of success with the translation function (Brünger, 1990).

2.5.2 Translational Search

The second step of the molecular replacement procedure is a three-dimesional positional search of the oriented search molecule with reference to the symmetry elements of the target unit cell. The fast translation function implemented in both CNS and AMoRe (Grosse-Kunstleve and Adams, 2001; Navaza and Vernoslova, 1995) was used for the translational search. Essentially, the fast

[4] $\mathcal{CC}(\Omega) = \mathcal{PC} = \frac{\langle |E_{obs}|^2 |E_{model(\Omega)}|^2 - \langle |E_{obs}|^2 \rangle \langle |E_{model(\Omega)}|^2 \rangle \rangle}{[\langle |E_{obs}|^4 - \langle |E_{obs}|^2 \rangle^2 \rangle \langle |E_{model(\Omega)}|^4 - \langle |E_{model(\Omega)}|^2 \rangle^2 \rangle]^{\frac{1}{2}}}$; where Ω is the rotational operator matrix, E_{obs} and $E_{model(\Omega)}$ are the observed and rotated model normalized structure factors, respectively, and $\langle\rangle$ denotes an average computed over all observed reflections.

translational search involves two tasks. First, the overlap of the target Patterson intermolecular or cross vectors is measured against those of the oriented search molecule as it ranges through the target unit cell. The correlation coefficient,[5] defined in terms of the structure factor amplitudes, is calculated for a number of potential peaks with top product translation function values and used as the main criterion for selecting solutions. Lastly, the translational solutions are optimized by rigid body refinement.

2.6 Model Refinement

The purpose of refinement is improve the agreement between the observed and calculated structure factors while maintaining reasonable chemical restraints. This is accomplished by modifying the atomic model such that it best matches the data. Refinement of APH(3')-IIIa structures described in this study was performed using the CNS software (Brünger *et al.*, 1998) and the progress of refinement was monitored by the crystallographic R_{cryst} value,[6] the average fractional disagreement. In addition, the R_{free} value was also used to assess the quality and validity of the model and to detect any over-fitting of data. The R_{free} is calculated in the same manner as the traditional R_{cryst}-factor using a subset of reflections that have been excluded from the modelling and refinement

[5] The target function is defined similarly to the direct rotational function as the linear correlation between the squared regular (unnormalized) structure factor with the rotational operator matrix replaced by a translational vector.

[6] $R_{cryst} = \frac{\Sigma||F_{obs}|-|F_{calc}||}{\Sigma|F_{obs}|}$; where $|F_{obs}|$ and $|F_{calc}|$ are, respectively, the observed and calculated structure factor amplitudes.

process. The R_{free} values for the APH(3')-IIIa structures were based on ten percent of reflections randomly selected from the data sets.

For the various APH(3')-IIIa complexes, a preliminary step of rigid body refinement was carried out if it had not been performed at the conclusion of the translational search algorithm. The ensuing refinement sequence consisted of iterative cycles of conjugate gradient positional minimization and B-factor refinement followed by manual remodelling in the graphic program O (Jones *et al.*, 1991). Initially, B-factors of all side chain atoms and all main chain atoms of each residue were refined collectively as two groups. Then, restrained individual isotropic B-factor refinement was utilized for the remainder of the refinement sequence. The choice was justified by the R_{free} statistic which progressively decreased upon individual B-factor refinement. After at least one cycle of positional and B-factor refinement, σ_A-weighted $2F_o$-F_c and F_o-F_c difference electron density maps (Read, 1986) were calculated and examined in the program O. The entire model was inspected and adjusted to best conform to the difference electron density maps. For regions that required significant rebuilding, simulated annealing model refinement and omit maps were used in addition to the difference electron density maps, as guides for manual remodelling. The manual refitting process can be facilitated by assessing the real space R-values between the observed and calculated density (Jones *et al.*, 1991; Chapman, 1995), using them as a guide to pinpoint regions of significant disagreement. Once a satisfactory model had been achieved, the simulated annealing omit and difference electron density maps in the active site region were examined and the appropriate

ligands, substrates or inhibitors were placed accordingly. When no improvement in the R-factors was observed upon further refinement and manual intervention, solvent molecules were located. Solvent molecules were accepted on the basis of electron density peaks, their surrounding environment, and hydrogen-bonding distances and geometry. The addition of solvent molecules can also be monitored by considering their temperature factors and the overall R_{free} value. The stereochemistry of the model was surveyed using the program PROCHECK (Laskowski *et al.*, 1993). A sample Ramachandran plot (Ramakrishnan and Ramachandran, 1965; Kleywegt and Jones, 1996) is shown in Figure 2–2. Model refinement continues until no further improvement in model statistics can be accomplished. In general, satisfactory crystal structure quality was achieved for all the APH(3')-IIIa complexes described in this thesis. The R_{cryst}- and R_{free}-values range from 0.20 to 0.25 and from 0.26 to 0.32, respectively; the number of solvent is, on average, 50 per molecule of APH(3')-IIIa, and at least 99.6% of residues fall into the allowed regions as defined by the Ramachandran analysis.

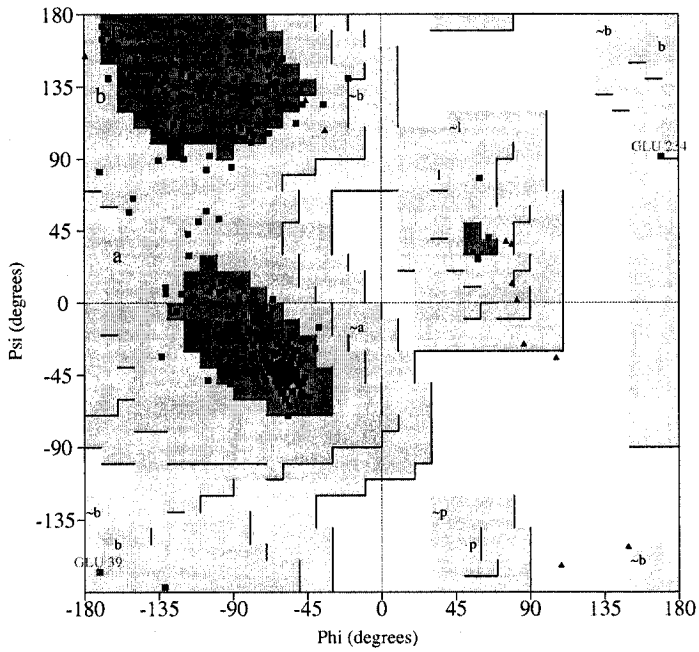

Plot statistics

Residues in most favoured regions [A,B,L]	200	85.5%
Residues in additional allowed regions [a,b,l,p]	32	13.7%
Residues in generously allowed regions [~a,~b,~l,~p]	2	0.9%
Residues in disallowed regions	0	0.0%
Number of non-glycine and non-proline residues	234	100.0%
Number of end-residues (excl. Gly and Pro)	71	
Number of glycine residues (shown as triangles)	14	
Number of proline residues	10	
Total number of residues	329	

Figure 2–2. Ramachandran plot produced by PROCHECK for APH(3')-IIIa–ADP–kanamycin A complex. Glycine residues are identified by triangles while all other residues are represented as squares. The most favourable combinations of ϕ-ψ angles are delimited by the red regions, additionally allowed combinations by the yellow regions, and the generously allowed combinations in the light yellow areas.

CHAPTER 3
Structural Basis of Plasticity in Substrate Specificity

Text and figures pertaining to the crystal structures of APH(3')-IIIa bound with ADP and kanamycin A or neomycin B were adapted from the journal article: Fong, D.H. and Berghuis, A.M. (2002) Substrate promiscuity of an aminoglycoside antibiotic resistance enzyme *via* target mimicry. *EMBO J.* **21**: 2323–2331. With permission from Nature Publishing Group.

3.1 Introduction

Due to the unusually broad spectrum of aminoglycosides that can be detoxified by APH(3')-IIIa (McKay *et al.*, 1994a; Wright and Thompson, 1999), much effort has been expended to understand the structural basis for its promiscuity in substrate recognition. For example, the crystal structures of APH(3')-IIIa in apo, ADP- and AMPPNP-bound forms have been determined (Burk *et al.*, 2001; Hon *et al.*, 1997); conformations of several aminoglycosides, such as amikacin and butirosin A, bound to APH(3')-IIIa have been studied using NMR (Cox *et al.*, 1996; Cox and Serpersu, 1997; Cox *et al.*, 2000; Mohler *et al.*, 1997); the binding of aminoglycosides to APH(3')-IIIa have been explored by examining the binding properties of synthetically constructed aminoglycoside variants (McKay

et al., 1996); and site-directed mutagenesis studies in combination with molecular docking experiments have been performed in order to predict the arrangement and conformation of different aminoglycosides in APH(3')-IIIa (Thompson *et al.*, 1999). These studies indicate the importance of electrostatic interactions for enzyme-substrate recognition and suggest that different aminoglycosides may have radically different conformations in the active site. However, no consensus can be established on the binding mode of aminoglycosides to APH(3')-IIIa, and thus, the structural basis for broad substrate specificity has remained enigmatic.

In this chapter, the three-dimensional crystal structure of APH(3')-IIIa in complex with ADP and either the 4,6-disubstituted aminoglycoside kanamycin A or the 4,5-disubstituted aminoglycoside neomycin B will be described. In addition, the crystal structure of APH(3')-IIIa with bound AMPPNP and butirosin A determined from two space groups will also be presented. These structures reveal the binding modes of the aminoglycosides and how the diverse structures of the substrates are accommodated by a versatile binding site consisting of three sub-sites and a flexible loop. Although the overall structure of APH(3')-IIIa is distinct from the ribosome, the arrangement of the amino acid side chains in the binding site of APH(3')-IIIa imitate that of the nucleotides in the A-site of the ribosome. These results suggest possible strategies for the design of novel antibacterial treatments. Furthermore, a detailed comparison between the crystal structures of kanamycin ternary complex and kanamycin-bound APH(3')-IIa will also be presented.

3.2 Experimental Procedures

3.2.1 Crystallization and Data Collection

ADP and Kanamycin A- or Neomycin B-bound APH(3')-IIIa. Crystals of the ternary complexes were grown at 4 °C using the hanging drop vapour diffusion method by combining 2 μL of a solution containing 12-15 mg/ml protein, 2.5 mM ADP, 2.5 mM aminoglycoside antibiotic, and 2 mM $MgCl_2$ with 2 μL of 35-40% (v/v) polyethylene glycol (PEG) 600 and 0.1 M CHES pH 9.0-9.5, and equilibrating it against 0.7 mL of the same solution. Crystals reach maximum size of 0.25mm x 0.25mm x 0.1mm in approximately 4 weeks. These crystals belonged to the tetragonal space group $P4_322$, with unit-cell dimensions a = b = 46.6 Å, c = 301 Å. All data collection was performed under cryogenic conditions (110 K). Prior to data collection, crystals were soaked for approximately one minute in 0.1 M CHES pH 9.0-9.5 and 55% (v/v) PEG 600 and flash frozen in liquid nitrogen. Diffraction data for APH(3')-IIIa–ADP–kanamycin were collected from two crystals and the two data sets were merged for structure determination. Data from the first crystal were collected on a Rigaku rotating copper anode X-ray generator using a MAR image plate to 2.9 Å, and data from a second crystal were collected at the X8C beamline of the NSLS at the BNL, using an ASDC Quantum CCD detector (λ = 1.072 Å) to 2.4 Å. Diffraction data for the ternary complex containing neomycin were collected from a single crystal at the X8C beamline of the NSLS, using an ASDC Quantum CCD detector (λ = 1.072 Å) to 2.7 Å. All data were processed using the HKL suite of programs (Otwinowski and Minor, 1997) giving statistics outlined in Table 3–1.

AMPPNP and Butirosin A-bound APH(3')-IIIa. Butirosin A-bound APH(3')-IIIa was crystallized in two space groups from a solution containing 15 mg/mL of protein, 2.5 mM of AMPPNP, 1.5 mM of butirosin A, and 2 mM $MgCl_2$ using the hanging drop technique. After one week at 22 °C, small needle shape crystals approximately 0.25 mm long appeared in one condition consisting of 40% (v/v) PEG 600, 0.1 M acetate pH 4.5, and 0.2 M magnesium chloride. Fine-screening of the precipitant concentration and buffer pH did not improve the crystal quality. Subsequently, Additive Screens I-III (Hampton Research) were used in attempt to enhance crystal quality. The Additive Screens contain a variety of small molecules which could perturb protein-protein and protein-solvent interactions, thereby altering process of crystal formation and consequently, the crystal quality. When using non-volatile additives in the crystallization experiment, each 5 μL drop is composed 2.5 μL of protein solution, 2 μL of crystallization reagent, and 0.5 μL of additive. For volatile additives, in addition to the procedure described, the volatile additive solution should constitute 10% of the total reservoir solution volume. Upon the inclusion of 0.5 μL of 30% (w/v) D(+)-sucrose, the size and shape of the crystals were considerably improved. The resultant crystals were egg-shaped of approximately 0.40 mm in length and 0.25 mm in the widest part in the middle. These crystals belonged to space group $P4_22_12$ with unit cell dimensions a = b = 80.1 Å, and c = 110 Å. A second crystal form in the shape of a plate with dimensions 0.37 mm x 0.30 mm x 0.03 mm grew at 4 °C in 30% (v/v) PEG 600, 0.1 M sodium cacodylate pH 6.5, 1 M NaCl, and 10% glycerol after approximately six months. These crystals were of space group $P4_322$ with cell dimensions a = b = 46.7 Å, and

c = 301 Å. These two crystals forms contained one APH(3')-IIIa molecule in each asymmetric unit. For both crystal forms, data were collected from a single crystal under cryogenic conditions at beamline X8C of the NSLS, equipped with an ASDC Quantum CCD detector (λ = 1.072 Å). 2.4 Å resolution data were collected from the crystal in space group $P4_22_12$ and data to 2.7 Å resolution were collected from the crystal in $P4_322$ space group. Intensities were integrated and scaled using the HKL program suite (Otwinowski and Minor, 1997) giving statistics summarized in Table 3–1.

3.2.2 Structure Determination and Refinement

ADP and Kanamycin A- or Neomycin B-bound APH(3')-IIIa. The structure of APH(3')-IIIa bound with ADP and kanamycin A was solved by molecular replacement using the CNS program (Brünger *et al.*, 1998) and the APH(3')-IIIa–ADP complex (Hon *et al.*, 1997; Burk *et al.*, 2001) as the search model. After the positioning of the model in the unit cell and several cycles of refinement using CNS, the kanamycin moiety was added adjacent to the nucleotide based on difference electron density maps ($2F_o$-F_c and F_o-F_c). Ideal stereochemistry applied to the aminoglycoside during subsequent refinement was based on the crystal structure of kanamycin A (Koyama and Iitaka, 1968). Examination of initial electron density maps showed that the loop located between helices αA and αB (residues 150 to 165) required remodelling. Based on difference electron density maps as well as simulated annealing omit map, this section of the protein structure was rebuilt using the program O (Jones *et al.*, 1991). Successive cycles of refinement alternated with manual intervention and addition of solvent

Table 3–1. Diffraction data collection statistics for APH(3')-IIIa complexed with ADP and kanamycin A or neomycin B, and AMPPNP and butirosin A.

Complexes	ADP & kanamycin A†	ADP & neomycin B	AMPPNP & butirosin A	AMPPNP & butirosin A
Space group	$P4_322$	$P4_322$	$P4_22_12$	$P4_322$
Unit cell parameters (Å,°)	a = b = 46.6 c = 301 $\alpha = \beta = \gamma = 90$	a = b = 46.4 c = 302 $\alpha = \beta = \gamma = 90$	a = b = 80.1 c = 111 $\alpha = \beta = \gamma = 90$	a = b = 47.1 c = 302 $\alpha = \beta = \gamma = 90$
Resolution limit (Å)	2.4	2.7	2.4	2.7
Reflections observed	93269	28072	200215	34208
Unique reflections	12532	8483	14576	8688
Data redundancy (outer shell)	7.4 (2.3)	3.4 (1.9)	13.7 (13.1)	3.9 (3.6)
Completeness (%) (outer shell)	88.4 (61.1)	80.8 (48.2)	99.1 (94.8)	86.1 (76.4)
Mean $I/\sigma(I)$ (outer shell)	13.7 (2.0)	15.4 (4.3)	45.9 (17.0)	11.1 (4.4)
R_{sym} (%) (outer shell)	10.1 (39.9)	4.8 (16.8)	4.3 (13.4)	10.0 (27.2)

†statistics for merged data

molecules were continued until no significant improvement in model statistics was observed.

A partially refined structure of APH(3')-IIIa–ADP–kanamycin complex, omitting the antibiotic and solvent molecules, was used to solve the structure of APH(3')-IIIa bound with ADP and neomycin B. Following rigid body refinement and simulated annealing, the neomycin B moiety was modelled into the positive electron density flanking the nucleotide. Stereochemical restraints employed for refinement of neomycin B were based on that of kanamycin A and information provided by Dr. J.R. Cox (Murray State University, Murray, KY). Refinement followed a strategy analogous to that described above for the kanamycin ternary complex of APH(3')-IIIa. Final refinement statistics for both ternary complex structures are given in Table 3–2.

AMPPNP and Butirosin A-bound APH(3')-IIIa. The structure of APH(3')-IIIa with AMPPNP and butirosin A crystallized in space group $P4_22_12$ was solved by molecular replacement using AMoRe (Navaza, 1994), part of the CCP4 suite of programs (Collaborative Computational Project Number 4, 1994). The structure of APH(3')-IIIa–ADP–kanamycin (Fong and Berghuis, 2002), excluding the ligands and solvent molecules, was used as the search model. After several cycles of refinement using CNS (Brünger *et al.*, 1998), AMPPNP, Mg^{2+}, and butirosin A molecules were placed in the active site based on difference electron density maps ($2F_o$-F_c and F_o-F_c). Ideal stereochemistry applied to butirosin A during subsequent refinement was based on those of neomycin B and values

from the energy minimized conformation obtained from the molecular mechanics program MM2 (Allinger, 1977; Burkert and Allinger, 1982) implemented in Chem3D (CambridgeSoft). Examination of initial electron density maps showed that the aminoglycoside-binding loop (residues 150-165) and the hinge region (residues 101-106) required remodelling. Based on difference electron density maps as well as simulated annealing, these sections were rebuilt using the program O (Jones *et al.*, 1991). Successive cycles of refinement were alternated with manual intervention, and the addition of solvent molecules was continued until no significant improvement in the model statistics was observed.

The ADP and kanamycin-bound structure of APH(3')-IIIa, excluding the ligands and solvent molecules, was used as the starting model for the refinement of APH(3')-IIIa–AMPPNP–butirosin A complex crystallized in the second space group, $P4_322$. After rigid body refinement and several rounds of positional and B-factor refinement using CNS (Brünger *et al.*, 1998), AMPPNP, Mg^{2+}, and butirosin A were added to the active site where positive electron density maps were observed. In addition, a 7σ peak was observed in the F_o-F_c map extending from the 5"-hydroxyl group of the aminoglycoside. Subsequently, a phosphate molecule was modelled into this positive peak density making the substrate a 5"-monophosphorylated product. The γ-phosphate of the nucleotide and the 5"-phosphate of butirosin A were subsequently refined at an occupancy value of 0.5 due to the elevated thermal factors of these atoms compared to the rest of the nucleotide and the aminoglycoside, respectively and the presence of negative features in the electron density maps. Upon further refinement, the B-factors

Table 3–2. Refinement statistics for APH(3')-IIIa complexed with ADP and kanamycin A or neomycin B, and AMPPNP and butirosin A.

APH(3')-IIIa Complexes	ADP & kanamycin A	ADP & neomycin B	AMPPNP & butirosin A	AMPPNP & butirosin A
Number of reflections				
Working set	10889	7175	14475	7614
Test set	1297	852	1473	856
Number of atoms				
Protein	2170	2170	2170	2170
Mg^{2+}	2	2	2	2
Co-factor	27	27	31	31
Substrate	33	42	38	42
Solvent	65	45	85	35
R_{cryst}	0.234	0.225	0.217	0.243
R_{free}	0.291	0.312	0.261	0.316
r.m.s.d.				
Bonds (Å)	0.007	0.008	0.007	0.007
Angles (°)	1.321	1.396	1.286	1.426

for the phosphate molecules fell to values more akin to atoms in their vicinities. Similar to the ternary complex crystallized in space group $P4_22_12$, the aminoglycoside-binding loop of the model also differed considerably from the difference electron density maps. Rebuilding and refinement followed a strategy analogous to that described above for the first crystal form. Final refinement statistics are given in Table 3–2.

3.3 Results

3.3.1 Overall Structure of Aminoglycoside-bound APH(3')-IIIa

Crystal structures are now available for each and every step of the reaction cycle of APH(3')-IIIa, namely, the apo-form (Burk *et al.*, 2001), the binary complex (i.e. with bound nucleotides ADP or ATP analogue AMPPNP) (Burk *et al.*, 2001; Hon *et al.*, 1997) and the ternary complex (i.e. with bound ADP or AMPPNP and kanamycin A, neomycin B or butirosin A (Figures 3–1 and 3–2). Comparison between the six crystal structures of APH(3')-IIIa shows that most of the APH(3')-IIIa protein structure appears to be rather rigid, and no gross domain movements are observed. Four segments can be identified which display differing conformations between the various APH(3')-IIIa structures: residues 21-26, 100-112, 147-170 and 226-238. Conformational differences observed for residues 100-112 and 226-238 can be attributed to inherent flexibility for these segments, as they are invariably associated with high thermal factors and poor electron density in $2F_o$-F_c and omit maps.

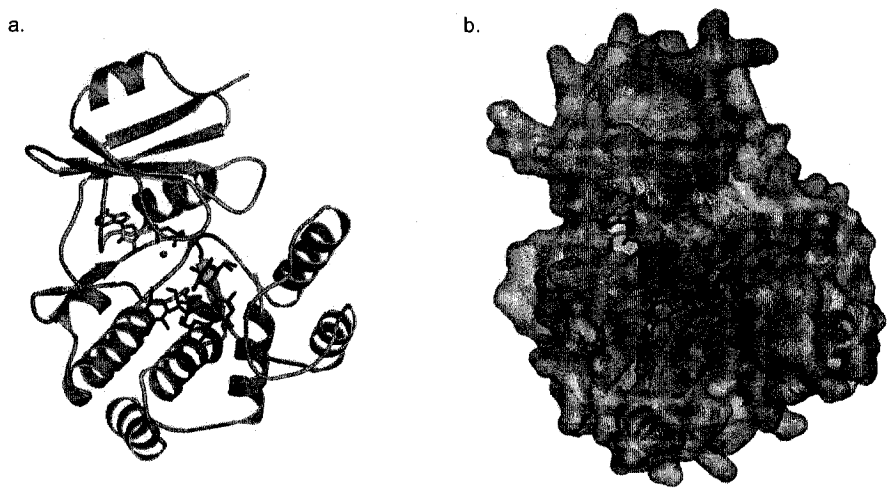

Figure 3–1. Crystal structures of APH(3')-IIIa in complex with ADP and kanamycin A or neomycin B and electrostatic potential surface of the nucleotide-bound enzyme. **a.** Ribbon representation of the APH(3')-IIIa ternary complexes showing the location of the antibiotic-binding site. Kanamycin (red) and neomycin (blue) are superimposed in the binding site. Magnesium ions are shown in green. Since the protein structure does not significantly differ between the two ternary complexes, only the kanamycin-bound APH(3')-IIIa is shown. *Reproduced with permission from Nature Publishing Group.* **b.** The molecular surface of APH(3')-IIIa coloured based on electrostatic potentials calculated using the ADP-bound structure. The nucleotide-bound enzyme is coloured grey and the ADP and magnesium ions are in black. Positive charges are shown in blue and negative charges are shown in red. The aminoglycosides from the ternary complexes are superposed onto the ADP-bound structure to show the accurate prediction of the aminoglycoside-binding site being the negatively-charged groove next to the ADP-binding pocket.

Conformational differences in residues 21-26 and 147-170 observed between the apo-form, the binary complex and the ternary complex structures of aminoglycoside phosphotransferase are associated with the nature of bound substrates. The conformation of residues 21-26, which form a loop above the phosphate moieties of the nucleotide that is structurally homologous to the GXGXXG motif in the related protein kinase superfamily, is dependent on the presence or absence of

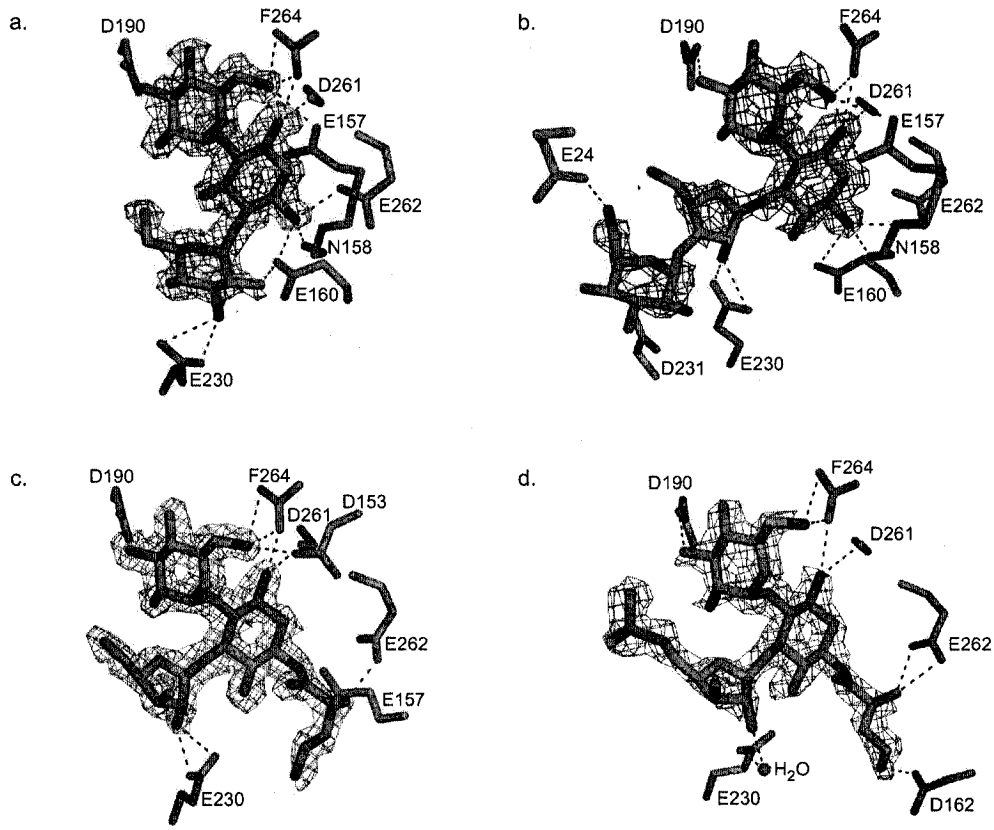

Figure 3–2. Simulated annealing F_o-F_c omit map, contoured at 2σ, for **a.** kanamycin A, **b.** neomycin B, **c.** butirosin A, and **d.** 5"-monophosphorylated butirosin A. Residues forming hydrogen bond interactions with their respective aminoglycoside substrates are also shown. *Panels a and b were reproduced with permission from Nature Publishing Group.*

the nucleotide co-factor. A detailed analysis of this has previously been reported (Burk *et al.*, 2001). Residues 147-170 adopt differing conformations depending on the presence or absence of antibiotic substrates. This segment, henceforth termed the aminoglycoside-binding loop is located between two helices (αA and αB). Previous crystallographic studies suggest that in the absence of aminoglycosides this loop is highly flexible (Burk *et al.*, 2001). In the kanamycin- and neomycin-bound structures of APH(3')-IIIa the aminoglycoside-binding loop is

folded over towards the antibiotic, and the shift observed at the tip of the loop (residue 160) is approximately 10 Å as compared to the nucleotide-bound enzyme crystal structure (Figure 3–3). As a consequence of the conformational changes in the aminoglycoside-binding loop upon substrate binding, several residues located in this loop are in a position to form interactions with the antibiotics, specifically Glu157, Asn158 and Glu160 (Figure 3–2a,b). In effect, the shift in the aminoglycoside-binding loop results in the completion of the aminoglycoside-binding pocket.

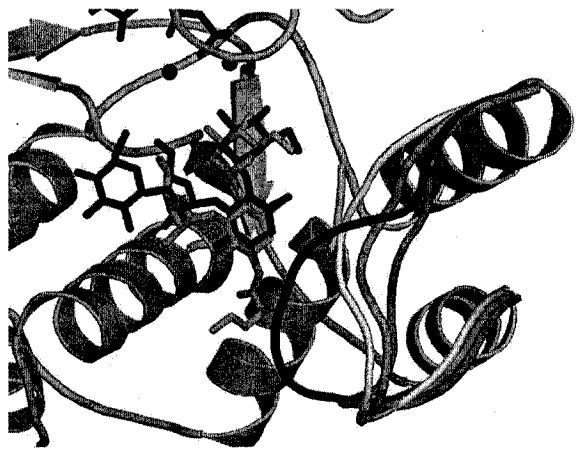

Figure 3–3. Structural changes observed in APH(3')-IIIa upon aminoglycoside binding. Shown is a ribbon diagram of the APH(3')-IIIa–neomycin B ternary complex in the vicinity of the antibiotic-binding pocket. The α-carbon trace of the aminoglycoside-binding loop (residues 150–165) is blue, the remainder of the protein is in grey, the antibiotic is also in blue, and the ADP co-factor and the magnesium ions are displayed in black. Overlayed with this is the backbone trace for residues 150–165 of the APH(3')-IIIa–ADP enzyme structure (Burk *et al.*, 2001), coloured in yellow. The aminoglycoside-binding loop represents the largest conformational difference between the kanamycin or neomycin ternary complexes and the nucleotide-bound binary enzyme structures. The α-carbon trace of the aminoglycoside-binding loop in the butirosin A and 5"-monophosphorylated butirosin A ternary complexes are also superposed and displayed in orange and green respectively. In the presence of a butirosin, the loop segment adopts a conformation resembling the one observed in the ADP-bound structure.

The overall structure of the AMPPNP- and butirosin A-bound APH(3')-IIIa determined from the two different space groups are identical except for the antibiotic-binding loop (residues 147-170) (Figure 3–4). The overall rmsd in C_α atoms is 1.34 Å whereas the corresponding value for the antibiotic-binding loop region is 3.14 Å. Since Cys156 is involved in the formation of a disulfide bond linking two APH(3')-IIIa molecules in adjacent asymmetric units, the discrepancy in the loop conformation can be partly attributed to the different space groups the complex was crystallized in. Compared to the kanamycin- and neomycin-bound ternary complexes, the antibiotic-binding loop adopts an open conformation in the presence of butirosin, akin to the conformation observed in the binary enzyme structures. The rmsd value in the antibiotic-binding loop between the ADP-bound and the butirosin-bound ternary structures determined from space groups $P4_22_12$ and $P4_322$ are 1.63 Å and 2.93 Å respectively. Moreover, the temperature factors in this region of butirosin-bound complexes are comparable to those of the nucleotide-bound enzyme structures, which are noticeably higher than those in the kanamycin and neomycin ternary structures. The average B-factor in the loop segment (residues 150-165) for the ADP-bound and butirosin-bound enzymes are 1.4 and 1.7 standard deviations above the mean, whereas the corresponding values for kanamycin- and neomycin-bound complexes are 0.4 and 1.0. The open loop conformation can be ascribed to the AHB at position N1 of the central ring which hinders the loop from approaching and forming as many interactions with the aminoglycoside (Figure 3–3).

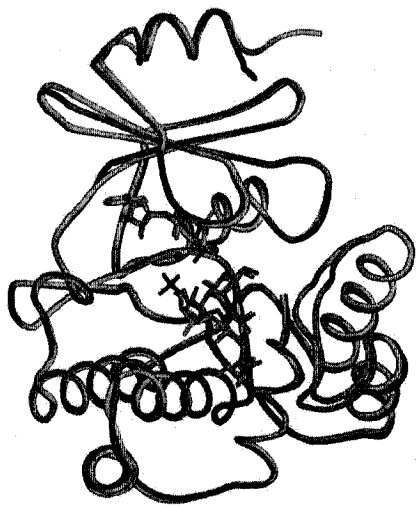

Figure 3–4. Superposition of the butirosin A and 5"-monophosphorylated butirosin A ternary complexes of APH(3')-IIIa. The alpha carbon trace of the AMPPNP- and butirosin A-bound structure is in light grey whereas the nucleotide and the antibiotic are shown in orange. Magnesium ions are in black. The 5"-monophosphorylated butirosin A-ternary complex is displayed in dark grey and the bound nucleotide and antibiotic are in green with the phosphate at the 5"-position coloured in magenta. The most significant difference between the two structures is located in the aminoglycsodie-binding loop region, which is highlighted in orange in the butirosin A-bound enzyme and in green for phosphorylated-butirosin A complex.

The butirosin ternary complexes are crystallized with AMPPNP, in contrast to ADP in the kanamycin and neomycin structures. The adenine and the α- and β-phosphates of the nucleotide could be unambiguously placed into the electron density found in the cleft between the N- and C-termini of both APH(3')-IIIa–butirosin complexes. However, in the structure determined from space group $P4_22_12$, the electron density indicates that the nitrogen atom connecting the β- and γ-phosphates is shifted by a distance of approximately 1.5 Å toward the nucleotide-binding loop, compared to the AMPPNP-bound enzyme. Manual remodelling and further refinement led to a rotation of 90° in the dihedral angle

(defined by the oxygen connecting the α- and β-phosphates, the β-phosphate, the nitrogen connecting the β- and γ-phosphate, and γ-phosphate) in this ternary complex.

3.3.2 Aminoglycoside-binding Site

The majority of residues located in the aminoglycoside-binding pocket are acidic in nature (3 Asp's, 5 Glu's and 1 C-terminal carboxylic acid group) and as a consequence the pocket is highly negatively charged (Figures 3–1b and 3–2). In fact, the enzyme provides only acceptor groups for hydrogen bond interactions with aminoglycoside substrates. The abundance of acidic residues in the aminoglycoside-binding pocket can be readily explained by noting that aminoglycosides are invariably positively charged molecules. The presence of negatively charged pockets for substrate binding has also been observed in enzymes that either adenylate or acetylate aminoglycosides so as to confer resistance (Perdersen *et al.*, 1995; Wolf *et al.*, 1998; Wybenga-Groot *et al.*, 1999; Kotra *et al.*, 2000; Vetting *et al.*, 2002, 2004). Related to the abundance of acidic residues is the large number of bifurcated hydrogen bonds (Figure 3–2). This feature of the aminoglycoside-binding pocket may provide for an inherent plasticity, allowing for various aminoglycosides to be bound to APH(3')-IIIa.

Kanamycin A- or Neomycin B-binding Site. The APH(3')-IIIa aminoglycoside-binding pocket in both the kanamycin- and neomycin-bound ternary complexes can be considered as consisting of three distinct sub-sites. Sub-site A forms interactions with the 2-deoxystreptamine ring and the hexose substituted at position 4 (often referred to as the prime ring). Although the functional groups

may vary, these two rings are the moieties common to most aminoglycosides (Mingeot-Leclercq *et al.*, 1999) and they have been shown to be the minimum essential components required for antibacterial activity (Fourmy *et al.*, 1998; Kotra *et al.*, 2000). Sub-site B can form interactions with moieties located at the 6 position of the 2-deoxystreptamine ring, e.g. the so-called double-prime ring of kanamycin. Since only a subset of aminoglycoside substrates of APH(3')-IIIa have 6 substituted 2-deoxystreptamine rings, sub-site B is not always employed. Those aminoglycosides that are substituted at the 5 instead of the 6 position (e.g. neomycin) employ the alternative sub-site C for binding to APH(3')-IIIa.

Most of the hydrogen bond interactions between the enzyme and kanamycin A or neomycin B are located in the A sub-site. Of specific interest are the interactions between the C-terminal carboxylic acid group and the 2-deoxystreptamine and prime rings, as well as the interaction between Asp190 and the 3'-OH group. The involvement of the C-terminus in substrate binding was previously predicted (Thompson *et al.*, 1999), and the Asp190–3'-OH hydrogen bond is significant in that the aminoglycoside 3'-hydroxyl group is the site of phosphorylation by APH(3')-IIIa and Asp190 has been suggested to be the catalytic base in the reaction mechanism (Hon *et al.*, 1997). When comparing kanamycin A and neomycin B binding to sub-site A, it is intriguing to note that the two aminoglycosides have different functional groups at the 2' position (OH and NH2 for kanamycin A and neomycin B, respectively), and that the enzyme does not form interactions with this variable substituent. Furthermore, no hydrogen bond interactions are observed with the 5-hydroxyl group of the 4,6-disubstituted 2-deoxystreptamine

ring of kanamycin A, or with the 6-hydroxyl group of the 4,5-disubstituted 2-deoxystreptamine ring of neomycin B.

As indicated above, both sub-site B and sub-site C provide much fewer hydrogen bond interactions with the aminoglycoside antibiotic than sub-site A. This limited number of specific interactions mirrors the greater variability present in the components that can occupy these two sub-sites, and hydrogen bonds are only made with functional groups that are highly conserved within the 4,6- or 4,5-disubstituted 2-deoxystreptamine aminoglycosides (Figure 1–3). Also notable is the fact that sub-site B is much smaller in size than sub-site C. While sub-site B has to provide room for only one hexose ring, sub-site C may be occupied by one (ribostamycin, butirosin), two (neomycin B, paromomycin I) or three (lividomycin A) rings.

Butirosin A-binding Site. Butirosin A occupies the substrate-binding pocket in the same manner as neomycin B, utilizing sub-sites A and C to make contact with the enzyme. In the presence of AMPPNP, a hydrogen bond is observed between a γ-phosphate oxygen and the 4'-OH of butirosin A. This interaction plausibly contributes to the proper alignment of the 3'-OH for catalysis. Most of the hydrogen bond interactions made between APH(3')-IIIa and butirosin A, kanamycin A, or neomycin B, notably those bonds made with the core moiety (the central 2-deoxystreptamine and the prime rings) of the aminoglycosides, are conserved. However, since the antibiotic-binding loop adopts an open conformation in order to accommodate the AHB, differences in the pattern of hydrogen bond interactions are observed (Figure 3–5). For example, the side

chain of Glu157 no longer makes contacts with the core moiety of butirosin A but is now involved in hydrogen bonding the hydroxyl of the butyryl group. In addition, the higher flexibility in the aminoglycoside-binding loop, as indicated by elevated temperature factor values, may result in less stable interactions with the aminoglycoside substrate. This may account for the lower binding affinity (higher K_m) of butirosin A relative to kanamycin A and neomycin B. The APH(3')-IIIa–AMPPNP–butirosin structure confirms the importance of the pliable aminoglycoside-binding loop in the recognition and binding of structurally diverse aminoglycoside substrates.

Although the two butirosin complex structures are highly similar in both overall architecture and aminoglycoside binding position, it was found that the butirosin in the structure determined in space group $P4_322$ had been monophosphorylated at the 5" position (Figure 3–4). Due to the relatively high B-factor values, the 5"-phosphate and the γ-phosphate of AMPPNP were refined at 0.5 occupancy. In other words, 50% of the APH(3')-IIIa nucleotide-binding sites in the crystal are occupied by ADP and the other half by AMPPNP, whereas 50% of the substrate-binding pockets are occupied by 5"-phosphorylated butirosin A and the remainder by unphosphorylated butirosin A.

There are differences in detail between the binding of butirosin A and the 5"-monophosphorylated butirosin A. The AHB groups have slightly different orientations in the two complexes. This portion of the antibiotic is relatively flexible due to the varying torsional angles this short segment can adopt. As a result, the end of the AHB tail of butirosin A rotates approximately 35° into the

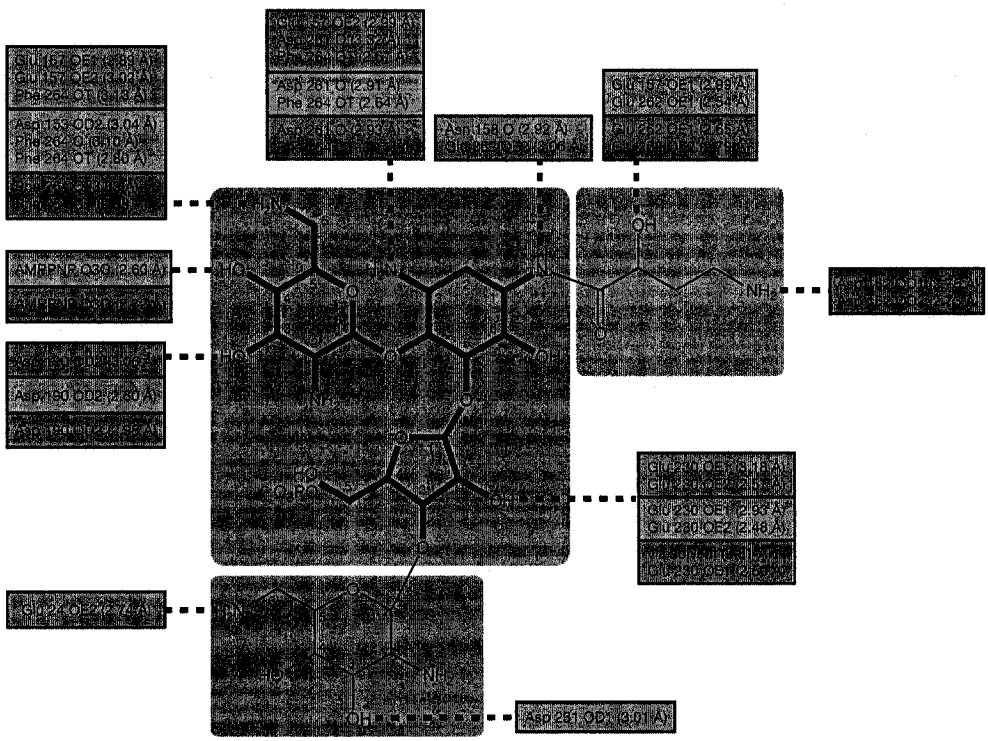

Figure 3–5. Schematic representation of hydrogen bond interactions between APH(3')-IIIa and 4,5-disubstituted aminoglycosides. A combined chemical structure of neomycin and butirosin is depicted here with the portion common to both highlighted in grey and that distinct to butirosin and neomycin highlighted in orange and blue respectively. Hydrogen bond interactions observed in the neomycin-bound structure of APH(3')-IIIa are shown in blue boxes. Hydrogen bonds formed between the enzyme and butirosin are displayed in orange boxes, whereas those between the enzyme and the phosphorylated butirosin substrate are in green boxes.

aminoglycoside-binding pocket with respect to the equivalent in the monophosphorylated butirosin A. The aminoglycoside-binding loop in the butirosin-bound enzyme is correspondingly positioned slightly closer to the aminoglycoside core. Moreover, the double prime ring of 5"-monophosphorylated butirosin A is tilted approximately 30° closer to the prime ring (Figure 3–4).

3.4 Discussion

3.4.1 Substrate-binding Mechanism of other Multiple-substrate Recognizing Enzymes

The ternary complexes of APH(3')-IIIa reported here were the first aminoglycoside kinase structures to be solved with a bound aminoglycoside. To date, at least one aminoglycoside-detoxifying enzyme from each class has been determined in the presence of an antibiotic substrate. The structures of APH(3')-IIa, a close relative of APH(3')-IIIa, as well as ANT(4')-Ia have been solved in complex with kanamycin A (Nurizzo *et al.*, 2003; Perdersen *et al.*, 1995, Section 3.4.3). Furthermore, the crystal structures of ternary complexes of AAC(6')-Iy with ribostamycin (Vetting *et al.*, 2004) and AAC(2')-Ic in complex with kanamycin A, tobramycin, or ribostamycin (Vetting *et al.*, 2002) have been determined. All these antibiotic-bound AMEs structures agree that the antibiotic-binding pocket is lined with many glutamate and aspartate residues, forming a negatively-charged binding area for the aminoglycoside substrate. Moreover, the majority of the interactions between the enzyme and the substrate are made *via* the 2-deoxystreptamine and the 2,6-dideoxy-2,6-diamino-glucose/prime rings of the aminoglycoside, with the double prime ring of the substrate generally more mobile.

In addition to aminoglycoside antibiotic-resistance enzymes, many other types of proteins are also capable of binding to diverse substrates. A few examples include various multidrug resistance (MDR) transporters, MDR transporter transcription activators, and P450s. Extensive research has been done in attempt

to elucidate the basis of broad substrate recognition by these enzymes. However, it was not until recently when crystal structures of some of these proteins were determined in the presence of substrates or inhibitors that multi-substrate recognition could be examined in atomic detail. The results indicate that diverse substrate recognition and binding are in part mediated by flexible domain movement, compliant and rigid sections in the active site, electrostatic interactions, and/or distinct substrate-binding sub-sites. For example, type II 3-hydroxyacyl-CoA dehydrogenase (HADH II) (Powell *et al.*, 2000) and aromatic amino acid aminotransferase (AroAT) (Okamoto *et al.*, 1998) contain highly flexible regions which undergo significant movement to close the active site upon substrate binding. Further analysis of AroAT bound to structurally related inhibitors shows that the active site can be divided into regions of rigidity and flexibility (Okamoto *et al.*, 1999). The residues in the rigid region remain in identical conformations upon the binding of various inhibitors. These residues interact with the portion of the substrate that is involved in the catalytic reaction to determine specificity and properly orient the substrate for efficient catalysis. Conversely, the residues in the flexible section of the binding site are able to adopt different conformations depending on the shape and size of the inhibitor bound. Additionally, adaptation to structurally diverse substrates can also be facilitated by multiple and overlapping substrate-binding sub-sites as observed in QacR (Schumacher *et al.*, 2001), a MDR transporter regulator. Another strategy employed by QacR and a number of other MDR transporter regulators, such as BmrR (Zheleznova *et al.*, 1999), which bind cationic substrates is the presence of glutamate residues buried in the binding pocket. The carboxylate group of glutamate complements

the positive charges on the cationic substrates and properly orients the substrate for catalysis.

These characteristics of substrate recognition and binding are also mirrored in APH(3')-IIIa. In APH(3')-IIIa, the flexible antibiotic-binding loop moves into close proximity of and forms key interactions with the aminoglycoside. The residues that interact with the 2-deoxystreptamine ring and the hexose at the 4 position in all ternary complexes of APH(3')-IIIa have essentially the same conformations, whereas the residues interacting with the remainder of the substrates are more flexible. The side chain of these residues (Glu230, Asp231, and Glu24) differ between the ternary structures. This is further supported by the higher than average thermal factor values in these residues. Another element of aminoglycoside binding to APH(3')-IIIa is electrostatic interactions (Thompson *et al.*, 1999). Aminoglycosides are cationic molecules and their binding site in APH(3')-IIIa is a negatively charged groove lined with glutamate and aspartate residues. Furthermore, the active site is composed of three distinct sub-sites in order to accommodate structurally different components of the substrate.

3.4.2 Comparison of Aminoglycoside-binding Mode in 16S Ribosomal RNA versus APH(3')-IIIa

As stated above, the intended cellular target for most aminoglycosides, including those that can be detoxified by APH(3')-IIIa, is the A-site of the bacterial ribosome (Kotra *et al.*, 2000; Mingeot-Leclercq *et al.*, 1999; Wright *et al.*, 1998). Solution structures have been determined of a fragment of the A-site in complex with gentamicin C_{1a} and paromomycin I (Yoshizawa *et al.*, 1998; Fourmy *et al.*,

1996). The crystal structure of an A-site fragment bound with tobramycin has also been solved (Vicens and Westhof, 2002). In addition, the crystal structure of the entire 30S ribosome in complex with various antibiotics, including paromomycin I, has been determined (Carter *et al.*, 2000). Of these structures, the complex structures with paromomycin I are of particular interest here since this aminoglycoside is also a substrate for APH(3')-IIIa. Paromomycin I is a 4,5-disubstituted aminoglycoside which differs from neomycin B by one functional group at position 6', where it possesses a hydroxyl instead of an amino group (Figure 1–3). A comparison of paromomycin I and neomycin B bound to the 16S rRNA (the intended target) and APH(3')-IIIa (a decoy for the antibiotics), respectively, can provide insight into the basis of the effectiveness of antibiotic resistance mechanisms.

Results from a comparison between neomycin B bound to APH(3')-IIIa versus paromomycin I bound to the ribosome can be summarized in three main points. First, the conformations of neomycin B and paromomycin I are effectively identical (rmsd of 1.7 Å; Figure 3–6a). This observation is surprising considering the large number of conformations these antibiotics are known to exhibit (Mikkelsen *et al.*, 2001). A probable explanation for this is that enzymes involved in the biosynthesis of aminoglycosides have evolved to produce products which, in their lowest energy conformation, are optimal for binding the A-site of the bacterial ribosome so as to enhance binding affinity through curtailing loss of entropy. Aminoglycoside modifying enzymes such as APH(3')-IIIa in turn evolved to capture this lowest-energy conformer so as to effectively

compete with the ribosome. Support for this explanation comes from molecular dynamics simulations of free solvated aminoglycosides (Hermann and Westhof, 1999), which confirm that the observed conformations of the two aminoglycosides correspond to their minimum-energy conformer. Second, the functional groups of the two aminoglycosides that are utilized in binding to APH(3')-IIIa or the bacterial ribosome are identical, with the exception of two, which are not employed for binding in the antibiotic resistance enzyme (Figure 3–6b). As expected, these functional groups correspond to those moieties that are predominantly conserved among 4,5-disubstituted aminoglycosides. Third, while the conformation of the aminoglycosides and the functional groups utilized for binding are effectively identical when comparing the neomycin B-bound structure of APH(3')-IIIa and the paromomycin I-bound structure of the 30S ribosome, there are significant differences when examining the van der Waals interactions. The most striking difference is that the face of the aminoglycosides that form most of the van der Waals interactions with the 16S rRNA is opposite to that observed with APH(3')-IIIa (Figure 3–6c and d).

The results of the analysis of 4,5-disubstituted aminoglycoside binding to the ribosome and to APH(3')-IIIa, i.e. identical conformation of the antibiotics and nearly identical hydrogen bond interactions but differing van der Waals interactions, is likely to also extend to 4,6-disubstituted aminoglycosides such as kanamycin A. Modelling of kanamycin A into the ribosome A-site employing the conformation seen in the APH(3')-IIIa ternary complex and employing hydrogen bond interactions akin to those observed for paromomycin I results in a

structure which is completely consistent with structural studies of tobramycin (a 4,6-disubstituted aminoglycoside) binding to the ribosome (Figures 3–6b and d) (Vicens and Westhof, 2002).

The above analyses provide an explanation for the structural basis of substrate promiscuity of APH(3')-IIIa and its effectiveness as an aminoglycoside antibiotic resistance enzyme. The aminoglycoside-binding pocket in APH(3')-IIIa mimics in nearly every important aspect the intended target site for these antibiotics, namely the A-site of the prokaryotic ribosome.

Although RNA and protein are chemically very different and are not expected to form the same shapes or to feature the same chemical properties, macromolecular mimicry between RNA and protein is not uncommon. The foremost example of mimicry is of Phe-tRNA–EF-Tu (Nissen *et al.*, 1995) by EF-G (al Karadaghi *et al.*, 1996; Czworkowski *et al.*, 1994). The overall structure of the two complexes are highly similar and the shape of part of the EF-G resembles the anticodon stem of the tRNA (Liljas, 1996; Nissen *et al.*, 2000). In addition to structural resemblance, molecular mimicry can also be defined based on common functions (Keene, 1996). For example, a particular RNA sequence can act as a decoy for antibodies specific for an autoantigenic epitope of the human insulin receptor (Doudna *et al.*, 1995). In our case, APH(3')-IIIa acts as a decoy of the A-site of the 16S ribosome. Though lacking resemblance in the shape of the overall structure, APH(3')-IIIa and the 16S ribosome utilize a highly homologous hydrogen bonding scheme for binding the same spectrum of substrates. In contrast to the other examples of molecular mimicry where the

a.

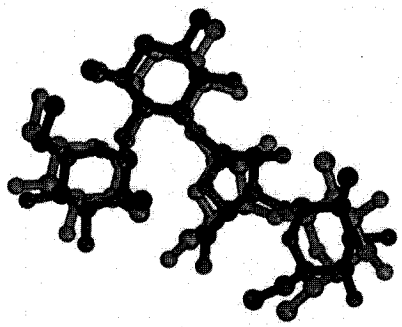

b.

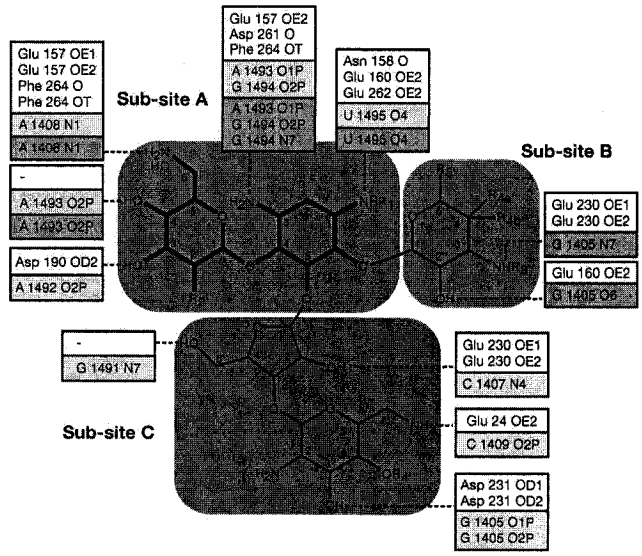
Glu 157 OE1
Glu 157 OE2
Phe 264 O
Phe 264 OT
A 1408 N1
A 1406 N1
-
A 1493 O2P
A 1493 O2P
Asp 190 OD2
A 1492 O2P
Sub-site A
Glu 157 OE2
Asp 261 O
Phe 264 OT
A 1493 O1P
G 1494 O2P
A 1493 O1P
G 1494 O2P
G 1494 N7
Asn 158 O
Glu 160 OE2
Glu 262 OE2
U 1495 O4
U 1495 O4
Sub-site B
Glu 230 OE1
Glu 230 OE2
G 1405 N7
Glu 160 OE2
G 1405 O6
-
G 1491 N7
Sub-site C
Glu 230 OE1
Glu 230 OE2
C 1407 N4
Glu 24 OE2
C 1409 O2P
Asp 231 OD1
Asp 231 OD2
G 1405 O1P
G 1405 O2P

c.

d.

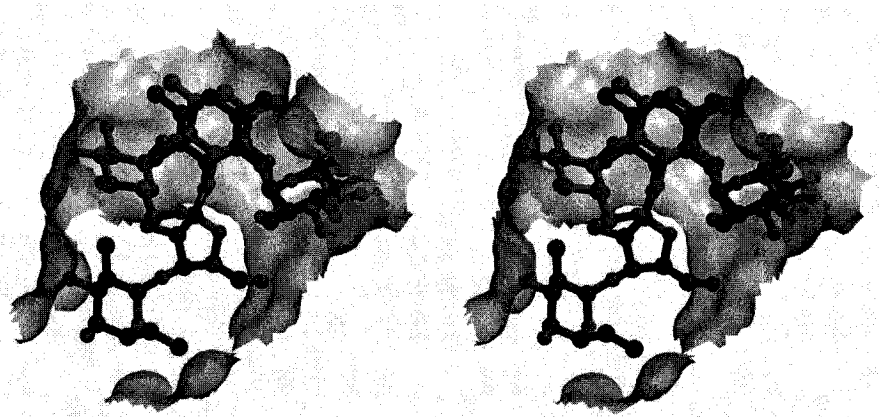

protein and RNA, during its biological function, may bind to another protein or RNA, the situation observed here is unique that the protein and RNA interact with a small molecule instead.

While mimicry of the ribosomal A-site by APH(3')-IIIa provides a structural explanation for this enzyme's effectiveness as a resistance factor, it also raises concerns for the development of new antibiotics that target the 16S RNA. However, the observation that APH(3')-IIIa and the ribosome differ in one crucial aspect with respect to aminoglycoside binding, namely van der Waals interactions, suggests possible strategies for the design of inhibitors and novel variant

Figure 3–6. (Page 92) Comparison of aminoglycoside binding to APH(3')-IIIa versus the bacterial ribosome. **a.** Superposition of neomycin B, in the conformation observed in the APH(3')-IIIa ternary complex, and paromomycin I in the conformation observed in the crystal structure of the 30S ribosomal subunit (Carter *et al.*, 2000). Neomycin B is shown in solid colours and paromomycin I is semi-transparent. **b.** Schematic overview of hydrogen bond interactions made by aminoglycosides with APH(3')-IIIa and the bacterial ribosome (Carter *et al.*, 2000; Vicens and Westhof, 2002). A combined generic chemical structure for 4,6- and 4,5-disubstituted aminoglycosides is shown, highlighting common functional groups (see also Figure 1–3). Hydrogen bond interactions made by APH(3')-IIIa with aminoglycosides are shown in white boxes, those made by the ribosome, as observed in the ribosome-paromomycin I crystal structure (Carter *et al.*, 2000), are shown in yellow boxes. Interactions made by an RNA construct containing the A-site, as observed in crystallographic studies of tobramycin (Vicens and Westhof, 2002), are displayed in green coloured boxes. **c.** Stereo view of the van der Waals surface of the APH(3')-IIIa aminoglycoside-binding pocket. Also shown are kanamycin A and neomycin B. **d.** Stereo view of the van der Waals surface of the bacterial ribosomal aminoglycoside-binding pocket. Also shown are paromomycin I and a modelled kanamycin A. Panel **d** has been subjected to a 180° rotation around the vertical axis with respect to panel **c**, to show that opposite faces of the aminoglycosides form predominant van der Waals interactions with either the ribosome or APH(3')-IIIa. *Reproduced with permission from Nature Publishing Group.*

aminoglycoside antibiotics that can interact with the ribosome A-site but are unable to be detoxified by APH(3')-IIIa and related enzymes. For example, the binding of aminoglycoside derivatives can be blocked by modifying the corresponding face with bulky chemical moieties (Vicens and Westhof, 2003).

3.4.3 Comparison to the Crystal Structure of APH(3')-IIa

Overall Structure. In addition to APH(3')-IIIa, APH(3')-IIa has also been extensively characterized (Kocabiyik and Perlin, 1992a,b; Kocabiyik *et al.*, 1992; Kocabivik and Perlin, 1994; Siregar *et al.*, 1994; Yang *et al.*, 1998; Kim *et al.*, 2004). The amino acid sequence of APH(3')-IIa and APH(3')-IIIa enzymes have 33% identity and the two enzymes have almost identical substrate spectra (Table 1–2). Their difference in substrate specificity is in part associated with the absence of phosphorylation at the 5"-hydroxyl group of 4,5-disubstituted aminoglycosides by APH(3')-IIa, thus eliminating lividomycin from its substrate profile. Recently, the crystal structure of APH(3')-IIa complexed with kanamycin A was solved (Nurizzo *et al.*, 2003). It is essentially identical to the structure of APH(3')-IIIa with an rmsd of about 1.7 Å for the C_α atoms. There is a small difference in the relative orientation of the N- and C-terminal lobes in the two structures. This difference was estimated to be a 4° rotation, bringing the two lobes of APH(3')-IIa closer together. The authors attributed the discrepancy in the relative domain orientation to the lack of conservation in the interdomain linker sequence between the two enzymes. The presence of a proline residue (Pro98) in APH(3')-IIa in place of an aspartate (Asp94) in APH(3')-IIIa may

have led to a conformational difference in this region due to a restricted Φ angle (Nurizzo *et al.*, 2003).

Figure 3–7. Superposition of the ADP-kanamycin A ternary complex of APH(3')-IIIa and kanamycin A-bound APH(3')-IIa (PDB code: 1ND4). The α-carbon trace of the APH(3')-IIIa structure is shown in light grey and the antibiotic in red. APH(3')-IIa is coloured in dark grey and the kanamycin in cyan. The two crystal structures differ most considerably in the nucleotide-binding and the aminoglycsodie-binding loops. These segments are highlighted in red for APH(3')-IIIa and in cyan for APH(3')-IIa.

Nucleotide-binding Pocket. Although the crystal structure of APH(3')-IIa was solved in the absence of a nucleotide, based on the overall structural congruity between APH(3')-IIa and APH(3')-IIIa as well as the conservation of most amino acid residues in the nucleotide-binding pocket, the authors were able to model an ATP molecule into the cleft between the N- and C-terminal lobes. The adenine of the modelled ATP was sandwiched between a hydrophobic pocket consisting of Phe48 (Tyr42, APH(3')-IIIa numbering), Met197 (Phe197), and Ile207 (Ile207). The N1 and N6 of the adenine ring forms two hydrogen bonds with the

main chain amide of Val97 (Ala93) and the carbonyl of Gly95 (Ser91), respectively. Although Pro194 (Ser194) is not conserved among APH(3') enzymes, only the main chain carbonyl of this residue is involved in the single hydrogen bond interaction with the ribose *via* the 3' oxygen. Asn195 and Asp208 were involved in the coordination of a Mg^{2+} ion, analogous to the Mg1 ion in APH(3')-IIIa. Although Lys50 adopts a different conformation than the corresponding Lys44 in APH(3')-IIIa, it is still capable of interacting with the α-phosphate of the modelled ATP and it is plausible that it may undergo a conformation change in the presence of a nucleotide (Nurizzo *et al.*, 2003).

The major difference between the nucleotide-binding region in APH(3')-IIa and APH(3')-IIIa resides in the nucleotide-binding loop (Figure 3–7). In the nucleotide-bound complexes of APH(3')-IIIa, the loop shields the ATP-binding pocket and OG atom of Ser27 makes a hydrogen bond with the β-phosphate. In contrast to the binary enzyme complexes, this loop in the apo APH(3')-IIIa structure shifts downward into the nucleotide-binding pocket thereby partially occupying the phosphate-binding space (Burk *et al.*, 2001). As with apo APH(3')-IIIa, above average temperature factors were observed in the nucleotide-binding loop of the nucleotide-free APH(3')-IIa structure. However, this segment behaves quite differently in APH(3')-IIa. The nucleotide-binding loop of APH(3')-IIa extends outward and upward, away from the phosphate-binding area, such that the side chain hydroxyl group of Ser32 is over 6 Å from the modelled β-phosphate (Nurizzo *et al.*, 2003). It is possible that a substantial conformation change may

be required to bring the loop in front of the bound nucleotide or perhaps, a completely different mechanism may take place in the presence of a nucleotide.

Aminoglycoside-binding Site. Not surprisingly, kanamycin A binds to a highly negatively-charged pocket in the C-terminus of APH(3')-IIa, delimited by the same secondary features as in the aminoglycoside-binding site of APH(3')-IIIa, namely, helix $\alpha 6$ (equivalent to $\alpha 5$ in APH(3')-IIIa), the loop connecting two antiparallel helices $\alpha 4$ (αA) and $\alpha 5$ (αB) or the aminoglycoside-binding loop, and the C-terminal helix. The position and orientation of kanamycin in APH(3')-IIa are almost identical to that in APH(3')-IIIa, occupying sub-sites A and B and forming very similar hydrogen bond interactions with the enzymes (Figure 3–8). The central and the prime rings overlay well but the deviation in the position of the double prime ring is more pronounced, with an estimated displacement of about 2 Å toward the aminoglycoside-binding loop of APH(3')-IIa (Nurizzo *et al.*, 2003).

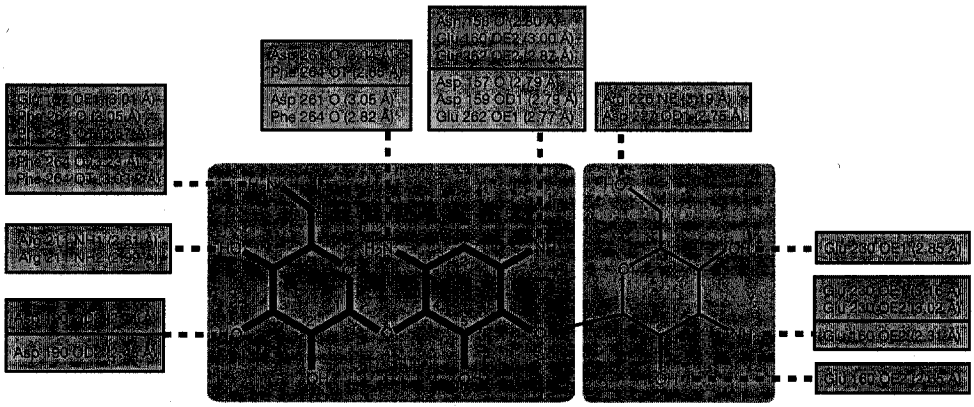

Figure 3–8. Schematic representation of hydrogen bonds made by kanamycin A with APH(3')-IIIa and APH(3')-IIa. Hydrogen bond contacts between kanamycin A and APH(3')-IIIa are displayed in red boxes and those between the antibiotic and APH(3')-IIa are shown in cyan.

Residues 260-264 in the C-terminus are highly conserved among APH(3') enzymes (Figure 1–2) and their importance in APH(3')-IIIa for aminoglycoside binding and recognition has been demonstrated by the ternary structures of APH(3')-IIIa described above as well as mutagenesis experiments (Thompson *et al.*, 1999). The crystal structure of APH(3')-IIa further corroborates the role of the C-terminal helix, particularly the terminal carboxylate, along with Asp190 in positioning the central and prime rings of the aminoglycoside, thereby presenting the 3'-OH to the γ-phosphate for efficient catalysis.

The amino acid sequence in the aminoglycoside-binding loop of APH(3')-IIa and APH(3')-IIIa is not well conserved and this might have resulted in differences in its conformation. Nonetheless, this segment in both enzymes is acidic in nature and partially covers the aminoglycoside-binding site forming many interactions with all three rings of the substrate (Figure 3–8). Sequence alignment has shown that although the distribution of the acidic residues differs, the acidic nature of this region is preserved amongst all APH(3') enzymes (Nurizzo *et al.*, 2003) (Figure 1–2).

The binding of the double prime ring to the enzyme occurs chiefly *via* helix α6 (residues 216–233) in APH(3')-IIa or the equivalent helix α5 in APH(3')-IIIa. This section of the aminoglycoside-binding area shows the most dissimilarity among APH(3') enzymes (Nurizzo *et al.*, 2003) (Figure 1–2). Only a few acidic residues are found in this region and they are concentrated in the C-terminal portion of the helix, in proximity to substrate-binding sub-sites B and C. Asp/Glu231 is well conserved among APH(3') enzymes. Both APH(3')-IIa

and APH(3')-IIIa have Glu230 and it is involved in contacting the double prime ring of the kanamycin. However, Asp227 is unique to APH(3')-II enzymes. This residue is replaced by Ser227 in APH(3')-IIIa. This amino acid substitution may have contributed to the displacement of the double prime ring of kanamycin in APH(3')-IIa since the side chain of aspartate is much larger relative to that of a serine residue. The aspartate side chain points into the aminoglycoside-binding cleft and may force the double prime ring to shift away from helix $\alpha 6$ and toward the aminoglycoside-binding loop.

The amino acid variations, the differing conformations in the aminoglycoside-binding loop, and the differences in the interactions that these two enzymes make with the same substrate may be the major contributors to the broad and distinct substrate specificity of the APH(3') enzymes. Nevertheless, a structure of APH(3')-IIIa bound with a 4,5-disubstituted aminoglycoside with the 5"-OH positioned for phosphorylation is required to resolve the difference in substrate specificity between APH(3')-IIa and APH(3')-IIIa and to discern the features dictating the substrate specificity and recognition of the APH(3') enzymes.

3.4.4 Binding of Aminoglycosides with a 4-amino-2-hydroxybutyrate (AHB)

The significance of the aminoglycoside-binding loop in accepting and positioning structurally diverse aminoglycosides in the binding pocket of APH(3')-IIIa is further emphasized by the structures of butirosin ternary complex. As mentioned in Section 1.4.1, the presence of the AHB at position N1 of butirosin results in a reduction in binding affinity toward most resistance factors, yet has

no effect on its bactericidal properties. It is believed that the AHB at position 1 of the central 2-deoxystreptamine ring hampers the binding of the aminoglycoside to the AMEs. Nonetheless, butirosin, amikacin, and isepamicin are unable to evade the recognition and inactivation by APH(3')-IIIa. The structure of the butirosin A ternary complex illustrates that the substrate-binding pocket of APH(3')-IIIa is highly malleable due to the flexible substrate-binding loop. The loop accommodates butirosin A by receding from the core of the aminoglcoside to make space for the AHB group at the central ring. It can, therefore, be extrapolated that the binding conformation of amikacin to APH(3')-IIIa would be similar to that of kanamycin, but that the AHB would point outward and away from the centre of the enzyme due to the steric hinderance of the double prime ring substituted at position 6. The AHB group would lead the antibiotic-binding loop to adopt a conformation akin to that of the butirosin-bound structures, or it might be placed even farther from the core of the aminoglycoside substrate thus making fewer and possibly less stable interactions with amikacin. Such a postulate would also be in agreement with the unusually high K_m value of amikacin relative to the other APH(3')-IIIa substrates.

3.4.5 Sequential and Regiospecific Diphosphorylation of 4,5 -disubstituted Aminoglycosides

In addition to having a broad substrate spectrum, APH(3')-IIIa is notable for its ability to inactivate lividomycin A (McKay *et al.*, 1994a). Studies have shown that although lividomycin A lacks a 3'-hydroxyl group, its hydroxyl group at position 5" can be targeted for phosphorylation by APH(3')-IIIa. In fact, APH(3')-IIIa can phosphorylate 4,5-disubstituted substrates such as neomycin

and butirosin at either 3'- or 5"-hydroxyl group alone, or at both sites (Thompson *et al.*, 1996b).

Although the aminoglycoside substrates in both the butirosin-bound ternary structures as well as the neomycin-bound complex are oriented with their 3'-OH directed toward the γ-phosphate, the most notable and surprising difference between the two butirosin A ternary complexes is the presence of a 5"-monophosphorylated version of the aminoglycoside substrate in its binding pocket. It is intriguing to observe a 5"-monophosphorylated butirosin A in the binding pocket, since the native function of the enzyme is to catalyze the phosphoryl transfer to the 3'-OH of the aminoglycoside and thus a preponderance of the 3'-monophosphorylated product is expected. Given that the same starting materials were used in both crystallization experiments, a possible explanation for the different forms of substrate could be the length of time it took for crystals to form. Although AMPPNP is a non-hydrolyzable analogue of ATP, it is possible that β-γ-phosphate bond could hydrolyze over time. Since the crystal in space group $P4_322$ (the one containing the phosphorylated form of butirosin A) took approximately 6 months to grow, it is very likely that the phosphoryl transfer reaction had taken place using AMPPNP. The phosphorylation could have occurred in solution before crystalline material began to form, or the phosphorylation could have taken place inside the crystal. So far, there are no data indicating how the aminoglycoside would bind for 5"-phosphorylation. If the phosphoryl transfer reaction occurred inside the crystal, the binding position and orientation of the aminoglycoside for both 3'- and 5"-phosphorylation would

have to be identical or very similar. However, this seems unlikely since it has been shown that APH(3')-IIIa catalyzes a direct phosphoryl transfer (Thompson *et al.*, 1996a) and the distance between the γ-phosphate and the 5"-OH is over 6 Å. Any changes in the position and conformation of the aminoglycoside would probably affect the architecture of the aminoglycoside-binding loop. This in turn could lead to changes in intermolecular, and hence crystal, contacts since Cys156 forms a disulfide bond with Cys19 of the adjacent protein molecule. Moreover, there was no ambiguity in the electron density for the substrate as to the orientation and conformation of the aminoglycoside. The aminoglycoside was modelled in only one conformation with the 3'-OH closest to the γ-phosphate and Asp190 of APH(3')-IIIa. Therefore, it can be concluded that the phosphorylation most likely occurred in solution before crystals began to form.

Multiple regiospecificity is not unique to APH(3')-IIIa. Numerous proteins can be multiply phosphorylated by a single protein kinase (Roach, 1991). Often the target sites are recognized through specific determinants in the polypeptide sequence. Several inositol phosphate kinases are able to target inositol at various phosphorylated states (Shears, 2004). This is proposed to be accomplished by presenting the enzyme with the same recognition motif by altering the substrate binding conformation. Other examples of enzymes with multiple positional specificity include a fatty acyl-acyl carrier protein (ACP) desaturase from English Ivy (*Hedera helix*) (Whittle *et al.*, 2005), various *S*-adenosyl-L-methionine-dependent flavonol and caffeoyl-CoA-specific *O*-methyltransferases (Ibdah *et al.*, 2003; Cacace *et al.*, 2003; Lavid *et al.*, 2002; Scalliet *et al.*, 2002)

and several phosphoethanolamine-specific *N*-methyltransferases (Nuccio *et al.*, 2000; Bolognese and McGraw, 2000; Charron *et al.*, 2002) as well as fatty acid lipoxygenases from both plants and mammals (Feussner and Wasternack, 2002). Although no concrete evidence regarding the mechanism of multiple positional specificity has been reported for these enzymes, hypotheses have been put forward to explain the phenomenon, namely, a spacious and/or flexible binding pocket (Feussner and Wasternack, 2002; Ibdah *et al.*, 2003) and distinct substrate binding orientation for each regiospecific reaction (Feussner and Wasternack, 2002; Whittle *et al.*, 2005).

The crystal structures of two AACs with differing regiospecificities, AAC(2')-Ic and AAC(6')-Iy, have recently been elucidated (Vetting *et al.*, 2002, 2004). Although lacking high sequence identity, the overall structural organization of the two enzymes is similar. However, the two active sites differ in shape and size due to the varying secondary structures and their arrangement. In addition, the aminoglycoside substrates adopt different binding orientations and conformations in the two enzymes in order to properly orient the target amino group toward the acetyl-CoA.

For APH(3')-IIIa, a crystal structure of the enzyme with the 5"-hydroxyl group of a 4,5-disubstituted aminoglycoside aligned with the γ-phosphate of AMPPNP is lacking to definitively illustrate the recognition mechanism of diphosphorylation, and unfortunately the existing data are unable to fully explain the substrate binding properties for the 5"-phosphorylation. Nonetheless, it is reasonable to propose that the binding mode of 4,5-disubstituted aminoglycosides

for 5"-phosphorylation must be distinct from that seen in the crystal structures described above in order to align the 5"-OH for the direct attack of the γ-phosphate. Moreover, the conformation of the aminoglycoside may also undergo changes in order to fit into the binding pocket.

CHAPTER 4
3'-Aminoglycoside Phosphotransferase Type IIIa complexed with a Eukaryotic Protein Kinase Inhibitor, CKI-7

Text and figures regarding the crystallization procedure of APH(3')-IIIa–CKI-7 complex were taken from the journal article: Fong, D.H. and Berghuis, A.M. (2004) Crystallization and preliminary crystallographic analysis of 3'-aminoglycoside kinase type IIIa complexed with a eukaryotic protein kinase inhibitor, CKI-7. *Acta crystallogr. D.* **60**: 1897–1899. With permission from the International Union of Crystallography.

4.1 Introduction

The investigation of aminoglycoside kinase inhibitors that target the nucleotide-binding pocket was motivated by the structural similarities between APH(3')-IIIa and serine/threonine and tyrosine ePKs (specifically around the nucleotide-binding pocket) as described in section 1.3. It was subsequently shown that APH(3')-IIIa is capable of phosphorylating serine residues of some peptide substrates of ePKs (Daigle *et al.*, 1999b). More importantly, it can also be inhibited by protein kinase inhibitors of the isoquinolinesulfonamide family which are competitive with ATP-binding (Daigle *et al.*, 1997). For example, the casein kinase 1 (CK1) inhibitor *N*-(2-aminoethyl)-5-chloro-isoquinoline-8-sulfonamide (CKI-7) has an inhibition constant of 65 μM for APH(3')-IIIa. Unfortunately, these

compounds are only able to inhibit the resistance enzymes *in vitro* and cannot rescue the function of aminoglycosides in enterococcal strains harboring *aph(3')-IIIa* genes (Daigle *et al.*, 1997). Nonetheless, the basis of this study was to identify starting compounds that can be modified to inhibitors with high affinity and selectivity for the nucleotide-binding site of APH(3')-IIIa, thus preventing the binding of ATP. As a result, the enzyme function is disrupted and the aminoglycoside is free to bind to its intended target and exert its bactericidal effects. A similar strategy has been employed to combat resistance to β-lactams due to β-lactamase activity (Therrien and Levesque, 2000). The use of drug-adjuvant therapy has lessened the use of cephalosporins, thus extending their effective life expectancy and allowing them to remain useful for more serious infections (Paterson, 1999). Ultimately, it is hoped that broad-spectrum inhibitors could be developed to target all AMEs that utilize ATP as a cofactor (i.e. APHs and ANTs), leading to renewed antimicrobial therapies using existing aminoglycosides with adjuvant AME inhibitors.

In this chapter, the three-dimensional structure of the APH(3')-IIIa in complex with CKI-7 will be described. Comparison of the APH(3')-IIIa–inhibitor complex with the nucleotide-bound APH(3')-IIIa, as well as the CKI-7-bound CK1 and various isoquinolinesulfonamides-bound cAPK complexes will be presented. The comparative analysis reveals the different inhibitor binding modes as well as topological features which could be exploited in the development of inhibitors with enhanced affinity and selectivity for APH(3')-IIIa. Furthermore,

the program LigBuilder (Wang *et al.*, 2000) was used for the construction of ligands based on CKI-7 and three-dimensional structure of its binding pocket.

4.2 Experimental Procedures

4.2.1 Crystallization

Past experiences have shown that APH(3')-IIIa can crystallize in a variety of crystal forms, depending on the presence and/or absence of ligands or ligand-analogues. The APH(3')-IIIa apo form crystallizes in space group $P4_32_12$ with cell dimensions a = b = 55, c = 185 Å (Burk *et al.*, 2001), the nucleotide-bound state crystallizes in space group $P2_12_12_1$ with cell dimensions a = 50, b = 91, c = 132 Å (Burk *et al.*, 2001; Hon *et al.*, 1997), and the ternary complex crystals possess either space group $P4_322$ with cell dimensions a = b = 47, c = 301 Å (Fong and Berghuis, 2002) or space group $P4_22_12$ with cell dimensions a = b = 80, c = 110 Å. The initial strategy for crystallizing APH(3')-IIIa in complex with CKI-7 was to pursue crystallization conditions and procedures akin to those used for obtaining nucleotide-bound or ternary complexes crystals, substituting the CK1 inhibitor for the nucleotide. These crystallization trials proved completely fruitless and thus a sparse-matrix screening approach was taken to obtain suitable crystallization conditions.

APH(3')-IIIa was expressed and purified using previously established procedures (McKay *et al.*, 1994a). The pure protein was then dialysed in 25 mM sodium cacodylate pH 7.0 and its concentration adjusted to 10 mg/mL. A 5-time molar excess of CKI-7 was added to the protein solution. Initial screening was carried out using methods detailed in section 2.3.2.

One condition from preliminary sparse-matrix crystallization experiments (20% (w/v) PEG 3000, 0.1 M 2-amino-2-(hydroxymethyl)1,3-propanediol (Tris) pH 7.0, and 0.2 M calcium acetate, at 4 °C) produced thin plate crystals with uneven edges and surfaces (Figure 4–1a). Extensive fine-screening by varying the protein concentration, the amounts of precipitant, salt and pH did not significantly improve crystal quality (Figure 4–1b). Subsequently, the microseeding method was attempted. A crystal was placed in a stabilizing solution (25–35% PEG 3000, 0.1 M Tris pH 7.5–8.0, and 0.2 M calcium acetate) and crushed using a Seed Bead (Hampton Research). This microseed stock was then diluted 10 to 10^3 times and 1 μL of the microseed slurry was added to drops containing reduced concentrations of precipitant and protein. Crystals appeared in these drops after approximately one week. Although these plate-shaped crystals were small and thin (Figure 4–1c), some had edges and surfaces much sharper and smoother than the ones grown in the absence of seeds. This procedure was repeated where an improved crystal was used as seed in the following cycle. Each subsequent round of the microseeding produced single rod-shaped crystals that were progressively larger and thicker (Figure 4–1d-f). The reservoir solutions for the fourth and final round of microseeding contained 10–12% (w/v) PEG 3000, 0.1 M Tris pH 7.0–8.5, and 0.2 M calcium acetate. Crystals grew to approximately 0.55 mm x 0.15 mm x 0.05 mm in about 4 weeks in drops containing 3.5 μL of reservoir solution, 3.5 μL of APH(3')-IIIa–CKI-7 solution at 6 mg/mL, and 1 μL of the microseed slurry diluted 10^3 times in a stabilizing solution containing 25% (w/v) PEG 3000, 0.1 M Tris pH 8.0 and 0.2 M calcium acetate.

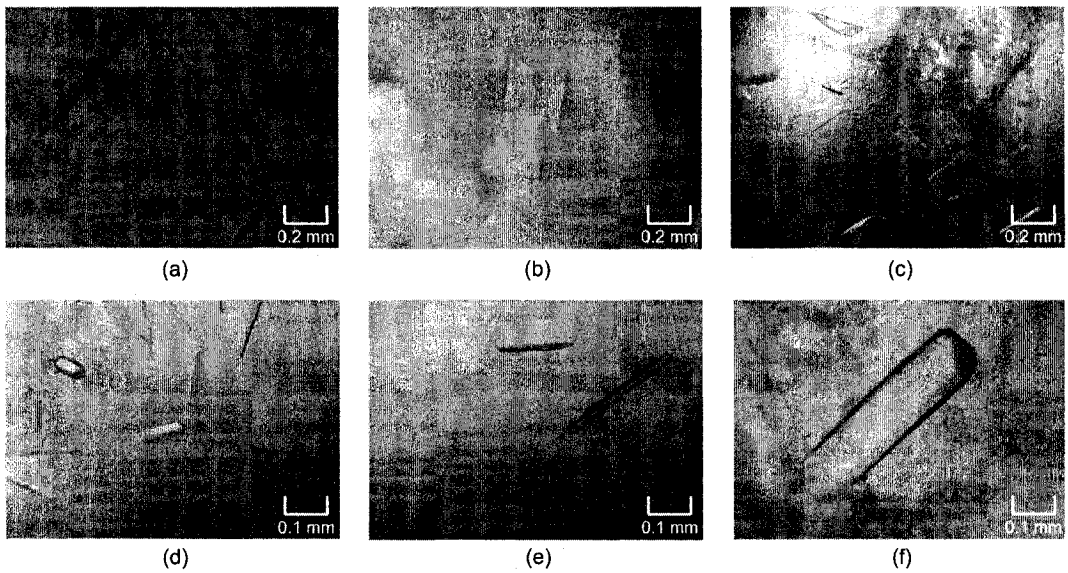

Figure 4–1. Typical crystals of the APH(3')-IIIa-CKI-7 complex at various stages of optimization. **a.** Crystals of APH(3')-IIIa with CKI-7 obtained from sparse-matrix screening. **b.** Crystals observed after refining protein and precipitant concentrations, as well as pH. **c.** Crystals grown from employing the microseeding technique. **d-f.** Typical crystals obtained from subsequent successive cycles of microseeding. Photographs were taken under polarized light. *Reproduced with permission from the International Union of Crystallography.*

4.2.2 Data Collection and Processing

Data from a single crystal were collected under cryogenic conditions (110 K) at beamline X8C of the NSLS at BNL, equipped with an ASDC Quantum CCD detector. The crystal was soaked for approximately two minutes in the mother liquor supplemented with 12.5% (v/v) 2-methyl-2,4-pentanediol (MPD) and 12.5% (v/v) PEG 600 before being flash-frozen in the cold stream for data collection. The crystal-to-detector distance was set at 200 mm and the data were collected with an oscillation angle of 1.0° and a wavelength of 1.072 Å. Intensities were integrated using HKL-2000 and scaled using the HKL program

suite (Otwinowski and Minor, 1997). Relevant data collection statistics are summarized in Table 4–1. Assuming the presence of two molecules per asymmetric unit, the Matthews coefficient (V_m) (Matthews, 1968) has a value of 2.4 Å^3/Da and the solvent content is about 49%.

Table 4–1. Data collection statistics for APH(3')-IIIa in complex with eukaryotic protein kinase inhibitor, CKI-7

Space group	$P2_12_12_1$
Unit cell parameters (Å,°)	$a = 49.84$ $b = 91.90$ $c = 131.2$ $\alpha = \beta = \gamma = 90$
Resolution limit (Å)	2.50
Reflections observed	101620
Unique reflections	21525
Data redundancy (outer shell)	4.7 (4.3)
Completeness (%) (outer shell)	99.6 (99.8)
Mean $I/\sigma(I)$ (outer shell)	24.9 (8.0)
R_{sym} (outer shell)	0.045 (0.124)

Reproduced with permission from the International Union of Crystallography.

4.2.3 Structure Determination and Refinement

Despite different crystal growth conditions, the APH(3')-IIIa–CKI-7 crystal was isomorphous with APH(3')-IIIa–nucleotide crystals. However, the crystallization conditions of the APH(3')-IIIa–CKI-7 complex are sufficiently different from those previously reported that it is understandable that our initial attempts to exploit previous crystallization conditions proved unsuccessful.

The APH(3')-IIIa–ADP structure (Hon *et al.*, 1997; Burk *et al.*, 2001), excluding the ligands and solvent molecules, was used as the starting model for the refinement of APH(3')-IIIa–CKI-7 complex using the program CNS (Brünger *et al.*, 1998). After rigid body refinement and one round of positional and grouped thermal factor refinement, one molecule of CKI-7 was modelled in each active site in the space where difference maps ($2F_o$-F_c and F_o-F_c) displayed positive electron density. The stereochemical parameters for CKI-7 used in subsequent refinement were based on the conformation of the inhibitor found in the crystal structure of CK1 (PDB code: 2CSN) (Xu *et al.*, 1996) in conjunction with values from the energy minimized conformation obtained from the molecular mechanics program MM2 (Allinger, 1977; Burkert and Allinger, 1982) implemented in Chem3D (CambridgeSoft).

Upon inspection, several regions required remodelling due to considerable deviations from the difference electron density maps. These areas were residues 21–27 (nucleotide-binding loop), residues 100–108 (hinge region), and residues 153–167 (aminoglycoside-binding loop). Rebuilding of these areas were accomplished in the program O (Jones *et al.*, 1991) based on difference electron density maps as well as a simulated-annealing omit map. Moreover, a strong electron density peak located between the antibiotic-binding loop and the C-terminal helix near residues 153 and 262 was observed. A solvent molecule was initially modelled at this position, however, the low thermal factor relative to its surrounding atoms and the apparent octahedral coordination suggested otherwise.

Consequently, a calcium ion, which would have originated from the crystallization solution, was modelled into the positive peak. Following that, cycles of positional and individual thermal factor refinement, alternated with manual refitting and addition of solvent molecules were repeated until no further improvement in model statistics could be obtained. Final refinement statistics are given in Table 4–2.

Table 4–2. Refinement statistics for APH(3')-IIIa in complex with eukaryotic protein kinase inhibitor, CKI-7

Number of reflections	
Working set	19106
Test set	2111
Number of atoms	
Protein	4340
Inhibitor	36
Ca^{2+}	2
Solvent	202
R_{cryst}	0.206
R_{free}	0.265
r.m.s.d.	
Bonds (Å)	0.006
Angles (°)	1.218

4.2.4 Inhibitor Design

The program LigBuilder (Wang *et al.*, 2000) was used for constructing ligand molecules based on CKI-7 substructures as seed molecules and according to the structural and chemical properties of the nucleotide-binding pocket of APH(3')-IIIa. First, the POCKET algorithm was used to analyze the nucleotide-binding

pocket of APH(3')-IIIa. The ADP-bound complex structure was used as the input for POCKET. The GROW module was then used for building ligands from a seed molecule pre-placed in the binding pocket. Three core substructures of CKI-7 were used for ligand building: isoquinoline, 8-isoquinolinesulfonamide, and 5-isoquinolinesulfonamide. The isoquinoline and the 8-isoquinolinesuflonamide were in the same binding mode as that of CKI-7 observed in the APH(3')-IIIa crystal structure. A second binding mode applied to the isoquinoline and the 5-isoquinolinesulfonamide is akin to that of the modelled H7 in APH(3')-IIIa. All available hydrogens on the seed molecules were designated for growing. Default building-block library, chemical rules, and forbidden structure and toxic structure libraries were used in the process. In addition, the following criteria were applied to ligand selection: the molecular weight of the ligand should fall in the range of 250 and 500 Da, the LogP value should lie between 3 and 6, a minimum of 2, but not exceeding 6, hydrogen bond donating or accepting atoms are allowed, and the ligand should have a binding affinity between 5 and 10 in pKd units. GROW was submitted with a population size of 3000 and a generation limit of 20. A maximum of 25 molecules were produced for each seed structure.

4.3 Results and Discussion

4.3.1 Overall Structure of CKI-7-bound APH(3')-IIIa

The APH(3')-IIIa–CKI-7 inhibitor complex was crystallized in the space group $P2_12_12_1$ and there were two inhibitor-bound enzyme molecules in the asymmetric unit, analogous to the nucleotide-bound enzyme complexes (Hon *et al.*, 1997; Burk *et al.*, 2001). The structure has been refined to 2.5 Å with

an R_{cryst} of 0.206 and R_{free} of 0.265. This crystal structure represents the first structure of an eukaryotic protein kinase inhibitor complexed to an enzyme that is not an eukaryotic protein kinase. The two molecules of APH(3')-IIIa–CKI-7 in the asymmetric unit were superposed with the ADP-bound APH(3')-IIIa dimer (Hon *et al.*, 1997; Burk *et al.*, 2001) using all main chain atoms by the least-squares method as implemented in the program LSQMAN (Kleywegt, 1996). The average rmsd for the main chain atoms between all the monomers in the two structures is 0.58 Å. In comparison to the rmsd values between the monomers in the ADP- or the CKI-7-bound structures, which are 0.42 and 0.39 respectively, the nucleotide- and inhibitor-bound APH(3')-IIIa do not display marked differences. Further examination between the overall structures of the inhibitor- and the nucleotide-bound enzyme indicate that only minor variations can be observed in the following segments: residues 21–27, 100–108, and 153–167. Residues 100-108 contains part of the tethering segment connecting the N- and C-terminal lobes of APH(3')-IIIa. Conformational differences in this section are observed in all 4 forms of APH(3')-IIIa crystal structures (the apo and nucleotide-bound enzymes (Hon *et al.*, 1997; Burk *et al.*, 2001), the ternary complexes (Fong and Berghuis, 2002, Chapter 3), and the inhibitor-bound enzyme described here) and can be ascribed to the inherent flexibility of this segment, as affirmed by poor electron density and thermal factors that are two to three standard deviations above average.

Residues 153–167 constitute the antibiotic-binding loop and its conformation is dictated by the absence or presence of the antibiotic substrate. In the

presence of an aminoglycoside, the loop moves toward and encloses the substrate (Fong and Berghuis, 2002, Section 3.3.2). Conversely, the antibiotic-binding loop in the binary enzyme structures, with no antibiotic substrate, is highly flexible (Burk *et al.*, 2001). In the structure of APH(3')-IIIa bound with CKI-7, the conformation of the antibiotic-binding loop closely resembles that of the nucleotide-bound enzyme complexes and requires only some minor remodelling. Cys156 adopts a different conformation; nonetheless, the disulfide bond between Cys19 and Cys156 that is observed in the binary enzyme structures is retained. The key difference in this region is the presence of a calcium ion, originating from the crystallization solution (Fong and Berghuis, 2004, Section 4.2.1) (Figure 4–2). The calcium ion is ligated to the main chain carbonyl of Asp153 and Glu262, side chain carboxyl group of Asp155 and Glu157, and two water molecules, forming an octahedral coordination geometry. Although, no solvent molecules are observed near the calcium ion in the second protomer of CKI-7-bound APH(3')-IIIa, the modelled calcium is retained at this location since the remaining ligand oxygen atoms from the protein satisfy the distance and geometry for calcium coordination. The calcium ion does not appear to play any role in either the structure or mechanism of the enzyme.

The third region that differs in the CKI-7-bound APH(3')-IIIa structure is located in residues 21–27 and it is structurally homologous to the glycine-rich loop in the ePK family. Similar to the antibiotic-binding loop, the conformation of this segment is governed by the nature of the bound ligand. In the nucleotide-bound enzyme structures, the polypeptide is positioned above the phosphate

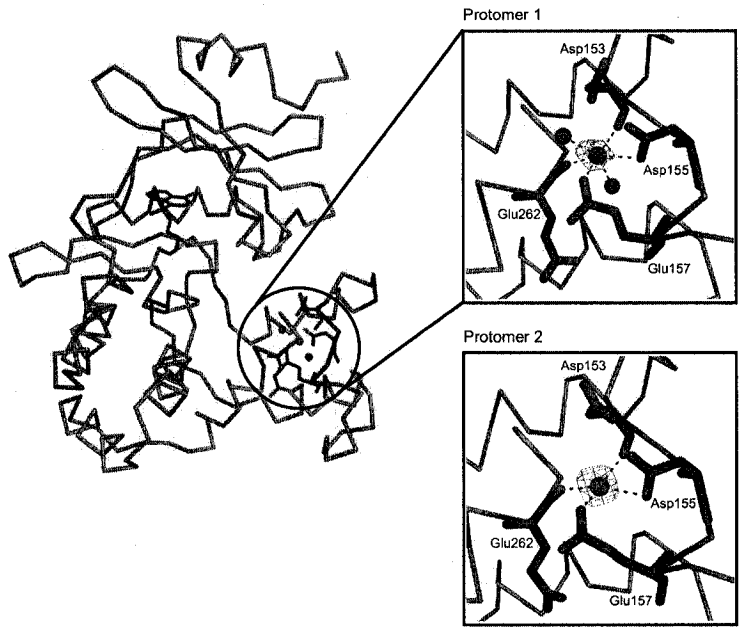

Figure 4–2. Calcium binding site in CKI-7-bound APH(3')-IIIa. The α-carbon trace of monomer 1 of CKI-7-bound APH(3')-IIIa is shown on the left in grey. The CKI-7 inhibitor is coloured blue. The calcium ion is shown as a green sphere; its coordinating amino acids and water molecules are shown in blue sticks and red spheres, respectively. The top and bottom panels on the right show a magnified view of the calcium binding site in monomers 1 and 2 of APH(3')-IIIa, respectively. The simulated annealing F_o-F_c omit map for the calcium ion, contoured at 3σ is also displayed.

moieties of the nucleotide and shielding them; whereas in apo APH(3')-IIIa, this segment moves downward into the vacant nucleotide-binding pocket and occupies part of the cavity (Burk *et al.*, 2001). In the APH(3')-IIIa–CKI-7 structure, the loop containing residues 21–27 adopts an intermediary conformation between those of the binary and the apo enzyme structures. The positions of residues 21–23 are similar to those in the nucleotide-bound enzyme structures, whereas Gly25 and Met26 rotates and extends into the nucleotide-binding pocket, occupying the space that houses the α- and β-phosphates of the nucleotide.

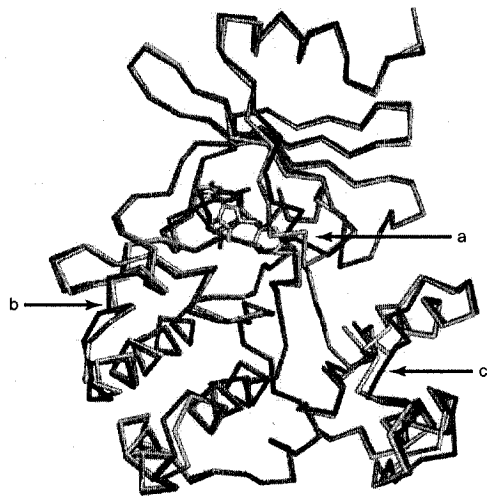

Figure 4–3. Superposition of the CKI-7-bound and ADP-bound APH(3')-IIIa. The α-carbon trace of the CKI-7-bound enzyme is shown in grey whereas the inhibitor is coloured blue. The ADP-bound enzyme is shown in light grey and the bound nucleotide is displayed in yellow. Differences between the two structures are isolated in the following three regions: (a) the nucleotide-binding loop, (b) the tethering segment, and (c) the antibiotic-binding loop. These areas are highlighted in blue and yellow in the CKI-7-bound and the ADP-bound APH(3')-IIIa, respectively.

4.3.2 Inhibitor Binding Site

As expected, the ATP-competitive inhibitor CKI-7 occupies the same location as the nucleotide, between the N- and C-terminal lobes of APH(3')-IIIa. The binding of the inhibitor did not alter the main or side chain conformation of any residues lining the binding pocket, except for the nucleotide-binding loop mentioned above. The isoquinoline ring of the inhibitor is buried in the hydrophobic adenine-binding cleft (Figure 4–4a) and its position and orientation mimic that of the adenine ring of the nucleotide. The binding orientation of the isoquinoline and adenine rings is dictated by the stacking interactions imposed

by the aromatic ring side chain of Tyr42 (Figure 4–4b). This residue is conserved as either a tyrosine or phenylalanine among most APH(3') and APH(2"), as well as APH(3") and APH(9) enzymes (Burk *et al.*, 2001) (Figure 1–2) and will likely induce a similar binding orientation of the adenine moiety in these APH enzymes. For example, the equivalent residue in APH(3')-IIa is Phe48 and when the crystal structure of the kanamycin-bound APH(3')-IIa is superposed with that of APH(3')-IIIa, the two aromatic ring side chains are in an identical orientation. A model of an ATP-bound APH(3')-IIa has been made where placing the adenine moiety in stacking conformation with Phe48 would satisfy the spatial requirements and other hydrophobic interactions expected between the nucleotide and the protein (Nurizzo *et al.*, 2003). Lastly, the CKI-7 is positioned such that its only cyclic nitrogen atom, N2, overlays with N1 of the adenine ring in ATP. A hydrogen bond analogous to the one between N1 of ATP and the amide of Ala93 is also observed in the CKI-7 complex between N2 and the main chain amide.

The remainder of the inhibitor, the aminoethyl-sulfonamide, is situated approximately 45° from the ribose of the nucleotide, toward the solvent exposed opening of the ATP-binding pocket (Figure 4–4b). Alternatively, using the terminology of the different compartments in the ATP-binding site of eukaryotic protein kinases (Cherry and Williams, 2004), the aminoethyl-sulfonamide lies adjacent to the ribose-binding pocket, bordering the specificity surface. This portion of the inhibitor is more flexible than the isoquinoline ring as reflected by the relatively higher thermal factors. Two hydrogen bonds are observed between

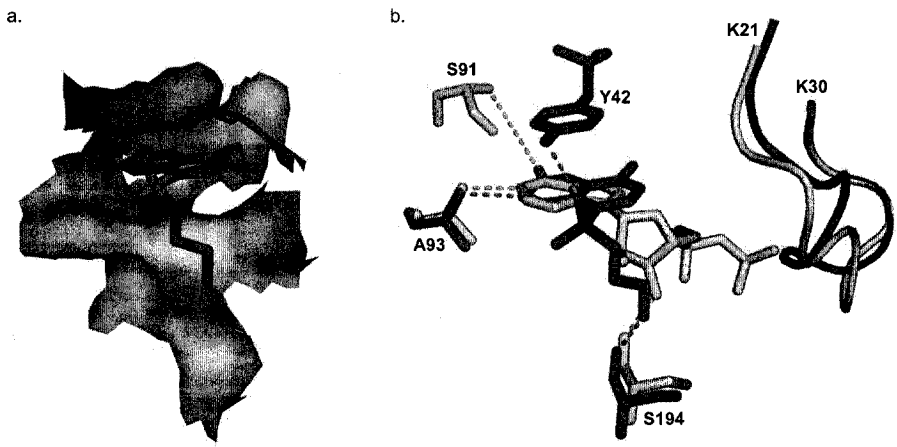

Figure 4–4. The inhibitor-binding pocket of APH(3')-IIIa. **a.** Molecular surface of the APH(3')-IIIa inhibitor-binding site. The inhibitor is represented in sticks. The surface is coloured according to atom type, where non-polar atoms are white, the positively- and negatively-charged atoms are coloured dark blue and red, respectively. The inhibitor-binding pocket is composed of mostly non-polar residues. **b.** Superposition of CKI-7 and ADP in their binding pocket in APH(3')-IIIa. The APH(3')-IIIa–CKI-7 is coloured blue and the APH(3')-IIIa–ADP is coloured yellow. The nucleotide-binding loop is shown in cartoon representation and the amino acid residues that form hydrogen bond interactions with the ligand are drawn as sticks. Hydrogen bonds are depicted as dash lines.

this section of the CKI-7 and the enzyme (Figure 4–4b). One of which is found between one of the oxygen atoms of the sulfonyl group (O2S) and the hydroxyl group of Tyr42. The second hydrogen bond is formed between the terminal nitrogen of the aminoethyl tail, N2', and the main chain carbonyl of Ser194. An analogous interaction is observed in the APH(3')-IIIa-nucleotide complex between the carbonyl of Ser194 and the O3' of the ribose, which overlaps roughly with the N2' atom.

4.3.3 Comparison of inhibitor-bound APH(3')-IIIa and eukaryotic protein kinases

Although many ePKs display similar affinity for ATP, their sensitivity to various classes of inhibitors competitive with ATP varies greatly (Fabian *et al.*, 2005). For example, cyclic-AMP-dependent protein kinases (cAPKs) are highly sensitive to the H-series isoquinolinesulfonamide compounds (Hidaka *et al.*, 1984; Inagaki *et al.*, 1985) whereas CKI-7, also a member of the isoquinolinesulfonamide family, targets CK1 (Chijiwa *et al.*, 1989); quercetin is an effective inhibitor of myosin-light-chain kinase (MLCK) and protein kinase C (PKC) (Hagiwara *et al.*, 1988), and staurosporine inhibits a number of ePKs including cAPK and PKC (Casnellie, 1991; Hidaka *et al.*, 1990). Likewise, APH(3')-IIIa is sensitive to inhibition by isoquinolinesulfonamides and FSBA, but not staurosporine, genistein, or wortmannin (Daigle *et al.*, 1997; Boehr *et al.*, 2001a). The binding modes, hence specificity, of these inhibitors are governed by the variations in the non-conserved amino acid residues and differences in the configuration in and around the ATP-binding pocket. Cross-selectivity of kinase inhibitors is often observed among closely related enzymes. In this case, detailed structural information of the binding site becomes invaluable. Numerous three-dimensional structures of ePK–nucleotide or ePK–inhibitor complexes have revealed differences in enzyme-ligand interactions (Xu *et al.*, 1996; Engh *et al.*, 1996; Prade *et al.*, 1997; Mohammadi *et al.*, 1997; Wilson *et al.*, 1997; Lawrie *et al.*, 1997; Furet *et al.*, 2002; Knighton *et al.*, 1991; Yang *et al.*, 2004; Xu *et al.*, 1995). Detailed analyses of these structures along with those of nucleotide- and inhibitor-bound APH(3')-IIIa would discern features that can be exploited for the design

or improvement of inhibitory compounds with increased selectivity and potency for APH(3')-IIIa.

CKI-7-bound APH(3')-IIIa *versus* CKI-7-bound casein kinase 1 (CK1). To date, CK1 isolated from *Schizosaccharomyces pombe* is the only enzyme, other then APH(3')-IIIa, whose structure has been solved with a CKI-7 inhibitor (Xu *et al.*, 1996) (Figure 4–5). CKI-7 targets CK1 with a K_i value of 8.5 μM (Chijiwa *et al.*, 1989) and it has been commonly used as a tool for investigating the physiological role and distribution of CK1 (Chijiwa *et al.*, 1989; Xu *et al.*, 1996).

Figure 4–5. Structures of CKI-7-bound APH(3')-IIIa, on the left, in blue, and CKI-7-bound CK1, on the right, in pink. The inhibitor is bound to deep cleft between the N- and C-termini in both enzymes and is shown in sticks and coloured orange.

As seen in APH(3')-IIIa, CKI-7 occupies the ATP-binding cleft between the N- and C-terminal domains of CK1 (Xu *et al.*, 1996) (Figure 4–5). The overall structures of the inhibitor- and nucleotide-bound CK1 are the same, differing

slightly in the glycine-rich loop. In the presence of the inhibitor, the aromatic side chain of Phe23 at the tip of the loop points down into the phosphate-binding site, whereas in the presence of the nucleotide the side chain points away from the core of the enzyme. The isoquinoline ring of the inhibitor is coplanar with the adenine moiety of ATP and the aminoethyl-sulfonamide points away from the ribose toward the solvent accessible opening of the binding pocket.

When the CKI-7-bound structures of APH(3')-IIIa and CK1 are superposed using the coordinates of the conserved active site residues (in APH(3')-IIIa numbering: Lys44, Glu60, Asp190, Arg195, and Asp208), it is apparent that the plane of the isoquinoline ring in the APH(3')-IIIa structure differs from that observed in CK1 by a rotation of approximately 40° (Figure 4–6a). This difference was also observed between the adenine rings in the nucleotide-bound APH(3')-IIIa and ePKs (Burk *et al.*, 2001) (Figure 4–6b). As mentioned above, the adenine and isoquinoline rings are in a stacking arrangement with the side chain of Tyr42, a residue highly conserved as a phenylalanine or tyrosine among many APH enzymes (Burk *et al.*, 2001) (Figure 1-2). It has been shown that when Tyr42 is mutated to valine, the affinity of ATP for APH(3')-IIIa is decreased 10-fold (Boehr *et al.*, 2002). Conversely, a Tyr-Phe mutation promoted tighter binding of ATP as well as a concomitant decrease in k_{cat}. These results demonstrated the significance of an aromatic residue at this position in the active site of APH(3')-IIIa. In contrast, the residue in the equivalent position in CK1 and most ePKs is an alanine, excluding a stacking interaction and requiring an alternate arrangement for the ring moiety.

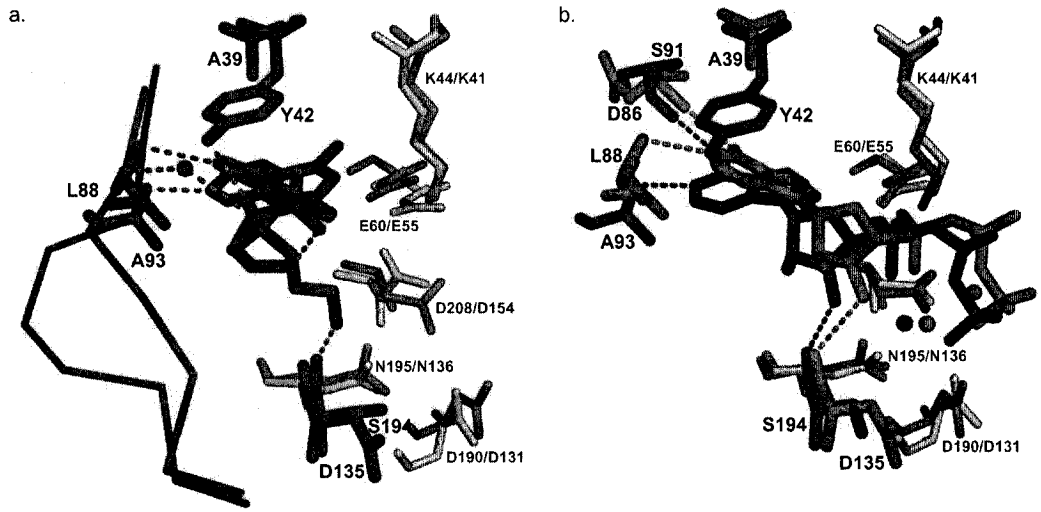

Figure 4–6. Comparison of the CKI-7-/nucleotide-binding pockets of APH(3')-IIIa and CK1. The figure demonstrates the difference in the orientation of the isoquinoline and adenine rings as well as the conserved hydrogen bond between the cyclic nitrogen and the main chain amide in the linker of the enzyme. APH(3')-IIIa and CK1 are superposed using the conserved residues. Conserved residues are drawn in sticks and coloured grey for APH(3')-IIIa and light grey for CK1. **a.** The amino acid residues that make contact with the the inhibitor are coloured blue and pink for APH(3')-IIIa and CK1 respectively. The solvent molecule that mediates contact between the CKI-7 and CK1 is represented as a pink sphere. The α-carbon trace of the linker region of the two enzymes are also shown. **b.** The amino acid residues that make contacts with AMPPNP are coloured dark blue for APH(3')-IIIa and light pink for CK1. The magnesium ions in APH(3')-IIIa are represented as green spheres, whereas the one found in CK1 is shown as a light green sphere.

Although the orientations of the isoquinoline ring of CKI-7 bound to APH(3')-IIIa and CK1 differ considerably, the hydrogen bonds between the cyclic nitrogen and a main chain amide (Ala93 in APH(3')-IIIa and Leu88 in CK1) in the linker region of the enzyme are maintained in both structures (Figure 4–6a). An equivalent hydrogen bond is observed between N1 of adenine and both APH(3')-IIIa and CK1 (Figure 4–6b). This interaction is conserved in all adenine-binding to

ePKs (Sowadski *et al.*, 1999). This hydrogen bond is not unique to isoquinolinesulfonamide type inhibitors binding to the two enzymes discussed here. A majority of ePK crystal structures complexed with an ATP-competitive inhibitor form at least one hydrogen bond with residues in the hinge region, mimicking the ones between N1 and/or the exocyclic N6 of the adenine and the enzyme (Cherry and Williams, 2004). The significance of the hydrogen bond interaction is corroborated by a previous observation in which naphthalene sulfonamide molecules did not display selective inhibition against ePKs until the all-carbon naphthalene ring is substituted with an isoquinoline (Hidaka *et al.*, 1984). This is an important detail to be taken into consideration when designing an inhibitor to occupy the adenine-binding site.

In the CK1–CKI-7 structure, Xu, *et. al.* (1996) noted that the chlorine atom at position 5 of the isoquinoline is within hydrogen bonding distance (3.5 Å) of the hydroxyl of Tyr59, a residue that is highly conserved in CK1 isoforms (Gross and Anderson, 1998; Spadafora *et al.*, 2002). Although, the chlorine atom is a poor hydrogen acceptor (Aullon *et al.*, 1998), dipole-dipole interactions may be important in facilitating the binding and orientation of the inhibitor to the enzyme. This is supported by the observation that *N*-(aminoethyl)isoquinoline-8-sulfonamide (CKI-6), the unchlorinated version of CKI-7, is 5 times less potent against CK1 relative to CKI-7 (Chijiwa *et al.*, 1989). However, the cholrine atom does not appear to be imporatnat in binding to APH(3')-IIIa. The corresponding residue of Tyr59 is Met64 in APH(3')-IIIa which contains no polar groups for interactions with the chlorine atom. Furthermore, due to the rotation of the

isoquinoline ring resulting from the stacking interactions imparted by Tyr42, the chlorine atom of CKI-7 in APH(3')-IIIa is in fact pointing approximately 40° above the plane of the isoquinoline in CK1 and is directed at the space between Met90 and the aliphatic portion of Lys44. Despite its new position, there is still no polar group in the vicinity to exert any polar effects. Nonetheless, in APH(3')-IIIa, the binding of CKI-7 may be compensated for by other polar interactions, such as those between the aminoethyl-sulfonamide and the enzyme.

In addition to the aromatic interactions between Tyr42 and the isoquinoline ring described above, a hydrogen bond is observed between the hydroxyl of the tyrosine residue and the axial sulfonyl oxygen of the inhibitor. In the APH(3')-IIIa structure, the aminoethyl tail of CKI-7 adopts an extended conformation such that the terminal nitrogen (N2') forms a hydrogen bond with the main chain carbonyl of Ser194 (Figure 4–6a). In contrast, the aminoethyl found in the CK1 structure points back at itself and forms an intramolecular interaction with the equatorial sulfonyl oxygen atom. One water-mediated interaction is found between the N_{β} of the inhibitor and the carbonyl of Leu88 in the hinge region of the CK1. No interactions, direct or water-mediated, are observed between the linker of APH(3')-IIIa and the aminoethyl of CKI-7 since this segment is one residue longer in APH(3')-IIIa and is situated over 6 Å away from the binding pocket compared to the equivalent in CK1 (Figure 4–6a).

As mentioned above, the orientations of the aminoethyl-sulfonamide of the CKI-7 in both structures deviate from the ribose and the phosphates of the nucleotide, pointing toward the opening of the binding pocket. This difference

in the binding location is a consequence of the location of the cyclic nitrogen in the isoquinoline ring. In the nucleotide-enzyme complexes, cyclic N1 in the pyrimidine makes a hydrogen bond interaction with the linker of the enzyme. In order to maintain this bond in the inhibitor-enzyme complex, the pyridine ring of the inhibitor must be rotated by 60° toward the hydrophobic pocket such that the cyclic N2 is in the same position as N1 of the pyrimidine. Concomitant with this turn, the aminoethyl portion is swung out toward the solvent exposed opening of the binding pocket.

The superposition of the inhibitor-bound structures of APH(3')-IIIa and CK1 reveals that sulfonamide moiety underwent a 110° rotation around the C8-S bond. As a result, the aminoethyl tail of CKI-7 in CK1 is more distal to the ribose-binding site than that in APH(3')-IIIa and is essentially perpendicular to the ribose and phosphates of the nucleotide.

CKI-7-bound APH(3')-IIIa *versus* H-series isoquinolinesulfonamide-bound cAPK. The H-series isoquinolinesulfonamides are a class of inhibitors in which the isoquinoline core found in the CKI-7-type inhibitors is substituted at position 5 with a sulfonamide group. The H-series inhibitors target an array of ePKs (Hidaka *et al.*, 1984; Inagaki *et al.*, 1985; Chijiwa *et al.*, 1990; Nagumo *et al.*, 2000; Sasaki *et al.*, 2002). X-ray structures of several H-series isoquinolinesulfonamide inhibitors complexed with cAPK have been solved, including 1-(5-isoquinolinesulfonyl)-2-methylpiperazine (H7), *N*-[2-(methylamino)-ethyl]-5-isoquinolinesulfonamide (H8), and *N*-[2-(*p*-bromocinnamylamino)ethyl]-5-isoquinolinesulfonamide (H89) (Engh *et al.*, 1996), as well

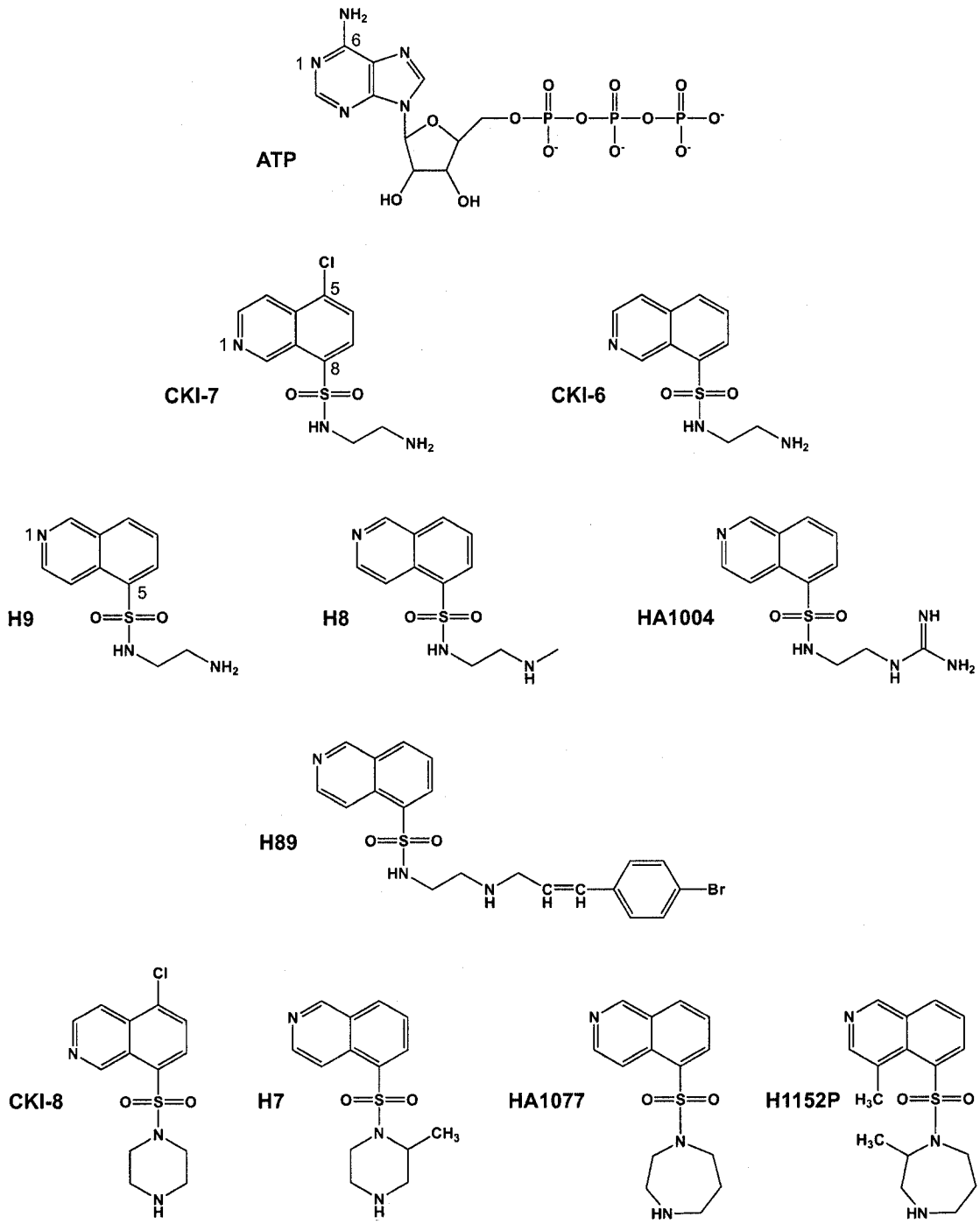

Figure 4–7. Chemical structures of ATP and several eukaryotic protein kinase inhibitors of the isoquinolinesulfonamide family.

as 1-(5-isoquinolinesulfonyl)-homopiperazine hydrochloride (HA1077) or Fasudil and (S)-(+)-2-Methyl-1-[(4-methyl-5-isoquinolynyl)sulfonyl]homopiperazine (H1152P) (Breitenlechner *et al.*, 2003) (Figure 4–7). Several members of this class of inhibitors have been shown to be capable of inhibiting the activity of APH(3')-IIIa. Among those of which X-ray structures are available, H7 has been tested, giving K_i value of 730 μM (Daigle *et al.*, 1997). Two other H-series isoquinolinesulfonamides *N*-(2-aminoethyl)-5-isoquinolinesulfonamide (H9) and *N*-(2-guanidino-ethyl)-5-isoquinolinesulfonamide (HA1004), have also been shown to effectively inhibit APH(3')-IIIa activity with K_i values of 138 μM and 48.9 μM, respectively. The crystal structure of cAPK–H7 is of particular interest since the information regarding the binding conformation of the inhibitor can be used to deduce a model of binding of H-series isoquinolinesulfonamides to APH(3')-IIIa.

The overall structures of the H-series inhibitor-bound cAPK are largely the same, but differ from the nucleotide-bound enzyme in the glycine-rich loop (Gly50 to Val57) (Figure 4–8). Evidence suggests that this region can adopt multiple conformations (Engh *et al.*, 1996; Breitenlechner *et al.*, 2003). A single loop conformation is observed in the H89-bound enzyme, in contrast to at least two conformations that can be modelled in the other H-isoquinolinesulfonamide-bound structures (Engh *et al.*, 1996; Breitenlechner *et al.*, 2003). The dominant conformation observed in these inhibitor-bound structures is more open compared to the ternary complex of cAPK (Engh *et al.*, 1996; Breitenlechner *et al.*,

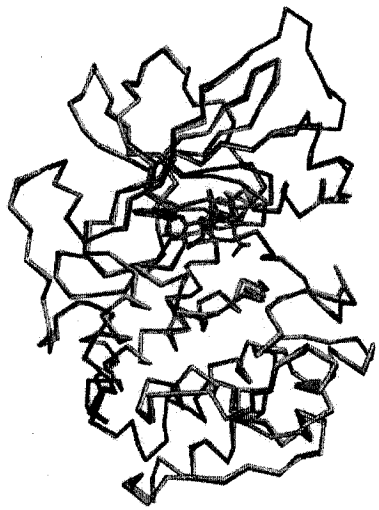

Figure 4–8. Superposition of the H89-bound and AMPPNP-bound cAPK. The α-carbon trace of the H89-bound enzyme is shown in grey whereas the inhibitor is coloured teal. The AMPPNP-bound enzyme is shown in light grey and the bound nucleotide is displayed in brown. The only notable difference between the two structures is localized in the glycine-rich loop, which assumes a more open conformation in the H89-bound enzyme. This area is highlighted in teal and brown in the H89-bound and the AMPPNP-bound cAPK, respectively.

2003). This upper, and the sole, conformation observed in the H89-bound enzyme is secured by the large bromocinnamylamino-ethyl moiety that fills the entire nucleotide-binding cavity and extends away from the peptide-binding site (Figure 4–8). The upper conformation is also observed in partial occupancy in the other inhibitor-bound structures; but a second middle, and possibly a third lower, conformation can also be modelled (Engh *et al.*, 1996; Breitenlechner *et al.*, 2003).

The superposition of the isoquinolinesulfonamide-bound structures of cAPK shows that the isoquinoline rings of H7, H8, H89, HA1077, and H1152P lie congruently in the hydrophobic adenine-binding pocket and are also coplanar with

the adenine ring of ATP (Figure 4–9), akin to ligand binding in the adenine-binding pocket in CK1 and APH(3')-IIIa. This observation emphasizes the role of aromatic interaction between Tyr42 in APH(3')-IIIa and the adenine/isoquinoline ring structure. The hydrogen bond between the cyclic N1 in the isoquinoline of the H-series inhibitors and the main chain amide of Val123 in the tethering segment in cAPK is also conserved, further underlining the significance of this polar interaction (Figure 4–11).

Relative to APH(3')-IIIa, CK1 and cAPK have a more compact specificity surface (Cherry and Williams, 2004) (Figure 4–10). As mentioned above, the linker region of APH(3')-IIIa has a one-residue insert compared to CK1 and it adopts a different conformation due to the structural divergence in the C-terminal lobe of the the two enzymes (Hon *et al.*, 1997). Although the linker region in cAPK is also one residue longer than that in CK1 thus forming a wider specificity surface, the C-terminus of cAPK stretches across the opening of the binding cleft and reduces the extent of the specificity surface. Furthermore, Ser91 on the periphery of the specificity surface in CK1 is replaced by a larger amino acid, Glu127, in cAPK, thus affecting ligand specificity (Figure 4–10).

The sulfonyl groups of H7, HA1077, and H1152P are oriented similarly to that in CKI-7 bound to APH(3')-IIIa (Figure 4–9b,c). However, the H8 and H89 sulfonyl groups differ from the others by a rotation of approximately 85° about the C5-S bond (Engh *et al.*, 1996) (Figure 4–9a). Regardless of the orientation of the oxygen atoms of the sulfonyl group, the sulfonamine group and the distinct parts of the H-series inhibitors superpose well with each other. Furthermore,

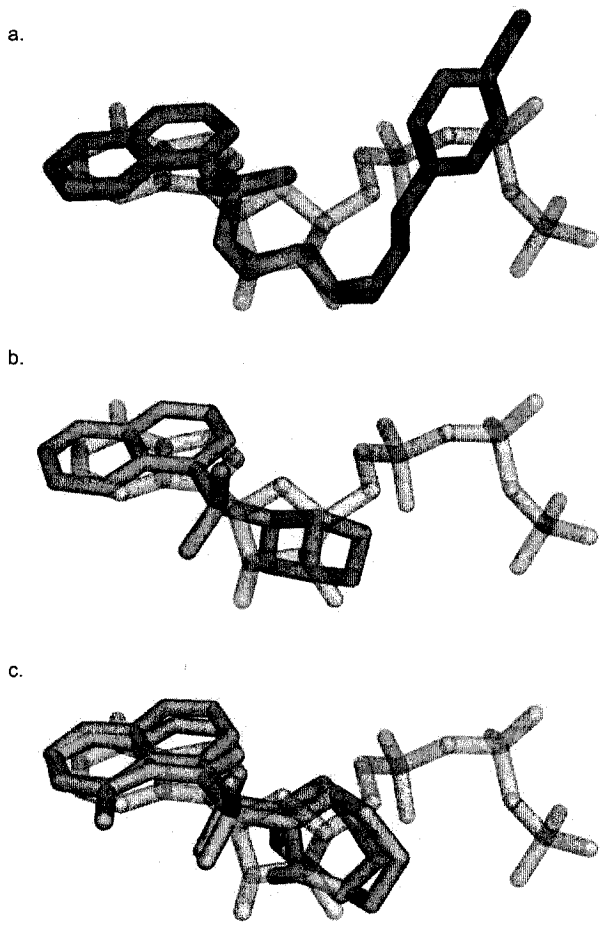

Figure 4–9. Comparison of the binding modes of H-isoquinolinesulfonamide inhibitors. ATP is shown in semi-transparent grey sticks. **a.** Superposition of H8, in green, and H89, in teal, with ATP. **b.** H7, coloured lime green, is superposed on ATP. **c.** Overlay of HA1077, in light green, H1152P, in light yellow, and ATP. These superpositions show congruency in the binding mode of the isoquinoline and adenine rings, as well as the colocalization of the tail fragment of the inhibitor and the ribose sugar of the nucleotide.

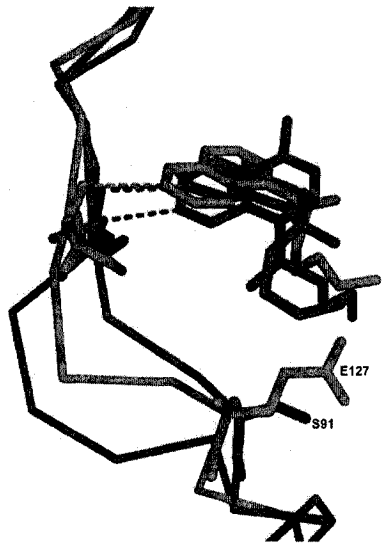

Figure 4–10. Comparison of the inhibitor-binding pocket near the linker regions of APH(3')-IIIa, CK1, and cAPK. The linker of the kinases are drawn in ribbon representation. APH(3')-IIIa is coloured in blue, CK1 in pink and cAPK in green. Ser93 and Leu88, whose amide form a hydrogen bond with the cyclic nitrogen of CKI-7 bound to APH(3')-IIIa and CK1, respectively, are shown in sticks. The equivalent residue in cAPK (Val123), whose amide form an equivalent hydrogen bond with H8, is also shown as stick representation. The inhibitors are coloured in the same scheme as the enzyme to which they are bound. Ser91 which borders the opening of the binding cleft in CK1 and its equivalent in cAPK, Glu127, are shown as sticks. The overlay of the binding cleft shows that CK1 has the narrowest specificity surface since it has a shorter linker segment.

compared to the inhibitor-bound structures of CK1 and APH(3')-IIIa, the tail of the inhibitors also superpose well with the ribose of the nucleotide (Figure 4–9). Unlike CKI-7 in which the inhibitor is rotated in order to align the cyclic N2 with the main chain amide of the enzyme linker, the cyclic N1 of the H-series inhibitors leads to a more parallel superposition between the isoquinoline and adenine rings. Hence, the groups substituted at position 5 of the isoquinoline are placed proximately to the ribose.

Despite variations in the size and structure of the tail section of the isoquinolinesulfonamide inhibitors, the number and pattern of polar interactions made with the enzymes are comparable (Figure 4–11). Apart from the hydrogen bond found between the isoquinoline cyclic nitrogen and the amide of Val123 in the linker region, all the H-series inhibitors, except H1152P, make additional polar contacts with the enzyme. The N4' atom in the H-series inhibitors forms a hydrogen bond with the carbonyl of Glu170 (Engh *et al.*, 1996; Breitenlechner *et al.*, 2003), equivalent to the hydrogen bond interaction found between N2' in CKI-7 and the carbonyl of Ser194. H8 and H89 make a water-mediated interaction with the side chain of Glu127 *via* N1', the nitrogen in the sulfonamide group; whereas in the HA1077-bound cAPK, a small shift in the side chain of Glu127 gives rise to a direct contact between the side chain $\epsilon 2$ oxygen and the homopiperazine amine (Breitenlechner *et al.*, 2003). Additional direct and solvent-mediated interactions are also observed and illustrated in Figure 4–11 (Engh *et al.*, 1996; Breitenlechner *et al.*, 2003).

The binding mode of H-series isoquinolinesulfonamides in APH(3')-IIIa can be speculated by extrapolating from existing data. The H-isoquinolinesulfonamide inhibitors could be viewed as comprised of two modules, the isoquinoline ring and the differing tail fragments, linked by the sulfonamide substituted at position 5 of the isoquinoline. Two requirements need to be fulfilled for the binding of the isoquinoline ring. First, the isoquinoline ring should lie coplanar to the adenine of the nucleotide, as observed in the existing structures. Therefore the plane of the isoquinoline ring moiety would also be rotated 40° relative to that

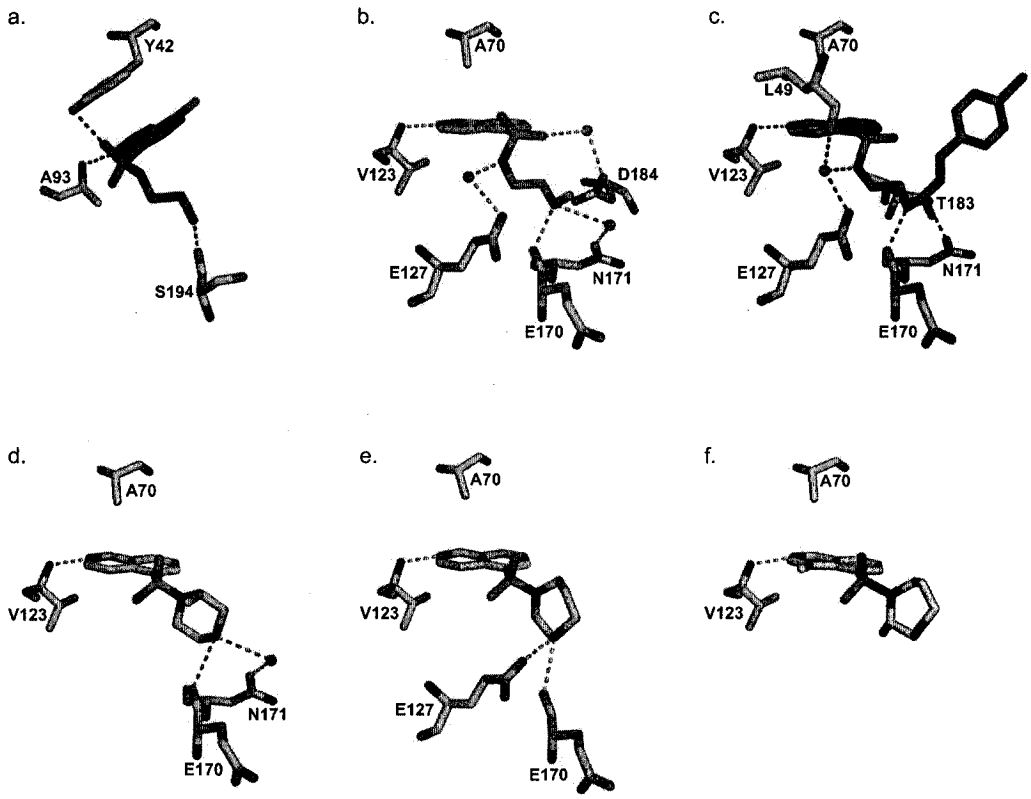

Figure 4–11. Hydrogen bonding interactions observed between various isoquinolinesulfonamides and APH(3')-IIIa or cAPK. The various inhibitors are coloured and shown in stick representation. Amino acid residues with which the inhibitors make contact are in grey and drawn as sticks. Water molecules are drawn as red spheres and the hydrogen bonds are depicted as dashed lines. **a.** CKI-7 in APH(3')-IIIa. **b.** H8 in cAPK (PDB code: 1YDS). **c.** H89 in cAPK (1YDT). **d.** H7 in cAPK (1YDR). **e.** HA1077 in cAPK (1Q8W). **f.** H1152P in cAPK (1Q8U). These illustrations show that all inhibitors form a hydrogen bond between its isoquinoline cyclic nitrogen and a main chain amide in the linker of the enzyme. In addition, all inhibitors except H1152P, make one or more direct or water-mediated interactions with the enzyme *via* the amide in the tail portion of the inhibitor. In contrast, the hydrogen bond between Y42 and the sulfonyl oxygen in CKI-7 is unique to APH(3')-IIIa, since the equivalent residue in cAPK is Ala70.

bound in cAPK. Second, the cyclic nitrogen in the isoquinoline should be aligned in such a way that it is in position to make the conserved hydrogen bond with the main chain amide of Ala93 in APH(3')-IIIa. The bond between the isoquinoline C5 and the sulfur atom should be rigid and thus, in maintaining the interaction between the isoquinoline nitrogen and the enzyme linker, the sulfonamide group should overlap the ribose. Due to the shift in location of the sulfonamide, the hydrogen bond between the axial oxygen of the sulfonyl and Tyr42 would no longer exist. Lastly, it is more difficult to predict the binding mode of the variable group substituted at the 5-sulfonamide. The conformation of the tail segment of the inhibitor that is constituted of an alkyl chain are generally flexible and depending on the neighboring amino acid residues, can adopt varying shapes. In comparison, the conformation of the ring structure substituted at the sulfonamide group of some H-series inhibitors are more rigid, however, it may be able to adopt different orientations. Regardless, due to the rigidity between the two modules of the inhibitor, the tail fragment will likely lie in the vicinity of the ribose-binding pocket, akin to the binding mode seen in cAPK. Based on this hypothesis, the binding mode of an H-series inhibitor, H7, to APH(3')-IIIa is postulated and illustrated in Figure 4–12, using the conformation found in the crystal structure of cAPK–H7.

4.3.4 Inhibitor Design

Considering the extensive sequence and structural conservation within the ATP-binding cleft among protein kinases, it was initially believed that the discovery or the design of ATP competitive inhibitors with high selectivity would

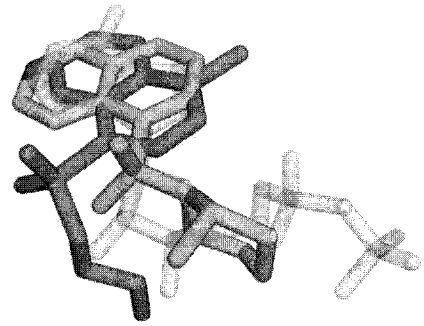

Figure 4–12. Comparison of the binding mode between the modelled H7, CKI-7, and ADP in APH(3')-IIIa. All three molecules are shown in stick representation. ADP is in yellow and is semi-transparent, CKI-7 is coloured blue, and H7 is in lime green except for its cyclic nitrogen, which is coloured in dark blue. The ring structures of all three molecules overlap and the ring nitrogen of H7 is aligned to form a hydrogen bond with the enzyme. Consequently, the entire structure of H7 is rotated such that the tail of the inhibitor occupies the ribose-binding area.

be an arduous task. However, data amassed from empirical screening and crystal structures of inhibitor-enzyme complexes have affirmed the feasibility of generating potent and specific inhibitors that target the ATP-binding pocket (Toledo *et al.*, 1999; Cherry and Williams, 2004). Structural data reveal that there are several elements in protein kinases that can be utilized for improving the selectivity of an inhibitory ligand. These include the non-conserved regions of the ATP-binding cavity, the pliant nucleotide-binding loop and interdomain flexibility. Based on the resemblance in overall structure, amino acid conservation in the ATP-binding site and sensitivity to inhibitors between ePKs and APH(3')-IIIa, the strategies employed for the design and development of protein kinase inhibitors can also be extrapolated to APH(3')-IIIa.

Crystal structures of protein kinases complexed with nucleotide show that the nucleotide does not fill the entire cavity of the binding cleft. Although the architecture and properties of the ATP-binding cleft are consistent among ePKs, the amino acid residues in the unoccupied regions, namely the hydrophobic pocket inward from the adenine pocket as well as the specificity surface outward of the adenine pocket (Cherry and Williams, 2004), are often diverse and therefore could be exploited for the development of selective ATP-competitive inhibitors (Toledo *et al.*, 1999; Cherry and Williams, 2004). The majority of the small molecule inhibitors examined so far mimic the shape and properties of the adenine and as a result, they often bind to the adenine pocket in a similar manner. The core of these inhibitors consists of a planar, hydrophobic, ring structure, decorated by various groups extending into the non-conserved areas, in order to confer specificity and affinity (Cherry and Williams, 2004). For example, the binding of purvalanol B to cyclin-dependent kinase 2 (CDK2) utilizes the specificity surface (Gray *et al.*, 1998), whereas the pyridinylimidazole-type inhibitors for p38 mitogen-activated protein kinase (MAPK) employs the hydrophobic pocket for selective binding (Wilson *et al.*, 1997; Tong *et al.*, 1997).

The glycine-rich loop that is highly conserved among ePKs has a structural equivalent in APH(3')-IIIa. This structural feature functions as a clamp stabilizing the phosphate groups in both types of enzymes. This loop is generally flexible and can be altered to varying degrees depending on the ligand bound to the cleft (Wang *et al.*, 1997; Taylor *et al.*, 1999; Chen *et al.*, 2000; Burk *et al.*, 2001). For example, the glycine-rich loop of cAPK complexed with H7, H8,

HA1077 and H1152P can adopt at least two conformations whereas, H89 stabilizes the loop in a single open conformation (Engh *et al.*, 1996). Moreover, the tip of the nucleotide-binding loop has been observed to fold in toward the inhibitor in several inhibitor-bound crystal structures such as APH(3')-IIIa–CKI-7, CK1–CKI-7 (Xu *et al.*, 1996), cAPK–stuarosporine (Prade *et al.*, 1997), cell cycle checkpoint kinase 1 (Chk1)–staurosporine derivative (Zhao *et al.*, 2002), fibroblast growth factor receptor 1 (FGFR1)–indolinone molecule (Mohammadi *et al.*, 1997), and p38 MAPK–pyridinylimidazole and its analogs (Wang *et al.*, 1998). This may be a consequence of the lack of the phosphate-moiety or a structural equivalent occupying the phosphate-binding pocket. The rearrangement of the loop therefore encloses the inhibitor-binding cleft and could increase the van der Waals interactions with the inhibitor. As a result, it may contribute to inhibitor potency and selectivity by enhancing the fit of the binding cleft.

Inhibitor selectivity of ePKs can also be guided by the interdomain movement observed in many ePKs as well as the residue side chain flexibility in the binding pocket. This is best illustrated by the staurosporine-bound enzyme crystal structures (Lawrie *et al.*, 1997; Prade *et al.*, 1997; Zhao *et al.*, 2002). Staurosporine is a potent but non-specific protein kinase inhibitor (Herbert *et al.*, 1990; Yanagihara *et al.*, 1991) that is much larger than adenine in size and is more rigid. These crystal structures showed that staurosporine binds to the adenine-binding pocket and anchors the enzyme in an open conformation compared to the nucleotide-bound structures (Lawrie *et al.*, 1997; Prade *et al.*, 1997; Zhao *et al.*, 2002). Staurosporine binding is accomplished by induced fit where

many residues surrounding the inhibitor display side chain rotamer alteration and displacement in order to accommodate the bulk of the inhibitor. Despite the indiscriminate inhibition of many ePKs, APH(3')-IIIa is unsusceptible to the inhibitory effects of staurosporine (Daigle *et al.*, 1997). APH(3')-IIIa is a rigid enzyme and no domain movement has been observed upon the binding of nucleotide and substrate (Burk *et al.*, 2001). Therefore, without the flexibility of domain movement, staurosporine may not be able to enter the constricted interdomain ATP-binding pocket of APH(3')-IIIa. Furthermore, several larger and less pliable residues are substituted in the adenine-binding pocket of APH(3')-IIIa. These substitutions may further hinder the entry and binding of staurosporine.

Among the protein kinase inhibitors tested for APH(3')-IIIa (Daigle *et al.*, 1997), HA1004 is the most potent, marginally more effective than CKI-7, with a K_i of 48.9 μM. HA1004 belongs to the H-series inhibitors. It consists of an 5-isoquinolinesulfonamide plus a guanidinoethyl tail (Figure 4–7). Comparing HA1004 and H9, the removal of the imidoformamide group reduces the potency of the inhibitor for APH(3')-IIIa by almost a factor of 3, whereas the replacement of the 5-isoquinolinesulfonamide in H9 with 5-chloroisoquinoline-8-sulfonamide to make CKI-7 doubles the inhibitory action. It was also shown that those isoquinolinesulfonamides that are substituted with a piperazine ring at the sulfonamide group, H7 and 1-(5-chloro-8-isoquinolinesulfonyl)-piperazine (CKI-8), are poor inhibitors for APH(3')-IIIa. Therefore, based on these results from

enzyme activity experiments, a plausible inhibitor for APH(3')-IIIa would contain a 5-chloroisoquinoline-8-sulfonamide and a guanidinoethyl group. Furthermore, with the availability of structural data of inhibitor-bound APH(3')-IIIa, additional suggestions can be proposed: Since the chlorine atom in CKI-7 does not appear to participate in any direct interactions with APH(3')-IIIa, a non-polar group could be considered as a possible candidate to replace the chlorine at C5 of the isoquinoline. To further improve the selectivity of a ligand for APH(3')-IIIa, a group could be appended to position C10. This group would be located in the specificity surface, adjacent to the linker of the enzyme. Since APH(3')-IIIa has a large specificity surface, the introduction of a non-polar group or a ring structure at this position could confer ligand specificity to the enzyme. Based on the observed binding orientation of the isoquinoline inhibitors to APH(3')-IIIa and cAPK, for a ligand containing a 5-substituted-isoquinoline, a functional group added to position 7 would more thoroughly utilize the ribose-binding pocket. Moreover, a large functional group analogous to the 2-(*p*-bromocinnamylamino)ethyl of H89 at this position could be devised to improve the shape complementarity to the phosphate-binding area and to increase van der Waals interactions with the active site (Hunenberger *et al.*, 1999).

The program LigBuilder (Wang *et al.*, 2000) was used to validate the proposed strategy of ligand design for APH(3')-IIIa based on the information obtained from the structure of CKI-7-bound enzyme complex. The binding pocket for which the ligands would be built is that of the ADP-bound APH(3')-IIIa

enzyme. The nucleotide-bound structure was chosen as the enzyme target instead of the inhibitor-bound complex since the nucleotide-binding loop adopts a more open conformation in the presence of a nucleotide and thus would allow the possibility of building ligands possessing variable fragments that could more thoroughly utilize the binding pocket. The resulting pharmacophore model from the POCKET module indicated the key interaction sites and confirmed that the adenine-binding site and the specificity surface are hydrophobic in nature and that the phosphate-binding area is hydrogen bond accepting. It also showed that the lower part of the binding pocket, near the ribose-binding area, was a hydrogen bond donating region (Figure 4–13).

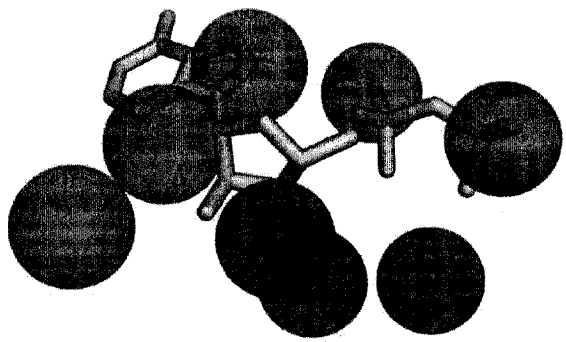

Figure 4–13. Pharmacophore model of the ADP-binding site. The ADP molecule drawn as yellow stick representation is shown to illustrate the shape of the binding pocket. The hydrophobic region of the binding cavity is represented by grey spheres, the hydrogen bond donating and accepting regions are represented by blue and red spheres, respectively.

Four seed molecules were used to initiate the ligand building process. Ligands built from 8-isoquinolinesulfonamide (Figure 4–14) and isoquinoline (Figure

4–15) in the CKI-7-binding mode corroborate with the above mentioned suggestions for modifications. Non-polar groups are substituted at position 5 of the isoquinoline, replacing the chlorine atom and confirming the employability of the hydrophobic pocket. Although no functional groups are observed to be added to C10, the largely non-polar ring structures appended to the sulfonamide or position 8 of the isoquinoline lie in the specificity surface. The variety of fragments appended to this position illustrate the extent of this region of the enzyme. As proposed earlier, fragments containing polar functional groups are attached to C7 of ligands constructed from isoquinoline. This moiety mainly overlaps with the ribose-binding area and the hydrogen bond donating region. Polar groups attached to the ring structures at the sulfonamide or C8 of isoquinoline compensate for ligands lacking a C7 substitution. Lastly, the addition of a methyl or methanol group at C2 of the isoquinolline is not among the suggested modifications.

Substructures of the H-series isoquinolinesulfonamides, 5-isoquinolinesulfonamide and isoquinoline, were also used as starting models for ligand building. The binding model of these seed molecules was taken from that of H7 modelled for the APH(3')-IIIa binding pocket (Figure 4–12). In general, the ligands built from 5-isoquinolinesulfonamide are quite uniform in structure (Figure 4–16) whereas ligands constructed from isoquinoline demonstrate great variability (Figure 4–17). For instance, no fragments were added to the sulfonamide group. All the ligands built from 5-isoquinolinesulfonamide are substituted at position 2 with large non-polar groups, typically consisting of a four- to seven-carbon chain

and/or at least one ring structure. This large fragment fills a significant portion of the specificity surface and resembles a cradle for the rest of the ligand, lying along the opening of the binding pocket. On the contrary, smaller functional groups are added to C2 of isoquinoline. Other modifications on the isoquinoline can be found bridged to positions 3 or 5, and also in the form of ring structures *peri*-fused to isoquinoline. Additions made to position 3 or as fused ring structures largely occupy the specificity surface, whereas groups added to position 5 occupy the ribose-binding area. Lastly, features observed in ligands constructed from both 5-isoquinolinesulfonamide and isoquinoline include the addition of a small functional group such as methyl or aldehyde at C10. Furthermore, the fragments appended to C7 show a large variety. The polar portion of the larger functional groups at C7 lies in the vicinity of the hydrogen bond accepting area specified by the pharmacophore model (Figure 4–13).

The ligands produced by LigBuilder (Wang *et al.*, 2000) demonstrate the substantial use of the specificity surface and the hydrophobic pocket of the ATP-binding site of APH(3')-IIIa (Figures 4–14 to 4–17). Based on the structural analyses presented in Section 4.3.3, APH(3')-IIIa has the most extensive specificity surface compared to CK1 and cAPK (Figure 4–10). Therefore, these LigBuilder-built molecules with large substitutions that occupy the specificity surface region are unlikely to fit in the more compact ATP-binding pockets of CK1 and cAPK. In other words, these molecules would bind to APH(3')-IIIa selectively. This can be illustrated by modelling the designed molecules into the

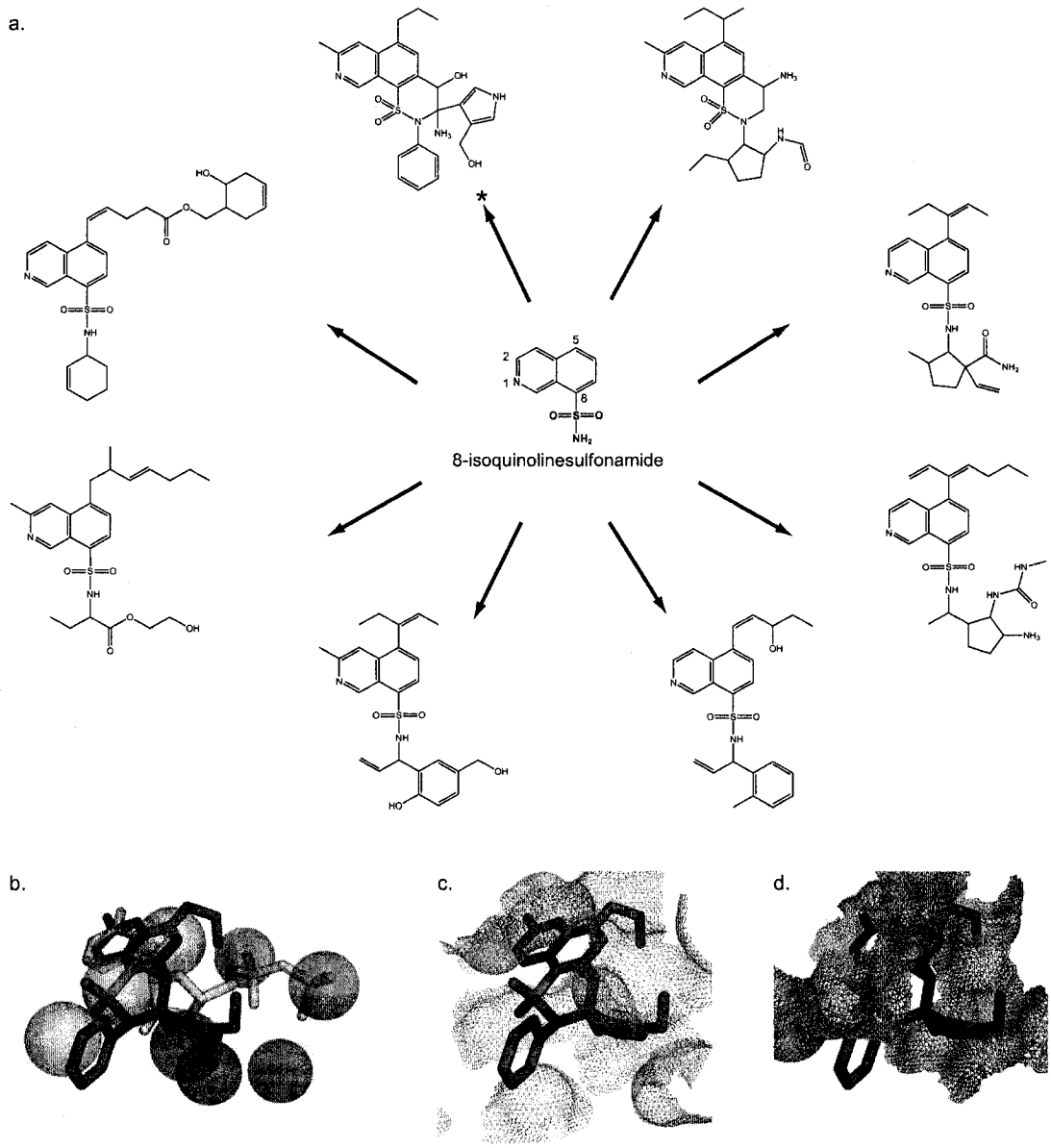

Figure 4–14. **a**. Chemical structures of examples of ligands produced by LigBuilder (Wang *et al.*, 2000) using 8-isoquinolinesulfonamide as the core. **b**. The ligand denoted by an asterisk (*) is drawn in light purple sticks and overlaid with ADP, drawn in semi-transparent sticks, and the pharmacophore model, shown in spheres. The colouring scheme of ADP and the pharmacophore model are the same as in Figure 4–13. **c**. The molecular surface of the ADP-binding pocket around the representative ligand is shown in mesh representation. **d**. The molecular surface of the ATP-binding pocket of CK1 around the ligand, shown in mesh representation.

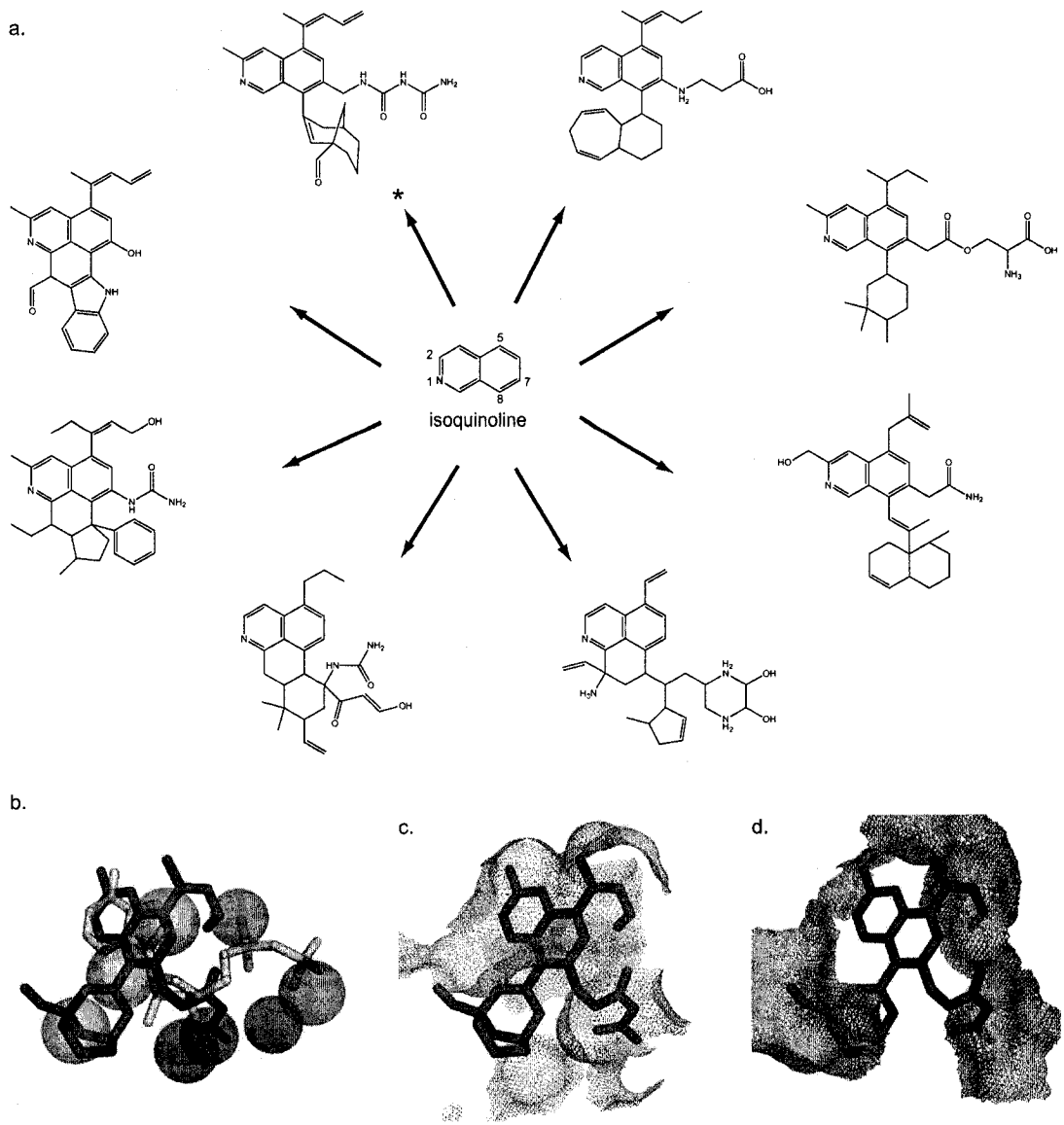

Figure 4–15. **a**. Chemical structures of examples of ligands built from an isoquinoline modelled in the binding pocket by analogy to CKI-7 using the LigBuilder program. **b**. The ligand denoted by an asterisk (*) is drawn in light purple sticks and overlaid with ADP, drawn in semi-transparent sticks, and the pharmacophore model, shown in spheres. The colouring scheme of ADP and the pharmacophore model are the same as in Figure 4–13. **c**. The molecular surface of the ADP-binding pocket around the representative ligand is shown in mesh representation. **d**. The molecular surface of the ATP-binding pocket of CK1 around the ligand, shown in mesh representation.

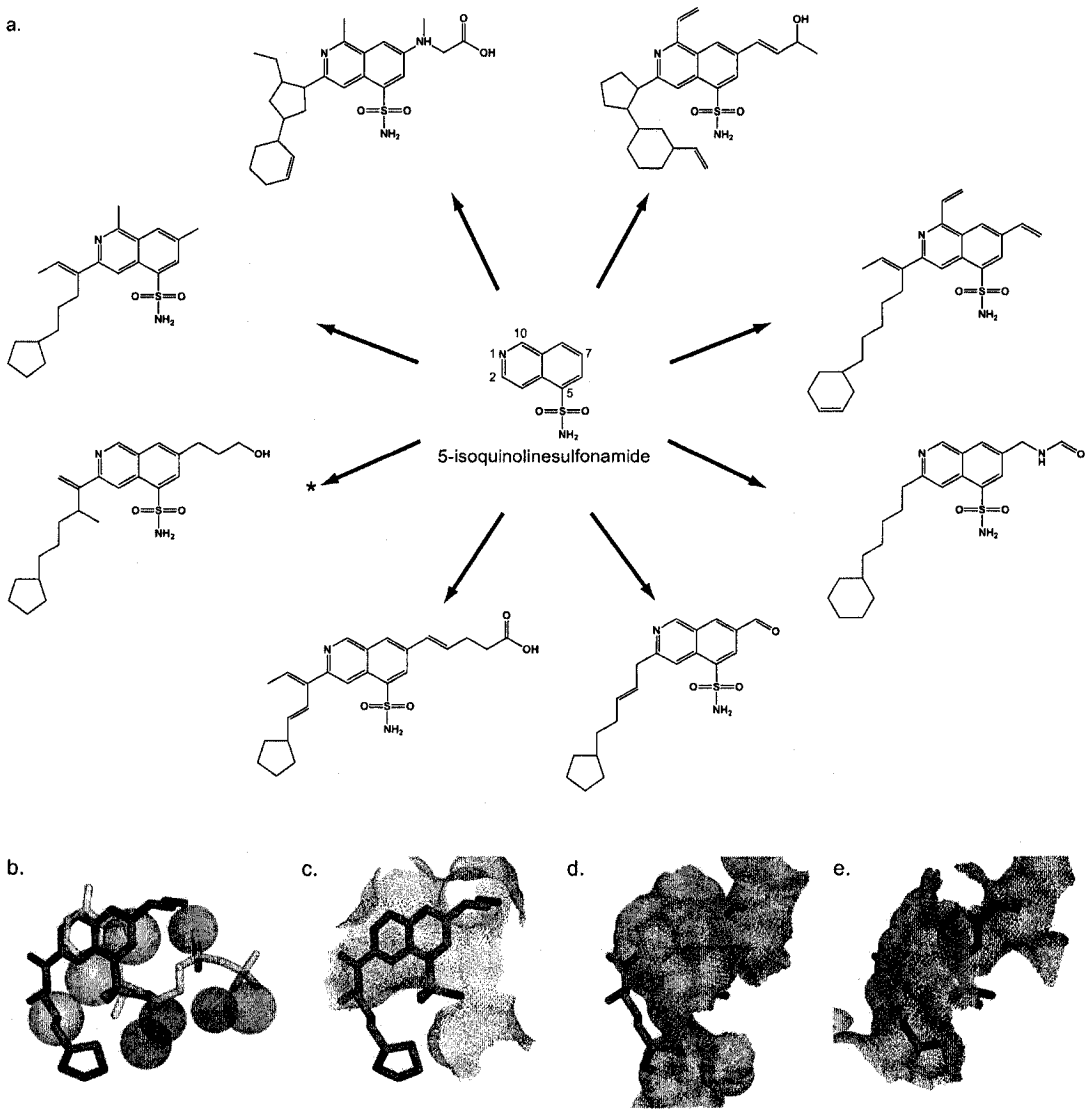

Figure 4–16. **a**. Chemical structures of examples of ligands produced by LigBuilder using, as the seed, 5-isoquinolinesulfonamide positioned according to the modelled binding mode of H7 in APH(3')-IIIa. **b**. The ligand denoted by an asterisk (*) is drawn in light purple sticks and overlaid with ADP, drawn in semi-transparent sticks, and the pharmacophore model, shown in spheres. The colouring scheme of ADP and the pharmacophore model are the same as in Figure 4–13. **c**. The molecular surface of the ADP-binding pocket around the sample ligand is shown in mesh representation. **d**. The molecular surface of the ATP-binding pocket of cAPK around the ligand. **e**. The molecular surface of the nucleotide-binding site of the staurosporine-bound cAPK around the ligand.

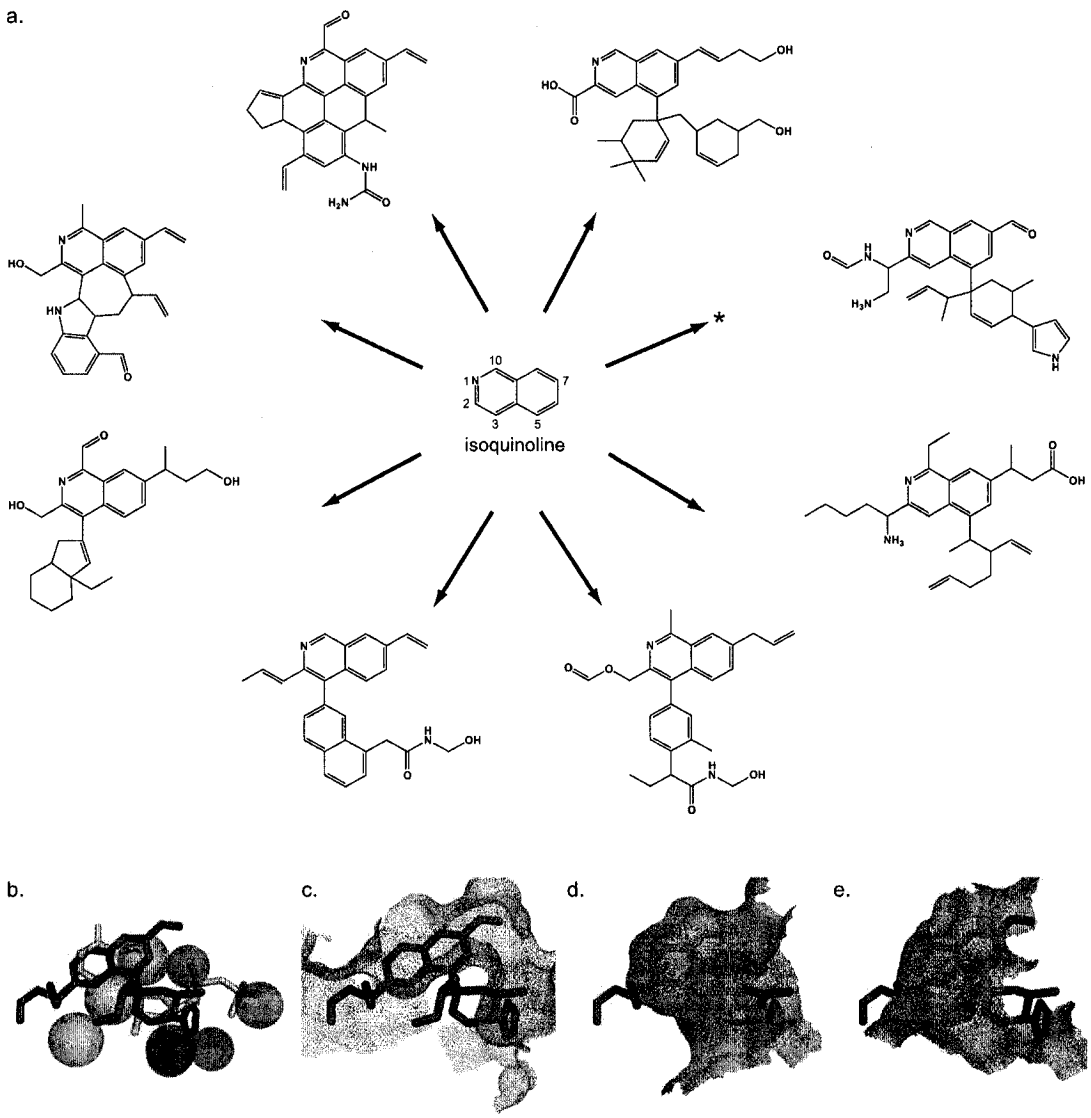

Figure 4–17. **a**. Chemical structures of examples of ligands constructed from an isoquinoline core positioned according to the modelled binding mode of H7 in APH(3')-IIIa. **b**. The ligand denoted by an asterisk (*) is drawn in light purple sticks and overlaid with ADP, drawn in semi-transparent sticks, and the pharmacophore model, shown in spheres. The colouring scheme of ADP and the pharmacophore model are the same as in Figure 4–13. **c**. The molecular surface of the ADP-binding pocket around the sample ligand is shown in mesh representation. **d**. The molecular surface of the ATP-binding pocket of cAPK around the ligand. **e**. The molecular surface of the nucleotide-binding site of the staurosporine-bound cAPK around the ligand.

ATP-binding pockets of the ePKs according to the observed and proposed binding modes of the isoquinoline inhibitors (Figures 4–14d to 4–17d). These figures show that the ligands built by LigBuilder are too large to be contained within the boundaries of the ATP-binding pockets of CK1 and cAPK. A limitation of LigBuilder is that the target binding pocket is treated as a rigid entity (Wang *et al.*, 2000), thus possible conformational changes of the enzyme cannot be predicted or accounted for. Nevertheless, this program is apposite for the *de Novo* design for APH(3')-IIIa inhibitors since no interdomain movement has been observed in APH(3')-IIIa (Burk *et al.*, 2001). However, interdomain flexibility has been noted for cAPK (Taylor *et al.*, 2004) and this property might allow the enzyme to accommodate the molecules constructed by LigBuilder. The ligands were also modelled into the ATP-binding site of the staurosporine-bound cAPK since it has been shown that staurosporine stabilizes cAPK in an open conformation (Lawrie *et al.*, 1997; Prade *et al.*, 1997; Zhao *et al.*, 2002). Although the ligands still cannot be completely contained inside the binding pocket, the combination of the open conformation and the changes in residue side chain position allow a larger portion of the molecules to lie inside the bounds (Figures 4–16e and 4–17e). Further shifts in amino acid residue positions in and around the nucleotide-binding pocket of cAPK could occur and adapt to the size and shape of the LigBuilder-built ligands. Subsequent experiments should include binding studies (Fabian *et al.*, 2005) of these ligands for APH(3')-IIIa and an array of ePKs in order to test their binding capabilities and selectivity.

CHAPTER 5
Summary and Conclusions

Section 5.3 has been taken from the following book chapter: Fong, D.H., Burk, D.L. and Berghuis, A.M. (2005) Aminoglycoside Kinases and Antibiotic Resistance. In Pinna, L.A. and Cohen, P.T.W. (eds.), Inhibitors of Protein Kinases and Protein Phosphatases. Springer, Berlin, Vol. 167, pp. 157–188. With kind permission of Springer Science and Business Media.

5.1 Summary of Experimental Results

In summary, the structures of four ternary (nucleotide- and aminoglycoside-bound) complexes and one inhibitor-bound structure of APH(3')-IIIa were determined by the molecular replacement method for this thesis work (Table 5–1). The ternary structures, along with the previously determined crystal structures of apo, ADP-, and AMPPNP-bound APH(3')-IIIa (Burk *et al.*, 2001; Hon *et al.*, 1997) complete the structural overview of the APH(3')-IIIa reaction cycle. The structures of ADP–kanamycin A, ADP–neomycin B, AMPPNP–butirosin A, and AMPPNP–5"-phoshporylated butirosin A definitively identify the location of the aminoglycoside-binding pocket and the binding mode of the structurally diverse

substrates. They also illustrate the basis for substrate promiscuity of APH(3')-IIIa, namely the compartmentalization of the binding pocket and a flexible substrate-binding loop. The comparison of the neomycin- and kanamycin-bound enzyme with the A-site of the ribosome, the cellular target of aminoglycosides, provides a structural explanation for this enzyme's effectiveness as a resistance factor and raises concerns for the development of new antibiotics that target the 16S RNA. Furthermore, a comparison between the kanamycin-bound APH(3')-IIIa and APH(3')-IIa (Nurizzo *et al.*, 2003) indicates that the main features utilized for aminoglycoside binding are likely to be conserved among all APHs, and possibly most, if not all, aminoglycoside-modifying enzymes. Together, these results will be useful in the design of novel variant aminoglycoside antibiotics that can interact with the target ribosome A-site but are unable to be detoxified by APH(3')-IIIa and related enzymes. In fact, information derived from the kanamycin A and neomycin B complexes of APH(3')-IIIa have furthered the progress of several studies on the design of 2-deoxystreptamine aminoglycosides with antibacterial activity against those strains known to be aminoglycoside-resistant and lower toxicity to humans (Russell *et al.*, 2003; Fridman *et al.*, 2003; Hainrichson *et al.*, 2005; Li *et al.*, 2005; Wang *et al.*, 2005).

The CKI-7-bound structure of APH(3')-IIIa represent the first crystal structure of an ePK inhibitor bound to a non-eukaryotic protein kinase. The structure confirms the conservation of the framework in the nucleotide-binding pocket of APH(3')-IIIa and ePKs and the feasibility of inhibiting APH(3')-IIIa by obstructing nucleotide binding. Moreover, detailed comparisons between the analogous

binding pockets reveal distinct features, such as the absence of ring stacking interactions with the adenine ring in ePKs and differences in the nucleotide-binding loop, that can be exploited to prevent cross-reactivity of the designer inhibitors with human protein kinases.

5.2 Future Directions

The crystal structures described in this thesis are APH(3')-IIIa complexes of 2-deoxystreptamine aminoglycosides whose 3'-hydroxyl group is positioned to accept a phosphate group. In order to decipher the manner in which 4,5-disubstituted aminoglycosides are recognized and bound to the enzyme for 5"-phsophorylation, it is necessary to obtain structural information of APH(3')-IIIa with a bound 4,5-disubstituted aminoglycoside in which the 5"-hydroxyl group is aligned with the γ-phosphate. Crystals of APH(3')-IIIa grown in the presence of AMPPNP and lividomycin A have been produced using 1,4-butanediol as the precipitant and a 2.7 Å data set has been collected. Although some electron density for four of the five rings of lividomycin was observed in the antibiotic-binding pocket, it was insufficient to unequivocally model in the aminoglycoside. Nonetheless, the sparse electron density present suggested an orientation in which the 3' position is aligned with the γ-phosphate. In retrospect, the results are not surprising since an aminoglycoside lacking a 3'-hydroxyl should be fully capable of binding to the enzyme in the same orientation as those containing a hydroxyl group at this position. This is illustrated by tobramycin, a 4,6-disubstituted aminoglycoside which can bind to and act as an inhibitor for APH(3')-IIIa (McKay *et al.*, 1994a). A strategy to deter the 3'-phosphorylation

Table 5–1. Summary of APH(3')-IIIa complexes determined

APH(3')-IIIa complex	Space Group	Resolution	R_{cryst}	R_{free}	Remarks	
ADP kanamycin	$P4_322$	2.4 Å	0.234	0.291	mechanism of binding: ·electrostatic interactions ·alternative binding subsites ·flexible substrate-binding loop	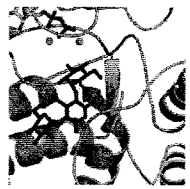
ADP neomycin	$P4_322$	2.7 Å	0.225	0.312	comparison to A-site-bound paromomycin: ·same substrate conformation ·equivalent H-bond pattern ·van der Waals interactions with opposite faces of substrate	
AMPPNP butirosin	$P4_22_12$	2.4 Å	0.217	0.261	·pliable substrate-binding loop accommodate AHB group at N1	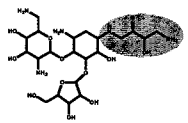
AMPPNP 5"-P-butirosin	$P4_322$	2.7 Å	0.243	0.316	·likely to have distinct binding mode for 5"-phosphorylation	
ePK inhibitor, CKI-7	$P2_12_12_1$	2.5 Å	0.206	0.265	·microseeding crystallization ·model for ATP-competitve inhibitor design	

binding mode is to co-crystallize APH(3')-IIIa with lividomycin A, or any 4,5-disubstituted aminoglycoside, derivated at the 3' position with a phosphate, nitrate, or sulfate group.

Studies following from the elucidation of CKI-7 complex of APH(3')-IIIa may include comparing the preliminary LigBuilder (Wang *et al.*, 2000) results to available small molecule databases and procuring the exact or comparable molecules for structure-activity relationship (SAR) studies against APH(3')-IIIa. These results could guide the design of appropriate ligands for APH(3')-IIIa with high selectivity and affinity. In addition to *in vitro* cell-free studies, it is also crucial to examine the ability of these potential inhibitors to restore antibacterial susceptibility in bacteria. There have been occasions in which the pursuit of target-optimized inhibitors in the nM range were terminated due to their inability to traverse the bacterial cell membranes to reach the target site (Overbye and Barrett, 2005). This issue is aptly illustrated by the class of inhibitors described here. Although, isoquinolinesulfonamides are proficient inhibitors of APH(3')-IIIa *in vitro*, they are incapable of recovering aminoglycoside susceptibility in cultures of *Enterococcus faecalis* harboring the *aph(3')-IIIa* gene (Daigle *et al.*, 1997).

5.3 Concluding Remarks

Despite the tremendous success of antibiotics over the past 50 years, infectious diseases remain a serious problem for public health due to the prevalence of antibiotic-resistant pathogens. Aminoglycoside resistance is no longer restricted to the hospital environment, but now represents a problem for communities in

both the developing and developed worlds. To date, there are no known inhibitors of aminoglycoside-modifying enzymes that can be used in combination with existing aminoglycosides in a clinical setting. Ideally, a single inhibitor would be designed to block the function of all the aminoglycoside-modifying enzymes. However, the design of a molecule that is capable to effectively bind to all three classes of enzymes would be extremely difficult. Although the negatively charged aminoglycoside-binding sites are a common feature in all three classes of resistant enzymes, differing ranges of substrate specificity and regiospecificity give rise to distinct features in the various classes of enzymes. However, it is plausible to develop a compound which would effectively block the activity of one family of enzymes, despite subtle differences between enzymes within each family. The design of new antibacterial agents that bind to the A-site of the bacterial ribosome is also equally challenging. A newly designed molecule has to fulfill an array of prerequisites before it can be considered as a drug candidate. It will have to be taken up into the bacterial cell, bind to the bacterial ribosome, interfere with protein translation, and be a poor substrate for resistance enzymes. Given the findings on aminoglycoside inhibition by APHs and as more mechanistic and structural information on aminoglycoside-modifying enzymes becomes available, it is possible that the restoration of current aminoglycosides as well as the development of new aminoglycoside derivatives with antibacterial activity may indeed be possible in the future.

Appendix

List of Publications

1. Published

   Refereed Papers

   (a) Fong, D.H., Yim, V.C.-N., D'Elia, M.A., Brown, E.D., and Berghuis, A.M. (2006)

   Crystal structure of CTP:glycerol-3-phosphate cytidylyltransferase from *Staphylococcus aureus*: Examination of structural basis for kinetic mechanism.

   Biochim. Biophys. Acta – Proteins and Proteomics. **1764**: 63–69.

   D.H.F and V.C.-N.Y. contributed equally to this work. D.H.F. did 20% of the structure refinement, performed 50% of the analysis, and wrote 70% of the manuscript.

   (b) Fong, D.H. and Berghuis, A.M. (2004)

   Crystallization and preliminary crystallographic analysis of 3'-aminoglycoside kinase type IIIa complexed with a eukaryotic protein kinase inhibitor, CKI-7.

   Acta crystallogr. D. **60**: 1897–1899.

   (c) Fong, D.H. and Berghuis, A.M. (2002)

   Substrate promiscuity of an antibiotic resistance enzyme due to target mimicry.

   EMBO J. **21**: 2323–2331.

Invited Publication

(a) Fong, D.H., Burk, D.L., and Berghuis, A.M. (2005)

Aminoglycoside kinases and antibiotic resistance.

In Pinna, L.A. and Cohen, P.T.W. (eds.), *Inhibitors of Protein Kinases and Protein Phosphatases.* Springer, Berlin, Vol. 167, pp. 157–188.

(b) Fong, D.H. and Berghuis, A.M. (2002)

Resistance to aminoglycoside antibiotics is due in part to target mimicry.

National Synchrotron Light Source Science Highlights.

`http://www.nsls.bnl.gov/newsroom/science/2002/09-Berghuis.htm`

2. In Preparation

(a) Fong, D.H. and Berghuis, A.M.

Structure of APH(3')-IIIa bound to an eukaryotic protein kinase inhibitor.

(b) Fong, D.H. and Berghuis, A.M.

Diphosphorylation mechanism of APH(3')-IIIa.

References

al Karadaghi S, Aevarsson A, Garber M, Zheltonosova J, and Liljas A (1996) The structure of elongation factor G in complex with GDP: conformational flexibility and nucleotide exchange. *Structure* **4**:555–565

Allinger N (1977) Conformational analysis. 130. MM2. A hydrocarbon force field utilizing V1 and V2 torsional terms. *Journal of American Chemical Society* **99**:8127–8134

Alper PB, Hendrix M, Sears P, and Wong CH (1998) Probing the specificity of aminoglycoside-ribosomal RNA interactions with designed synthetic analogs. *J Am Chem Soc* **120**:1965–1978

Amstutz P, Binz HK, Parizek P, Stumpp MT, Kohl A, Grutter MG, Forrer P, and Pluckthun A (2005) Intracellular kinase inhibitors selected from combinatorial libraries of designed ankyrin repeat proteins. *J Biol Chem* **280**:24715–24722

Aullon G, Bellamy D, Brammer L, Bruton EA, and Orpen AG (1998) Metal-bound chlorine often accepts hydrogen bonds. *Chem Commun* **6**:653–654

Beck E, Ludwig G, Auerswald EA, Reiss B, and Schaller H (1982) Nucleotide sequence and exact localization of the neomycin phosphotransferase gene from transposon Tn5. *Gene* **19**:327–336

Berman J and Fleckenstein L (1991) Pharmacokinetic justification of antiprotozoal therapy. A US perspective. *Clin Pharmacokinet* **21**:479–493

Boehr DD, Draker K, Koteva K, Bains M, Hancock RE, and Wright GD (2003) Broad-spectrum peptide inhibitors of aminoglycoside antibiotic resistance enzymes. *Chem Biol* **10**:189–196

Boehr DD, Farley AR, Wright GD, and Cox JR (2002) Analysis of the π-π stacking interactions between the aminoglycoside antibiotic kinase APH(3')-IIIa and its nucleotide ligands. *Chem Biol* **9**:1209–1217

Boehr DD, Lane WS, and Wright GD (2001a) Active site labeling of the gentamicin resistance enzyme AAC(6')-APH(2") by the lipid kinase inhibitor wortmannin. *Chem Biol* **8**:791–800

Boehr DD, Thompson PR, and Wright GD (2001b) Molecular mechanism of aminoglycoside antibiotic kinase APH(3')-IIIa: roles of conserved active site residues. *J Biol Chem* **276**:23929–23936

Bolognese CP and McGraw P (2000) The isolation and characterization in yeast of a gene for Arabidopsis S-adenosylmethionine:phospho-ethanolamine N-methyltransferase. *Plant Physiol* **124**:1800–1813

Bradford MM (1976) A rapid and sensitive method for the quantitation of microgram quantities of protein utilizing the principle of protein-dye binding. *Anal Biochem* **72**:248–254

Breitenlechner C, Gassel M, Hidaka H, Kinzel V, Huber R, Engh RA, and Bossemeyer D (2003) Protein kinase A in complex with Rho-kinase inhibitors Y-27632, Fasudil, and H-1152P: structural basis of selectivity. *Structure (Camb)* **11**:1595–1607

Brünger A, Adams P, Clore G, DeLano W, Gros P, Grosse-Kunstleve R, Jiang JS, Kuszewski J, Nilges M, Pannu N, Read R, Rice L, Simonson T, and Warren

G (1998) Crystallography & NMR system: a new software suite for macromolecular structure determination. *Acta Crystallogr D* **54**:905–921

Brünger AT (1990) Extension of molecular replacement: a new search strategy based on Patterson correlation refinement. *Acta Crystallographica Section A* **46**:46–57

Burk DL and Berghuis AM (2002) Protein kinase inhibitors and antibiotic resistance. *Pharmacol Ther* **93**:283–292

Burk DL, Hon WC, Leung AK, and Berghuis AM (2001) Structural analyses of nucleotide binding to an aminoglycoside phosphotransferase. *Biochemistry* **40**:8756–8764

Burkert U and Allinger N (1982) *Molecular Mechanics.* American Chemical Society, Washington, D.C.

Cacace S, Schroder G, Wehinger E, Strack D, Schmidt J, and Schroder J (2003) A flavonol O-methyltransferase from Catharanthus roseus performing two sequential methylations. *Phytochemistry* **62**:127–137

Carter AP, Clemons WM, Brodersen DE, Morgan-Warren RJ, Wimberly BT, and Ramakrishnan V (2000) Functional insights from the structure of the 30S ribosomal subunit and its interactions with antibiotics. *Nature* **407**:340–348

Casnellie JE (1991) Protein kinase inhibitors: probes for the functions of protein phosphorylation. *Adv Pharmacol* **22**:167–205

Chang S, Sievert DM, Hageman JC, Boulton ML, Tenover FC, Downes FP, Shah S, Rudrik JT, Pupp GR, Brown WJ, Cardo D, and Fridkin SK (2003) Infection with vancomycin-resistant Staphylococcus aureus containing the vanA resistance gene. *N Engl J Med* **348**:1342–7

Chapman MS (1995) Restrained real-space macromolecular atomic refinement using a new resolution-dependent electron-density function. *Acta Crystallographica Section A* **51**:69–80

Charron JBF, Breton G, Danyluk J, Muzac I, Ibrahim RK, and Sarhan F (2002) Molecular and biochemical characterization of a cold-regulated phosphoethanolamine N-methyltransferase from wheat. *Plant Physiol* **129**:363–373

Chen P, Luo C, Deng Y, Ryan K, Register J, Margosiak S, Tempczyk-Russell A, Nguyen B, Myers P, Lundgren K, Kan CC, and O'Connor PM (2000) The 1.7 Å crystal structure of human cell cycle checkpoint kinase Chk1: implications for Chk1 regulation. *Cell* **100**:681–92

Chenna R, Sugawara H, Koike T, Lopez R, Gibson TJ, Higgins DG, and Thompson JD (2003) Multiple sequence alignment with the Clustal series of programs. *Nucleic Acids Res* **31**:3497–3500

Cherry M and Williams DH (2004) Recent kinase and kinase inhibitor X-ray structures: mechanisms of inhibition and selectivity insights. *Curr Med Chem* **11**:663–73

Chijiwa T, Hagiwara M, and Hidaka H (1989) A newly synthesized selective casein kinase I inhibitor, N-(2-aminoethyl)-5-chloroisoquinoline-8-sulfonamide, and affinity purification of casein kinase I from bovine testis. *J Biol Chem* **264**:4924–7

Chijiwa T, Mishima A, Hagiwara M, Sano M, Hayashi K, Inoue T, Naito K, Toshioka T, and Hidaka H (1990) Inhibition of forskolin-induced neurite outgrowth and protein phosphorylation by a newly synthesized selective inhibitor

of cyclic AMP-dependent protein kinase, N-[2-(p-bromocinnamylamino)ethyl]-5-isoquinolinesulfonamide (H-89), of PC12D pheochromocytoma cells. *J Biol Chem* **265**:5267–5272

Chopra I, Hesse L, and O'Neill AJ (2002) Exploiting current understanding of antibiotic action for discovery of new drugs. *J Appl Microbiol* **92 Suppl**:4S–15S

Cohen M (2000) Changing patterns of infectious disease. *Nature* **406**:762–767

Collaborative Computational Project Number 4 (1994) The *CCP*4 suite: programs for protein crystallography. *Acta Crystallogr D* **50**:760–763

Conly J (2002) Antimicrobial resistance in Canada. *CMAJ* **167**:885–91

Cox J, McKay G, Wright G, and Serpesu E (1996) Arrangement of substrates at the active site of an aminoglycoside antibiotic 3'-phosphotransferase as determined by NMR. *J Am Chem Soc* **118**:1295–1301

Cox J and Serpersu E (1997) Biologically important conformations of aminoglycoside antibiotics bound to an aminoglycoside 3'-phosphotransferase as determined by transferred nuclear Overhauser effect spectroscopy. *Biochemistry* **36**:2353–2359

Cox JR, Ekman DR, DiGiammarino EL, Akal-Strader A, and Serpersu EH (2000) Aminoglycoside antibiotics bound to aminoglycoside-detoxifying enzymes and RNA adopt similar conformations. *Cell Biochem Biophys* **33**:297–308

Cundliffe E (1989) How antibiotic-producing organisms avoid suicide. *Annu Rev Microbiol* **43**:207–233

Czworkowski J, Wang J, Steitz T, and Moore P (1994) The crystal structure of elongation factor G complexed with GDP at 2.7Å resolution. *EMBO J* **13**:3661–3668

Daigle DM, Hughes DW, and Wright GD (1999a) Prodigious substrate specificity of AAC(6')-APH(2"), an aminoglycoside antibiotic resistance determinant in enterococci and staphylococci. *Chem Biol* **6**:99–110

Daigle DM, McKay GA, Thompson PR, and Wright GD (1999b) Aminoglycoside antibiotic phosphotransferases are also serine protein kinases. *Chem Biol* **6**:11–18

Daigle DM, McKay GA, and Wright GD (1997) Inhibition of aminoglycoside antibiotic resistance enzymes by protein kinase inhibitors. *J Biol Chem* **272**:24755–24758

Davies JE (1991) Aminoglycoside-aminocyclitol antibiotics and their modifying enzymes. In V Lorian (ed.) *Antibiotics in laboratory medicine*, Williams & Wilkins, Baltimore, 691–713

DeLano WL and Brünger AT (1995) The direct rotation function: Patterson correlation search applied to molecular replacement. *Acta Crystallographica Section D* **51**:740–748

Doudna J, Cech T, and Sullenger B (1995) Selection of an RNA molecule that mimics a major autoantigenic epitope of human insulin receptor. *Proc Natl Acad Sci USA* **92**:2355–2359

Engh RA, Girod A, Kinzel V, Huber R, and Bossemeyer D (1996) Crystal structures of catalytic subunit of cAMP-dependent protein kinase in complex with

isoquinolinesulfonyl protein kinase inhibitors H7, H8, and H89. Structural implications for selectivity. *J Biol Chem* **271**:26157–26164

Fabian MA, Biggs WH, Treiber DK, Atteridge CE, Azimioara MD, Benedetti MG, Carter TA, Ciceri P, Edeen PT, Floyd M, Ford JM, Galvin M, Gerlach JL, Grotzfeld RM, Herrgard S, Insko DE, Insko MA, Lai AG, Lelias JM, Mehta SA, Milanov ZV, Velasco AM, Wodicka LM, Patel HK, Zarrinkar PP, and Lockhart DJ (2005) A small molecule-kinase interaction map for clinical kinase inhibitors. *Nat Biotechnol* **23**:329–336

Ferretti JJ, Gilmore KS, and Courvalin P (1986) Nucleotide sequence analysis of the gene specifying the bifunctional 6'-aminoglycoside acetyltransferase 2-aminoglycoside phosphotransferase enzyme in *Streptococcus faecalis* and identification and cloning of gene regions specifying the two activities. *J Bacteriol* **167**:631–638

Feussner I and Wasternack C (2002) The lipoxygenase pathway. *Annu Rev Plant Biol* **53**:275–297

Fong DH and Berghuis AM (2002) Substrate promiscuity of an aminoglycoside antibiotic resistance enzyme via target mimicry. *EMBO J* **21**:2323–2331

Fong DH and Berghuis AM (2004) Crystallization and preliminary crystallographic analysis of 3'-aminoglycoside kinase type IIIa complexed with a eukaryotic protein kinase inhibitor, CKI-7. *Acta Crystallogr D* **60**:1897–1899

Forge A and Schacht J (2000) Aminoglycoside antibiotics. *Audiol Neurootol* **5**:3–22

Forrer P, Stumpp MT, Binz HK, and Pluckthun A (2003) A novel strategy to design binding molecules harnessing the modular nature of repeat proteins.

FEBS Lett **539**:2–6

Fourmy D, Recht MI, Blanchard SC, and Puglisi JD (1996) Structure of the A site of *Escherichia coli* 16S ribosomal RNA complexed with an aminoglycoside antibiotic. *Science* **274**:1367–1371

Fourmy D, Recht MI, and Puglisi JD (1998) Binding of neomycin-class aminoglycoside antibiotics to the A-site of 16 S rRNA. *J Mol Biol* **277**:347–362

Fridman M, Belakhov V, Yaron S, and Baasov T (2003) A new class of branched aminoglycosides: pseudo-pentasaccharide derivatives of neomycin B. *Org Lett* **5**:3575–3578

Fujimura S, Tokue Y, Takahashi H, Kobayashi T, Gomi K, Abe T, Nukiwa T, and Watanabe A (2000) Novel arbekacin- and amikacin-modifying enzyme of methicillin-resistant *Staphylococcus aureus*. *FEMS Microbiol Lett* **190**:299–303

Fujimura S, Tokue Y, Takahashi H, Nukiwa T, Hisamichi K, Mikami T, and Watanabe A (1998) A newly recognized acetylated metabolite of arbekacin in arbekacin-resistant strains of methicillin-resistant *Staphylococcus aureus*. *J Antimicrob Chemother* **41**:495–497

Furet P, Meyer T, Strauss A, Raccuglia S, and Rondeau JM (2002) Structure-based design and protein X-ray analysis of a protein kinase inhibitor. *Bioorg Med Chem Lett* **12**:221–4

Georgopapadakou NH (2002) Infectious disease 2001: drug resistance, new drugs. *Drug Resist Updat* **5**:181–191

Gray GS and Fitch WM (1983) Evolution of antibiotic resistance genes: the DNA sequence of a kanamycin resistance gene from *Staphylococcus aureus*. *Mol Biol Evol* **1**:57–66

Gray NS, Wodicka L, Thunnissen AM, Norman TC, Kwon S, Espinoza FH, Morgan DO, Barnes G, LeClerc S, Meijer L, Kim SH, Lockhart DJ, and Schultz PG (1998) Exploiting chemical libraries, structure, and genomics in the search for kinase inhibitors. *Science* **281**:533–8

Greenberg WA, Priestley ES, Sears PS, Alper PB, Rosenbohm C, Hendrix M, Hung SC, and Wong CH (1999) Design and synthesis of new aminoglycoside antibiotics containing neamine as an optimal core structure: correlation of antibiotic activity with in vitro inhibition of translation. *J Am Chem Soc* **121**:6527–6541

Gross SD and Anderson RA (1998) Casein kinase I: spatial organization and positioning of a multifunctional protein kinase family. *Cell Signal* **10**:699–711

Grosse-Kunstleve RW and Adams PD (2001) Patterson correlation methods: a review of molecular replacement with *CNS*. *Acta Crystallographica Section D* **57**:1390–1396

Haddad J, Kotra LP, Llano-Sotelo B, Kim C, Azucena EF Jr, Liu M, Vakulenko SB, Chow CS, and Mobashery S (2002) Design of novel antibiotics that bind to the ribosomal acyltransfer site. *J Am Chem Soc* **124**:3229–3237

Haddad J, Vakulenko S, and Mobashery S (1999) An antibiotic cloaked by its own resistance enzyme. *J Am Chem Soc* **121**:11922–11923

Hagiwara M, Inoue S, Tanaka T, Nunoki K, Ito M, and Hidaka H (1988) Differential effects of flavonoids as inhibitors of tyrosine protein kinases and serine/threonine protein kinases. *Biochem Pharmacol* **37**:2987–92

Hainrichson M, Pokrovskaya V, Shallom-Shezifi D, Fridman M, Belakhov V, Shachar D, Yaron S, and Baasov T (2005) Branched aminoglycosides: biochemical studies and antibacterial activity of neomycin B derivatives. *Bioorg Med Chem* **13**:5797–5807

Herbert JM, Seban E, and Maffrand JP (1990) Characterization of specific binding sites for [3H]-staurosporine on various protein kinases. *Biochem Biophys Res Commun* **171**:189–95

Hermann T and Westhof E (1999) Docking of cationic antibiotics to negatively charged pockets in RNA folds. *J Med Chem* **42**:1250–1261

Hidaka H, Hagiwara M, and Chijiwa T (1990) Molecular pharmacology of protein kinases. *Neurochem Res* **15**:431–4

Hidaka H, Inagaki M, Kawamoto S, and Sasaki Y (1984) Isoquinolinesulfonamides, novel and potent inhibitors of cyclic nucleotide dependent protein kinase and protein kinase C. *Biochemistry* **23**:5036–41

Holm SE, Hill B, Lowestad A, Maller R, and Vikerfors T (1983) A prospective, randomized study of amikacin and gentamicin in serious infections with focus on efficacy, toxicity and duration of serum levels above the MIC. *J Antimicrob Chemother* **12**:393–402

Hon WC, McKay GA, Thompson PR, Sweet RM, Yang DS, Wright GD, and Berghuis AM (1997) Structure of an enzyme required for aminoglycoside antibiotic resistance reveals homology to eukaryotic protein kinases. *Cell* **89**:887–895

Hotta K, Sunada A, Ishikawa J, Mizuno S, Ikeda Y, and Kondo S (1998) The novel enzymatic 3"-N-acetylation of arbekacin by an aminoglycoside 3-N-acetyltransferase of Streptomyces origin and the resulting activity. *J Antibiot (Tokyo)* **51**:735–742

Hotta K, Zhu CB, Ogata T, Sunada A, Ishikawa J, Mizuno S, Ikeda Y, and Kondo S (1996) Enzymatic 2'-N-acetylation of arbekacin and antibiotic activity of its product. *J Antibiot (Tokyo)* **49**:458–464

Hunenberger PH, Helms V, Narayana N, Taylor SS, and McCammon JA (1999) Determinants of ligand binding to cAMP-dependent protein kinase. *Biochemistry* **38**:2358–66

Ibdah M, Zhang XH, Schmidt J, and Vogt T (2003) A novel Mg(2+)-dependent O-methyltransferase in the phenylpropanoid metabolism of Mesembryanthemum crystallinum. *J Biol Chem* **278**:43961–43972

Ida T, Okamoto R, Shimauchi C, Okubo T, Kuga A, and Inoue M (2001) Identification of aminoglycoside-modifying enzymes by susceptibility testing: epidemiology of methicillin-resistant *Staphylococcus aureus* in Japan. *J Clin Microbiol* **39**:3115–3121

Inagaki M, Watanabe M, and Hidaka H (1985) N-(2-Aminoethyl)-5-isoquinolinesulfonamide, a newly synthesized protein kinase inhibitor, functions as a ligand in affinity chromatography. Purification of Ca2+-activated, phospholipid-dependent and other protein kinases. *J Biol Chem* **260**:2922–2925

Inouye S, Tamura A, Niizato T, Takeuchi T, Hamada M, and Kondo S (1996) Antibacterial activity and nephrotoxicity of two novel 2-amino derivatives of

arbekacin. *J Infect Chemother* **2**:84–89

Jacob AE and Hobbs SJ (1974) Conjugal transfer of plasmid-borne multiple antibiotic resistance in *Streptococcus faecalis* var. zymogenes. *J Bacteriol* **117**:360–72

Jancarik J and Kim SH (1991) Sparse matrix sampling: a screening method for crystallization of proteins. *J Appl Crystallogr* **24**:409–411

Johnson LN, Noble ME, and Owen DJ (1996) Active and inactive protein kinases: structural basis for regulation. *Cell* **85**:149–158

Jones TA, Zou JY, Cowan SW, and Kjeldgaard M (1991) Improved methods for building protein models in electron density maps and the location of errors in these models. *Acta Crystallogr A* **47**:110–119

Kadokura H, Katzen F, and Beckwith J (2003) Protein disulfide bond formation in prokaryotes. *Annu Rev Biochem* **72**:111–135

Kawaguchi H, Naito T, Nakagawa S, and Fujisawa KI (1972) BB-K 8, a new semisynthetic aminoglycoside antibiotic. *J Antibiot (Tokyo)* **25**:695–708

Keene JD (1996) RNA surfaces as functional mimetics of proteins. *Chemistry and Biology* **3**:505–513

Kim C, Haddad J, Vakulenko SB, Meroueh SO, Wu Y, Yan H, and Mobashery S (2004) Fluorinated aminoglycosides and their mechanistic implication for aminoglycoside 3'-phosphotransferases from Gram-negative bacteria. *Biochemistry* **43**:2373–2383

Kleywegt GJ (1996) Use of non-crystallographic symmetry in protein structure refinement. *Acta Crystallogr D Biol Crystallogr* **52**:842–857

Kleywegt GJ and Jones TA (1996) Phi/psi-chology: Ramachandran revisited. *Structure* **4**:1395–400

Knighton DR, Zheng JH, Ten Eyck LF, Ashford VA, Xuong NH, Taylor SS, and Sowadski JM (1991) Crystal structure of the catalytic subunit of cyclic adenosine monophosphate-dependent protein kinase. *Science* **253**:407–414

Kocabivik S and Perlin MH (1994) Amino acid substitutions within the analogous nucleotide binding loop (P-loop) of aminoglycoside 3'-phosphotransferase-II. *Int J Biochem* **26**:61–66

Kocabiyik S, Mullins C, Breeding C, and Perlin MH (1992) Structure-function analyses for aminoglycoside 3'-phosphotransferase II (APH(3')-II). *SAAS Bull Biochem Biotechnol* **5**:58–63

Kocabiyik S and Perlin MH (1992a) Altered substrate specificity by substitutions at Tyr218 in bacterial aminoglycoside 3'-phosphotransferase-II. *FEMS Microbiol Lett* **72**:199–202

Kocabiyik S and Perlin MH (1992b) Site-specific mutations of conserved C-terminal residues in aminoglycoside 3'-phosphotransferase II: phenotypic and structural analysis of mutant enzymes. *Biochem Biophys Res Commun* **185**:925–931

Kohl A, Amstutz P, Parizek P, Binz HK, Briand C, Capitani G, Forrer P, Pluckthun A, and Grutter MG (2005) Allosteric inhibition of aminoglycoside phosphotransferase by a designed ankyrin repeat protein. *Structure (Camb)* **13**:1131–1141

Kondo S and Hotta K (1999) Semisynthetic aminoglycoside antibiotics: Development and enzymatic modifications. *J Infect Chemother* **5**:1–9

Kondo S, Iinuma K, Yamamoto H, Ikeda Y, and Maeda K (1973a) Letter: Synthesis of (S)-4-amino-2-hydroxybutyryl derivatives of 3',4'-dideoxykanamycin B and their antibacterial activities. *J Antibiot (Tokyo)* **26**:705–707

Kondo S, Iinuma K, Yamamoto H, Maeda K, and Umezawa H (1973b) Letter: Syntheses of 1-n-(S)-4-amino-2-hydroxybutyryl)-kanamycin B and -3', 4'-dideoxykanamycin B active against kanamycin-resistant bacteria. *J Antibiot (Tokyo)* **26**:412–415

Kondo S, Ikeda Y, Ikeda D, Takeuchi T, Usui T, Ishii M, Kudo T, Gomi S, and Shibahara S (1994) Synthesis of 2"-amino-2"-deoxyarbekacin and its analogs having potent activity against methicillin-resistant *Staphylococcus aureus*. *J Antibiot (Tokyo)* **47**:821–832

Kondo S, Shibahara S, Usui T, Kudo T, Tamura A, Gomi S, Ikeda Y, Ikeda D, and Takeuchi T (1993a) New 2"-amino derivatives of arbekacin, potent aminoglycoside antibiotics against methicillin-resistant *Staphylococcus aureus*. *J Antibiot (Tokyo)* **46**:531–534

Kondo S, Tamura A, Gomi S, Ikeda Y, Takeuchi T, and Mitsuhashi S (1993b) Structures of enzymatically modified products of arbekacin by methicillin-resistant. *Staphylococcus aureus*. *J Antibiot (Tokyo)* **46**:310–315

Kotra LP, Haddad J, and Mobashery S (2000) Aminoglycosides: perspectives on mechanisms of action and resistance and strategies to counter resistance. *Antimicrob Agents Chemother* **44**:3249–3256

Koyama G and Iitaka Y (1968) The crystal structure of kanamycin. *Tetrahedron Letters* **15**:1875–1879

Laskowski R, MacArthur M, Moss D, and Thornton J (1993) PROCHECK: a program to check the sterochemical quality of protein structures. *J Appl Crystallogr* **26**:283–291

Lavid N, Wang J, Shalit M, Guterman I, Bar E, Beuerle T, Menda N, Shafir S, Zamir D, Adam Z, Vainstein A, Weiss D, Pichersky E, and Lewinsohn E (2002) O-methyltransferases involved in the biosynthesis of volatile phenolic derivatives in rose petals. *Plant Physiol* **129**:1899–1907

Lawrie AM, Noble ME, Tunnah P, Brown NR, Johnson LN, and Endicott JA (1997) Protein kinase inhibition by staurosporine revealed in details of the molecular interaction with CDK2. *Nat Struct Biol* **4**:796–801

Leclercq R, Dutka-Malen S, Brisson-Noel A, Molinas C, Derlot E, Arthur M, Duval J, and Courvalin P (1992) Resistance of enterococci to aminoglycosides and glycopeptides. *Clin Infect Dis* **15**:495–501

Li J, Chen HN, Chang H, Wang J, and Chang CWT (2005) Tuning the regioselectivity of the Staudinger reaction for the facile synthesis of kanamycin and neomycin class antibiotics with N-1 modification. *Org Lett* **7**:3061–3064

Liljas A (1996) Imprinting through molecular mimicry. Protein synthesis. *Curr Biol* **6**:247–249

Liu M, Haddad J, Azucena E, Kotra LP, Kirzhner M, and Mobashery S (2000) Tethered bisubstrate derivatives as probes for mechanism and as inhibitors of aminoglycoside 3'-phosphotransferases. *J Org Chem* **65**:7422–7431

Livermore DM (2003) Bacterial resistance: origins, epidemiology, and impact. *Clin Infect Dis* **36**:S11–23

Llano-Sotelo B, Azucena EF Jr, Kotra LP, Mobashery S, and Chow CS (2002) Aminoglycosides modified by resistance enzymes display diminished binding to the bacterial ribosomal aminoacyl-tRNA site. *Chem Biol* **9**:455–463

Madhusudan EA Trafny, Xuong NH, Adams JA, Ten Eyck LF, Taylor SS, and Sowadski JM (1994) cAMP-dependent protein kinase: crystallographic insights into substrate recognition and phosphotransfer. *Protein Sci* **3**:176–187

Martel A, Masson M, Moreau N, and Le Goffic F (1983) Kinetic studies of aminoglycoside acetyltransferase and phosphotransferase from *Staphylococcus aureus* RPAL. Relationship between the two activities. *Eur J Biochem* **133**:515–521

Matthews BW (1968) Solvent content of protein crystals. *J Mol Biol* **33**:491–497

McCaig LF, Besser RE, and Hughes JM (2003) Antimicrobial drug prescription in ambulatory care settings, United States, 1992-2000. *Emerg Infect Dis* **9**:432–437

McKay G, Thompson P, and Wright G (1994a) Broad spectrum aminoglycoside phosphotransferase type III from Enterococcus: overexpression, purification, and substrate specificity. *Biochemistry* **33**:6936–6944

McKay GA, Robinson RA, Lane WS, and Wright GD (1994b) Active-site labeling of an aminoglycoside antibiotic phosphotransferase (APH(3')-IIIa). *Biochemistry* **33**:14115–14120

McKay GA, Roestamadji J, Mobashery S, and Wright GD (1996) Recognition of aminoglycoside antibiotics by enterococcal-staphylococcal aminoglycoside 3'-phosphotransferase type IIIa: role of substrate amino groups. *Antimicrob Agents Chemother* **40**:2648–2650

McKay GA and Wright GD (1995) Kinetic mechanism of aminoglycoside phosphotransferase type IIIa. Evidence for a Theorell-Chance mechanism. *J Biol Chem* **270**:24686–24692

McKay GA and Wright GD (1996) Catalytic mechanism of enterococcal kanamycin kinase (APH(3')-IIIa): viscosity, thio, and solvent isotope effects support a Theorell-Chance mechanism. *Biochemistry* **35**:8680–5

Mikkelsen NE, Johansson K, Virtanen A, and Kirsebom LA (2001) Aminoglycoside binding displaces a divalent metal ion in a tRNA- neomycin B complex. *Nat Struct Biol* **8**:510–514

Mingeot-Leclercq MP, Glupczynski Y, and Tulkens PM (1999) Aminoglycosides: activity and resistance. *Antimicrob Agents Chemother* **43**:727–737.

Moazed D and Noller HF (1987) Interaction of antibiotics with functional sites in 16S ribosomal RNA. *Nature* **327**:389–394

Moellering RC (2003) Linezolid: the first oxazolidinone antimicrobial. *Ann Intern Med* **138**:135–42

Mohammadi M, McMahon G, Sun L, Tang C, Hirth P, Yeh BK, Hubbard SR, and Schlessinger J (1997) Structures of the tyrosine kinase domain of fibroblast growth factor receptor in complex with inhibitors. *Science* **276**:955–60

Mohler ML, Cox JR, and Serpersu EH (1997) Aminoglycoside phosphotransferase (3')-IIIa (APH(3')-IIIa)-bound conformation of the aminoglycoside lividomycin A characterized by NMR. *Carbohydr Lett* **3**:17–24

Nagabhushan TL, Cooper AB, Tsai H, Daniels PJ, and Miller GH (1978) The syntheses and biological properties of 1-N-(S-4-amino-2-hydroxybutyryl)-gentamicin B and 1-N-(S-3-amino-2-hydroxypropionyl)-gentamicin B. *J Antibiot (Tokyo)* **31**:681–687

Nagumo H, Sasaki Y, Ono Y, Okamoto H, Seto M, and Takuwa Y (2000) Rho kinase inhibitor HA-1077 prevents Rho-mediated myosin phosphatase inhibition in smooth muscle cells. *Am J Physiol Cell Physiol* **278**:57–65

Navaza J (1994) *AMoRe*: an automated package for molecular replacement. *Acta Crystallogr A* **50**:157–163

Navaza J (2001) Implementation of molecular replacement in *AMoRe*. *Acta Crystallographica Section D* **57**:1367–1372

Navaza J and Vernoslova E (1995) On the fast translation functions for molecular replacement. *Acta Crystallographica Section A* **51**:445–449

Nicolaou K and Boddy CN (2001) Behind Enemy Lines. *Sci Am* **284**:54–61

Nissen P, Kjeldgaard M, and Nyborg J (2000) Macromolecular mimicry. *Embo J* **19**:489–495

Nissen P, Kjeldgaard M, Thirup S, Polekhina G, Reshetnikova L, Clark B, and J N (1995) Crystal structure of the ternary complex of Phe-tRNAPhe, EF-Tu and a GTP analogue. *Science* **270**:1464–1472

Nuccio ML, Ziemak MJ, Henry SA, Weretilnyk EA, and Hanson AD (2000) cDNA cloning of phosphoethanolamine N-methyltransferase from spinach by complementation in Schizosaccharomyces pombe and characterization of the recombinant enzyme. *J Biol Chem* **275**:14095–14101

Nurizzo D, Shewry SC, Perlin MH, Brown SA, Dholakia JN, Fuchs RL, Deva T, Baker EN, and Smith CA (2003) The crystal structure of aminoglycoside-3'-phosphotransferase-IIa, an enzyme responsible for antibiotic resistance. *J Mol Biol* **327**:491–506

Ogle JM, Brodersen DE, Clemons WM, Tarry MJ, Carter AP, and Ramakrishnan V (2001) Recognition of cognate transfer RNA by the 30S ribosomal subunit. *Science* **292**:897–902

Ogle JM, Murphy FV, Tarry MJ, and Ramakrishnan V (2002) Selection of tRNA by the ribosome requires a transition from an open to a closed form. *Cell* **111**:721–732

Oka A, Sugisaki H, and Takanami M (1981) Nucleotide sequence of the kanamycin resistance transposon Tn903. *J Mol Biol* **147**:217–226

Okamoto A, Ishii S, Hirotsu K, and Kagamiyama H (1999) The active site of Paracoccus denitrificans aromatic amino acid aminotransferase has contrary properties: flexibility and rigidity. *Biochemistry* **38**:1176–1184

Okamoto A, Nakai Y, Hayashi H, Hirotsu K, and Kagamiyama H (1998) Crystal structures of Paracoccus denitrificans aromatic amino acid aminotransferase: a substrate recognition site constructed by rearrangement of hydrogen bond network. *J Mol Biol* **280**:443–61

Otwinowski Z and Minor W (1997) Processing of X-ray diffraction data collected in oscillation mode. *Methods Enzymol* **276**:307–326

Overbye KM and Barrett JF (2005) Antibiotics: where did we go wrong? *Drug Discov Today* **10**:45–52

Owen DJ, Noble ME, Garman EF, Papageorgiou AC, and Johnson LN (1995) Two structures of the catalytic domain of phosphorylase kinase: an active protein kinase complexed with substrate analogue and product. *Structure* **3**:467–482

Papadopoulou B and Courvalin P (1988) Dispersal in Campylobacter spp. of aphA-3, a kanamycin resistance determinant from gram-positive cocci. *Antimicrob Agents Chemother* **32**:945–948

Pape T, Wintermeyer W, and Rodnina MV (2000) Conformational switch in the decoding region of 16S rRNA during aminoacyl-tRNA selection on the ribosome. *Nat Struct Biol* **7**:104–107

Paterson DL (1999) β-lactamase inhibitors and new β-lactamases. *Current Treatment Options in Infectious Diseases* **1**:85–87

Perdersen L, Benning M, and Holden H (1995) Structural investigation of the antibiotic and ATP-binding sites in kanamycin nucleotidyltransferase. *Biochemsitry* **34**:13305–13311

Pfaller MA, Jones RN, Doern GV, and Kugler K (1998) Bacterial pathogens isolated from patients with bloodstream infection: frequencies of occurrence and antimicrobial susceptibility patterns from the SENTRY antimicrobial surveillance program (United States and Canada, 1997). *Antimicrob Agents Chemother* **42**:1762–70

Powell AJ, Read JA, Banfield MJ, Gunn-Moore F, Yan SD, Lustbader J, Stern AR, Stern DM, and Brady RL (2000) Recognition of structurally diverse substrates by type II 3-hydroxyacyl-CoA dehydrogenase (HADH II)/amyloid-beta binding alcohol dehydrogenase (ABAD). *J Mol Biol* **303**:311–327

Powis G, Bonjouklian R, Berggren MM, Gallegos A, Abraham R, Ashendel C, Zalkow L, Matter WF, Dodge J, Grindey G, and et al (1994) Wortmannin, a potent and selective inhibitor of phosphatidylinositol-3-kinase. *Cancer Res* **54**:2419–2423

Prade L, Engh RA, Girod A, Kinzel V, Huber R, and Bossemeyer D (1997) Staurosporine-induced conformational changes of cAMP-dependent protein kinase catalytic subunit explain inhibitory potential. *Structure* **5**:1627–37

Ramakrishnan C and Ramachandran GN (1965) Stereochemical criteria for polypeptide and protein chain conformations. II. Allowed conformations for a pair of peptide units. *Biophys J* **5**:909–933

Rao VD, Misra S, Boronenkov IV, Anderson RA, and Hurley JH (1998) Structure of type IIbeta phosphatidylinositol phosphate kinase: a protein kinase fold flattened for interfacial phosphorylation. *Cell* **94**:829–839

Read R (1986) Improved Fourier coefficients for maps using phases from partial structures with errors. *Acta Crystallogr A* **42**:140–149

Roach PJ (1991) Multisite and hierarchal protein phosphorylation. *J Biol Chem* **266**:14139–14142

Rodnina MV, Daviter T, Gromadski K, and Wintermeyer W (2002) Structural dynamics of ribosomal RNA during decoding on the ribosome. *Biochimie* **84**:745–754

Roestamadji J, Grapsas I, and Mobashery S (1995a) Loss of individual electrostatic interactions between aminoglycoside antibiotics and resistance enzymes as an effective means to overcoming bacterial drug resistance. *J Am Chem Soc* **117**:11060–11069

Roestamadji J, Grapsas I, and Mobashery S (1995b) Mechanism-based inactivation of bacterial aminoglycoside 3'-phosphotransferases. *J Am Chem Soc* **117**:80–84

Roestamadji J and Mobashery S (1998) The use of neamine as a molecular template: inactivation of bacterial antibiotic resistance enzyme aminoglycoside 3'-phosphotransferase type IIa. *Bioorg Med Chem Lett* **8**:3483–3486

Russell RJ, Murray JB, Lentzen G, Haddad J, and Mobashery S (2003) The complex of a designer antibiotic with a model aminoacyl site of the 30S ribosomal subunit revealed by X-ray crystallography. *J Am Chem Soc* **125**:3410–3411

Rutschmann O and Domino M (2004) Antibiotics for upper respiratory tract infections in ambulatory practice in the United States, 1997-1999: Does physician specialty matter? *J Am Board Fam Pract* **17**:196–200

Sasaki Y, Suzuki M, and Hidaka H (2002) The novel and specific Rho-kinase inhibitor (S)-(+)-2-methyl-1-[(4-methyl-5-isoquinoline)sulfonyl]-homopiperazine as a probing molecule for Rho-kinase-involved pathway. *Pharmacol Ther* **93**:225–232

Scalliet G, Journot N, Jullien F, Baudino S, Magnard JL, Channeliere S, Vergne P, Dumas C, Bendahmane M, Cock JM, and Hugueney P (2002) Biosynthesis of the major scent components 3,5-dimethoxytoluene and 1,3,5-trimethoxybenzene by novel rose O-methyltransferases. *FEBS Lett* **523**:113–118

Schatz A, Bugie E, and Waksman S (1944) Streptomycin, a substance exhibiting antibiotic activity against gram-positive and gram-negative bacteria. *Proc Soc Exp Biol Med* **55**:66–69

Schentag JJ, Hyatt JM, Carr JR, Paladino JA, Birmingham MC, Zimmer GS, and Cumbo TJ (1998) Genesis of methicillin-resistant *Staphylococcus aureus* (MRSA), how treatment of MRSA infections has selected for vancomycin-resistant *Enterococcus faecium*, and the importance of antibiotic management and infection control. *Clin Infect Dis* **26**:1204–1214

Schmitz FJ, Fluit AC, Gondolf M, Beyrau R, Lindenlauf E, Verhoef J, Heinz HP, and Jones ME (1999) The prevalence of aminoglycoside resistance and corresponding resistance genes in clinical isolates of staphylococci from 19 European hospitals. *J Antimicrob Chemother* **43**:253–259

Schumacher MA, Miller MC, Grkovic S, Brown MH, Skurray RA, and Brennan RG (2001) Structural mechanisms of QacR induction and multidrug recognition. *Science* **294**:2158–2163

Serpersu EH, Cox JR, DiGiammarino EL, Mohler ML, Ekman DR, Akal-Strader A, and Owston M (2000) Conformations of antibiotics in active sites of aminoglycoside- detoxifying enzymes. *Cell Biochem Biophys* **33**:309–321

Shaw K, Rather P, Hare R, and Miller G (1993) Molecular genetics of aminoglycoside resistance genes and familial relationships of the aminoglycoside-modifying enzymes. *Microbiol Rev* **57**:138–163

Shears SB (2004) How versatile are inositol phosphate kinases? *Biochem J* **377**:265–280

Siregar JJ, Lerner SA, and Mobashery S (1994) Purification and characterization of aminoglycoside 3'-phosphotransferase type IIa and kinetic comparison with a new mutant enzyme. *Antimicrob Agents Chemother* **38**:641–647

Siregar JJ, Miroshnikov K, and Mobashery S (1995) Purification, characterization, and investigation of the mechanism of aminoglycoside 3'-phosphotransferase type Ia. *Biochemistry* **34**:12681–12688

Smith CA and Baker EN (2002) Aminoglycoside antibiotic resistance by enzymatic deactivation. *Curr Drug Targets Infect Disord* **2**:143–160

Sowadski JM, Epstein LF, Lankiewicz L, and Karlsson R (1999) Conformational diversity of catalytic cores of protein kinases. *Pharmacol Ther* **82**:157–64

Spadafora C, Repetto Y, Torres C, Pino L, Robello C, Morello A, Gamarro F, and Castanys S (2002) Two casein kinase 1 isoforms are differentially expressed in Trypanosoma cruzi. *Mol Biochem Parasitol* **124**:23–36

Sucheck SJ, Wong AL, Koeller KM, Boehr DD, Draker Ka, Sears P, Wright GD, and Wong CH (2000) Design of bifunctional antibiotics that target bacterial rRNA and inhibit resistance-causing enzymes. *J Am Chem Soc* **122**:5230–5231

Taylor DE, Yan W, Ng LK, Manavathu EK, and Courvalin P (1988) Genetic characterization of kanamycin resistance in *Campylobacter coli*. *Ann Inst Pasteur Microbiol* **139**:665–676

Taylor SS, Knighton DR, Zheng J, Ten Eyck LF, and Sowadski JM (1992) Structural framework for the protein kinase family. *Annu Rev Cell Biol* **8**:429–462

Taylor SS, Radzio-Andzelm E, Madhusudan, Cheng X, Ten Eyck L, and Narayana N (1999) Catalytic subunit of cyclic AMP-dependent protein kinase: structure and dynamics of the active site cleft. *Pharmacol Ther* **82**:133–41

Taylor SS, Yang J, Wu J, Haste NM, Radzio-Andzelm E, and Anand G (2004) PKA: a portrait of protein kinase dynamics.

Teale CJ (2002) Antimicrobial resistance and the food chain. *J Appl Microbiol* **92 Suppl**:85S–9S

Theorell H and Chance B (1951) Studies on liver alcohol dehydrogenase II. The kinetics of the compound of horse liver alcohol dehydrogenase and reduced diphosphopyridine nucleotide. *Acta Chemica Scandinavica* **5**:1127–1144

Therrien C and Levesque RC (2000) Molecular basis of antibiotic resistance and beta-lactamase inhibition by mechanism-based inactivators: perspectives and future directions. *FEMS Microbiol Rev* **24**:251–62

Thompson J, Skeggs PA, and Cundliffe E (1985) Methylation of 16S ribosomal RNA and resistance to the aminoglycoside antibiotics gentamicin and kanamycin determined by DNA from the gentamicin-producer, Micromonospora purpurea. *Mol Gen Genet* **201**:168–173

Thompson PR, Boehr DD, Berghuis AM, and Wright GD (2002) Mechanism of aminoglycoside antibiotic kinase APH(3')-IIIa: role of the nucleotide positioning loop. *Biochemistry* **41**:7001–7

Thompson PR, Hughes DW, and Wright GD (1996a) Mechanism of aminoglycoside 3'-phosphotransferase type IIIa: His188 is not a phosphate-accepting residue. *Chem Biol* **3**:747–755

Thompson PR, Hughes DW, and Wright GD (1996b) Regiospecificity of aminoglycoside phosphotransferase from Enterococci and Staphylococci (APH(3')-IIIa). *Biochemistry* **35**:8686–8695

Thompson PR, Schwartzenhauer J, Hughes DW, Berghuis AM, and Wright GD (1999) The COOH terminus of aminoglycoside phosphotransferase (3')-IIIa

is critical for antibiotic recognition and resistance. *J Biol Chem* **274**:30697–30706

Toledo LM, Lydon NB, and Elbaum D (1999) The structure-based design of ATP-site directed protein kinase inhibitors. *Curr Med Chem* **6**:775–805

Tong L, Pav S, White DM, Rogers S, Crane KM, Cywin CL, Brown ML, and Pargellis CA (1997) A highly specific inhibitor of human p38 MAP kinase binds in the ATP pocket. *Nat Struct Biol* **4**:311–6

Trieu-Cuot P and Courvalin P (1983) Nucleotide sequence of the *Streptococcus faecalis* plasmid gene encoding the 3'5-aminoglycoside phosphotransferase type III. *Gene* **23**:331–341

Tsukiura H, Saito K, Kobaru S, Konishi M, and Kawaguchi H (1973) Aminoglycoside antibiotics. IV. BU-1709 E1 and E2, new aminoglycoside antibiotics related to the butirosins. *J Antibiot (Tokyo)* **26**:386–388

Udo EE and Dashti AA (2000) Detection of genes encoding aminoglycoside-modifying enzymes in staphylococci by polymerase chain reaction and dot blot hybridization. *Int J Antimicrob Agents* **13**:273–279

Umezawa H, Umezawa S, Tsuchiya T, and Okazaki Y (1971a) 3',4'-dideoxykanamycin B active against kanamycin-resistant *Escherichia coli* and *Pseudomonas aeruginosa*. *J Antibiot (Tokyo)* **24**:485–487

Umezawa S, Tsuchiya T, Muto R, Nishimura Y, and Umezawa H (1971b) Synthesis of 3'-deoxykanamycin effective against kanamycin-resistant *Escherichia coli* and *Pseudomonas aeruginosa*. *J Antibiot (Tokyo)* **24**:274–276

Vakulenko SB and Mobashery S (2003) Versatility of aminoglycosides and prospects for their future. *Clin Microbiol Rev* **16**:430–450

Vetting MW, Hegde SS, Javid-Majd F, Blanchard JS, and Roderick SL (2002) Aminoglycoside 2'-N-acetyltransferase from Mycobacterium tuberculosis in complex with coenzyme A and aminoglycoside substrates. *Nat Struct Biol* **9**:653–658

Vetting MW, Magnet S, Nieves E, Roderick SL, and Blanchard JS (2004) A bacterial acetyltransferase capable of regioselective N-acetylation of antibiotics and histones. *Chem Biol* **11**:565–573

Vicens Q and Westhof E (2002) Crystal structure of a complex between the aminoglycoside tobramycin and an oligonucleotide containing the ribosomal decoding a site. *Chem Biol* **9**:747–55

Vicens Q and Westhof E (2003) Molecular recognition of aminoglycoside antibiotics by ribosomal RNA and resistance enzymes: An analysis of x-ray crystal structures. *Biopolymers* **70**:42–57

Walker EH, Pacold ME, Perisic O, Stephens L, Hawkins PT, Wymann MP, and Williams RL (2000) Structural determinants of phosphoinositide 3-kinase inhibition by wortmannin, LY294002, quercetin, myricetin, and staurosporine. *Mol Cell* **6**:909–919

Walsh C (2000) Molecular mechanisms that confer antibacterial drug resistance. *Nature* **406**:775–781

Wang J, Li J, Chen HN, Chang H, Tanifum CT, Liu HH, Czyryca PG, and Chang CWT (2005) Glycodiversification for the optimization of the kanamycin class aminoglycosides. *J Med Chem* **48**:6271–6285

Wang R, Gao Y, and Lai L (2000) LigBuilder: A Multi-Purpose Program for Structure-Based Drug Design. *Journal of Molecular Modeling* **6**:498–516

Wang Z, Canagarajah BJ, Boehm JC, Kassisa S, Cobb MH, Young PR, Abdel-Meguid S, Adams JL, and Goldsmith EJ (1998) Structural basis of inhibitor selectivity in MAP kinases. *Structure* **6**:1117–28. 0969-2126 eng Journal Article England 9418985

Wang Z, Harkins PC, Ulevitch RJ, Han J, Cobb MH, and Goldsmith EJ (1997) The structure of mitogen-activated protein kinase p38 at 2.1-Å resolution. *Proc Natl Acad Sci U S A* **94**:2327–32

Whittle E, Cahoon EB, Subrahmanyam S, and Shanklin J (2005) A multifunctional acyl-acyl carrier protein desaturase from Hedera helix L. (English ivy) can synthesize 16- and 18-carbon monoene and diene products. *J Biol Chem* **280**:28169–28176

Wilson KP, McCaffrey PG, Hsiao K, Pazhanisamy S, Galullo V, Bemis GW, Fitzgibbon MJ, Caron PR, Murcko MA, and Su MS (1997) The structural basis for the specificity of pyridinylimidazole inhibitors of p38 MAP kinase. *Chem Biol* **4**:423–31

Wolf E, Vassilev A, Makino Y, Sali A, Nakatani Y, and Burley S (1998) Crystal structure of a GCN5-related N-acetyltransferase: Serratia marcescens aminoglycoside 3-N-acetyltransferase. *Cell* **94**:439–449

World Health Organization (1999) Removing obstacles to healthy development. Report on infectious diseases 1999

World Health Organization (2000) Overcoming antimicrobial resistance. Report on infectious diseases 2000

Wright GD, Berghuis AM, and Mobashery S (1998) Aminoglycoside antibiotics. Structures, functions, and resistance. *Adv Exp Med Biol* **456**:27–69

Wright GD and Thompson PR (1999) Aminoglycoside phosphotransferases: proteins, structure, and mechanism. *Front Biosci* **4**:D9–21

Wright JJ (1976) Synthesis of 1-N-ethylsisomicin: A broad-spectrum semisynthetic aminoglycoside antibiotic. *J Chem Soc Chem Commun* **6**:206–208

Wu M, Maier E, Benz R, and Hancock RE (1999) Mechanism of interaction of different classes of cationic antimicrobial peptides with planar bilayers and with the cytoplasmic membrane of *Escherichia coli*. *Biochemistry* **38**:7235–7242

Wybenga-Groot LE, Draker K, Wright GD, and Berghuis AM (1999) Crystal structure of an aminoglycoside 6'-N-acetyltransferase: defining the GCN5-related N-acetyltransferase superfamily fold. *Structure Fold Des* **7**:497–507

Wymann MP, Bulgarelli-Leva G, Zvelebil MJ, Pirola L, Vanhaesebroeck B, Waterfield MD, and Panayotou G (1996) Wortmannin inactivates phosphoinositide 3-kinase by covalent modification of Lys-802, a residue involved in the phosphate transfer reaction. *Mol Cell Biol* **16**:1722–1733

Xu RM, Carmel G, Kuret J, and Cheng X (1996) Structural basis for selectivity of the isoquinoline sulfonamide family of protein kinase inhibitors. *Proc Natl Acad Sci U S A* **93**:6308–6313

Xu RM, Carmel G, Sweet RM, Kuret J, and Cheng X (1995) Crystal structure of casein kinase-1, a phosphate-directed protein kinase. *EMBO J* **14**:1015–1023

Yamaguchi H and Hendrickson WA (1996) Structural basis for activation of human lymphocyte kinase Lck upon tyrosine phosphorylation. *Nature* **384**:484–489

Yanagihara N, Tachikawa E, Izumi F, Yasugawa S, Yamamoto H, and Miyamoto E (1991) Staurosporine: an effective inhibitor for Ca^{2+}/calmodulin-dependent protein kinase II. *J Neurochem* **56**:294–8

Yang J, Ten Eyck LF, Xuong NH, and Taylor SS (2004) Crystal structure of a cAMP-dependent protein kinase mutant at 1.26 Å: new insights into the catalytic mechanism. *J Mol Biol* **336**:473–87

Yang Y, Roestamadji J, Mobashery S, and Orlando R (1998) The use of neamine as a molecular template: identification of active site residues in the bacterial antibiotic resistance enzyme aminoglycoside 3'-phosphotransferase type IIa by mass spectroscopy. *Bioorg Med Chem Lett* **8**:3489–3494

Yoshikawa TT (2002) Antimicrobial resistance and aging: beginning of the end of the antibiotic era? *J Am Geriatr Soc* **50**:S226–9

Yoshizawa S, Fourmy D, and Puglisi JD (1998) Structural origins of gentamicin antibiotic action. *EMBO J* **17**:6437–6448.

Zhao B, Bower MJ, McDevitt PJ, Zhao H, Davis ST, Johanson KO, Green SM, Concha NO, and Zhou BB (2002) Structural basis for Chk1 inhibition by UCN-01. *J Biol Chem* **277**:46609–15

Zheleznova EE, Markham PN, Neyfakh AA, and Brennan RG (1999) Structural basis of multidrug recognition by BmrR, a transcription activator of a multidrug transporter. *Cell* **96**:353–362

Zheng J, Knighton DR, ten Eyck LF, Karlsson R, Xuong N, Taylor SS, and Sowadski JM (1993) Crystal structure of the catalytic subunit of cAMP-dependent protein kinase complexed with MgATP and peptide inhibitor. *Biochemistry* **32**:2154–2161

Zhou J and Adams JA (1997) Is there a catalytic base in the active site of cAMP-dependent protein kinase? *Biochemistry* **36**:2977–2984